Investigating the Therapeutic and Biological Impact of MNK1/2 Kinases

Sathyen Alwin Prabhu

Division of Experimental Medicine

Faculty of Medicine

McGill University

Montréal, Québec,

Canada

April, 2023

A thesis submitted to McGill University in partial fulfillment of the requirements of the degree of Doctor of Philosophy (Ph.D.) in Experimental Medicine

Co-supervised by

Dr. Wilson H. Miller Jr. and Dr. Sonia del Rincón

Table of Contents

Abstract

The MAPK and PI3K pathways are among the most deregulated pathways in cancer. At the nexus of these pathways lies the MNK1/2-eIF4E axis. The Mitogen activated protein kinase-interacting kinases 1 and 2 (MNK1/2) are activated downstream of the MAP kinases ERK1/2 and p38. Downstream of the PI3K pathway, the availability of the 5' cap binding protein eIF4E is tightly regulated by mTOR kinase activity. MNK1 and MNK2 are the exclusive kinases for eIF4E at serine 209 and numerous studies have implicated a role for activated MNK1/2 and phosphorylated eIF4E in cancer development and progression. While indispensible for normal development, the phosphorylation of eIF4E enhances the translation of a subset of mRNAs that code for proteins with functions in invasion, metastasis and cell survival. Hence, I wanted to identify effective therapeutic combinations with MNK1/2 inhibitors. Additionally, I delved deeper into MNK1/2 biology to identify novel interactors and substrates of the kinases.

We have identified a new therapeutic combination of MNK1/2 and CDK4/6 inhibitors as a potential strategy for the management of melanoma and breast cancer. We identified that the efficacy of the CDK4/6 inhibitor, palbociclib is limited by its ability to promote the phosphorylation of eIF4E.

We thus hypothesized that the addition of a MNK1/2 inhibitor would result in an improved cellular response to palbociclib. Indeed, we observed that genetic or pharmacologic inhibition of MNK1/2 resulted in increased sensitivity of cells to palbociclib in melanoma and breast cancer resulting in increased G1 cell cycle arrest

and senescence. Moreover, we discovered that acquired resistance to palbociclib is partly mediated by an increase in phosphorylated eIF4E compared to their therapy naïve counterparts and the treatment of these palbociclib-resistant cells with a MNK1/2 inhibitor results in resensitization to palbociclib. Importantly, we demonstrate that the drug combination delays tumor outgrowth and significantly improves the overall survival in murine models of melanoma.

Next we attempted to identify and characterize novel substrates of MNK1. We discovered that MNK1, but not MNK2, interacts with the RNA-binding protein binding protein LARP1. Similar to eIF4E, LARP1 binds the 5' m7GTP of TOP mRNA. While the function of LARP1 in regulating mRNA translation has been controversial, its significance in cancer is emerging. We have verified that MNK1 and LARP1 indeed interact using a number of complimentary approaches, including data that endogenous LARP1 co-immunoprecipitates with endogenous MNK1 in a number of cell lines. We have also characterized the regions on LARP1 and MNK1 that are necessary for the interaction.

One outcome of the MNK1:LARP1 interaction is that MNK1 phosphorylates LARP1 on threonine 449, as shown by mass spectrometry and in vitro kinase assays. Mechanistically we show that, the Kd apparent ratio between poly (A25) and RPS6 TOP motif RNAs was lower in the T449A phosphodeficient La-Module, than the WT La-Module suggesting that the T449A mutant likely has a higher affinity for RNA compared with WT LARP1.

Overall these data improve our understanding of the role that MNK1/2 kinases play in mRNA translation and open up new avenues for further investigation.

Résumé

Les voies de signalisation MAPK et PI3K sont parmi les voies les plus dérégulées dans le cancer. Au croisement de ces voies se trouve l'axe MNK1/2-eIF4E. Les protéines “Mitogen activated protein kinase-interacting kinases 1 and 2” (MNK1/2) sont activées en aval des “MAP kinases” ERK1/2 et p38. D'un côté, en aval de la voie PI3K, la disponibilité de la protéine de liaison à la coiffe 5' de l’ARNm, eIF4E, est étroitement régulée par l'activité de la kinase mTOR. D'un autre côté, MNK1 et MNK2 sont les seules kinases connues capables de phosphoryler eIF4E sur la sérine 209 et de nombreuses études ont montré le rôle entre l’activation des MNK1/2 et la phosphorylation d’eIF4E dans le développement et la progression du cancer. Bien que dispensable pour le développement de cellules normales, la phosphorylation d’eIF4E augmente la traduction d'un sous-ensemble d'ARNm qui codent pour des protéines impliqués dans l’invasion, la métastase et la survie cellulaire. J'ai donc voulu déterminer des combinaisons thérapeutiques avec les inhibiteurs MNK1/2 et approfondir nos connaissance sur la biologie moléculaires des MNK1/2 afin identifier de nouveaux interacteurs et substrats de ces kinases.

Nous avons identifié une nouvelle thérapie basée sur la combinaison d’inhibiteurs de MNK1/2 et de CDK4/6 comme stratégie potentielle pour le traitement du mélanome et du cancer du sein. Nous avons observé que l'efficacité de l'inhibiteur contre les CDK4/6, le palbociclib, est limitée due à sa capacité d’induire la phosphorylation d’eIF4E. Nous avons donc émis l'hypothèse qu'ajouter un inhibiteur de MNK1/2 entraînerait une amélioration de la réponse au palbociclib. En effet, nous avons

remarqué que l'inhibition génétique, ou pharmacologique de MNK1/2 accentuait la réponse des cellules de mélanome et de cancer du sein au palbociclib, en exacerbant l'arrêt du cycle cellulaire en G1 et de la sénescence. De plus, nous avons découvert que la résistance acquise au palbociclib est en partie médiée par une augmentation de la phosphorylation d'eIF4E et que le traitement avec un inhibiteur de MNK1/2 entraîne une resensibilisation au palbociclib. Fait important, nous avons démontré dans des modèles murins de mélanome que la combinaison de ces thérapies retarde la croissance tumorale et améliore considérablement leur survie globale.

Par la suite, nous avons tenté de caractériser de nouveaux substrats de MNK1. Nous avons découvert que MNK1, mais pas MNK2, interagit avec la protéine de liaison à l'ARNm LARP1. Similaire à eIF4E, LARP1 se lie à la coiffe 5' m7GTP de l'ARNm TOP. Bien que la fonction de LARP1 dans la régulation de la traduction de l'ARNm a été controversée, son importance dans le développement du cancer est en émergence. Nous avons confirmé que MNK1 et LARP1 interagissent effectivement ensemble en utilisant méthodologies complémentaires, notamment par immuno-précipitation, où LARP1 endogène co-immunoprécipite avec MNK1 endogène dans plusieurs lignées cellulaires. Nous avons également identifié les régions au sein des protéines LARP1 et MNK1 nécessaires à leur interaction. Résultat interessant de cette étude sur l'interaction entre MNK1 et LARP1, MNK1 phosphoryle LARP1 sur la thréonine 449, comme l'ont démontré la spectrométrie de masse et des expériences de phosphorylation par kinase *in vitro*. D'un point de vue mécanistique, nous montrons que le coefficient de dissociation (Kd) entre les ARN poly (A25) et RPS6 TOP était plus

faible dans le module “La” de la protéine LARP1 portant la mutation T449A que dans celui de la protéine LARP1 WT, suggèrant que le mutant T449A a probablement une affinité plus élevée pour l'ARN par rapport à WT LARP1.

Dans l'ensemble, ces données améliorent notre compréhension du rôle que jouent les kinases MNK1/2 dans la traduction de l'ARNm et ouvrent de nouvelles voies pour une études plus approfondies sur ces protéines.

Acknowledgments

If I were to go back 10 years and tell my former self that I would one day graduate with a Ph.D., together we would probably have a good laugh. I always knew I wanted to pursue graduate school, but, like everyone starting their career, I doubted my ability to achieve such a feat. On top of that, my mediocre GPA and a string of rejections made it feel impossible. Hence, first and foremost, I am grateful that I moved past my fears, without which I'm certain I would not be in the position I am today. I am honored to have completed my doctoral studies at **McGill University** and the **Lady Davis Institute of Medical Research**. The **staff** and **faculty** at these institutes have made my Ph.D. immensely fruitful; whether it is through providing funding opportunities, ensuring we have the appropriate facilities, or overall creating a collegial environment.

Doctoral studies kind of feel like an emotional rollercoaster. There are many lows and highs. However, having worked with **Dr. Sonia del Rincón** and **Dr. Wilson H. Miller Jr.** has made my lows seem high and my highs even higher. Somehow, in the midst of dealing with their lives and priorities, they always made time to keep me and my projects from derailing. Hands down, their mentorship has made me a better scientist and person. I feel a deep sense of gratitude for their guidance and support. I am also sincerely grateful for our shared lab meetings with **Dr. Koren Mann**, **Dr. April Rose**, and their teams. Having to consider three equitable points of view makes you want to pull your hair out, but when you're past that, it makes for an amazing learning experience and a fun story. I hope to be fortunate in my future to work with scientists that test my caliber like they have.

Fortunately, rollercoasters aren't single-seaters, and I've shared this tumultuous ride with some incredible people. I am super grateful to have met and worked alongside **Omar Moussa**, **Judith LaPierre**, **Christophe Goncalves**, **Sai Sakktee Krisna**, **Dr. Francois Santinon**, **Raul González**, **Dr. Alexandre Benoit**, **Dr. Kiran Makhani**, **Rowa Bakadlag**, and **Dr. Henry Yu**. While we all had our own challenges, in one way or another we made the time to support each other. I wish them tremendous fortune in their future endeavors.

I also would like to thank **Dr. Andrea Berman** and her team, **Nicholas Arredondo** and **Jahree Sosa**, for providing me with a lab home during my research stay at the University of Pittsburgh. Not only did they provide me with all the resources I needed to get my experiments done, they consistently tested me as a scholar and as a person.

I am very grateful for all the training I have received through the years leading up to my doctoral program. I have had the amazing opportunity to work with world-class scientists especially, but not limited to, **Dr. Chhavi Sharma**, **Dr. Jennifer Amengual**, **Dr. Owen O'Connor**, **Dr. Luigi Scotto**, **Dr. Michael Mangone**, and **Dr. Mark Lipstein**.

Finally, I want to give out a special thanks to my parents, **Priscilla D'souza** and **Alwin D'souza**, my brothers **Vinay** and **Rohit Prabhu**, my sister-in-law **Dandy Rodrigues** and my two nephews **Aiden** and **Gabriel Prabhu**. Their emotional support during my graduate studies was instrumental to my success. Family wouldn't be so without including my fiancé, **Hsiang Chou**. I have known no one with the patience and

love to deal with my shenanigans like she has and still love me more than I can love myself. From the bottom of my heart, I thank you, my love.

It’s difficult to remember to thank everyone, especially when you’re trying to write your thesis. To all those that have been forgotten, in paper, I genuinely appreciate your support and love.

Original Contributions to Knowledge

The MNK1 and MNK2 kinases are key regulators of cellular mRNA translation, with potential roles in cancer and other diseases. However, our current understanding about these proteins is limited. In this thesis, I will present data demonstrating the potential of MNK1/2 inhibitors in enhancing the anti-neoplastic capabilities of currently approved therapies. Moreover, this work will also describe the discovery of a novel interacting partner, and potential substrate, of MNK1 which may provide us with a better understanding of the role of MNK1 in cells, with the overarching goal of developing better MNK1/2 inhibitors. Contributions to original knowledge and significance of studies presented in this thesis are highlighted as follows:

1. In **Chapter 2** of this thesis, we demonstrate that the efficacy of the FDA approved CDK4/6 inhibitor, palbociclib, is limited by its ability to promote the phosphorylation of eIF4E, an event exclusively catalyzed by MNK1/2 kinases.
    - In this study, we are the first to demonstrate that cellular exposure to the CDK4/6 inhibitor palbociclib can result in the increased phosphorylation of the MNK1/2 substrate eIF4E.
    - We are also the first to demonstrate that blocking this increase in phosphorylated eIF4E using selective MNK1/2 inhibitors results in further repression of cell growth, increased G1 cell cycle arrest, and increased senescence in breast cancer and melanoma cells. Furthermore, we demonstrate that the combination of the two inhibitors further delays tumor outgrowth and improves the overall survival in murine models of melanoma.

- Finally this study is also the first to identify that cells that acquire resistance to palbociclib have elevated levels of phosphorylated eIF4E and moreover, inhibition of MNK1/2 in this context, resensitized these cells to palbociclib.

2. In **Chapter 3** of this thesis, we used a proteomics-based approach with the goal of identifying novel interactors and substrates of the MNK1.
    - In this study, we are the first to demonstrate and validate that MNK1, but not MNK2, is able to co-immunoprecipitate the RNA-binding protein, LARP1 in immortalized and transformed cells.
    - This study is also the first to show that MNK1 binds the LARP1 protein through its La-Module, while LARP1 interacts with MNK1 by potentially interacting with the N-terminal polybasic region on the latter.
    - Furthermore, using phosphoproteomics and in vitro kinase assays, we are the first to demonstrate that MNK1 can phosphorylate LARP1 on the La-Module at threonine 449.
    - Finally, we are the first to begin to understand the impact of the T449 phosphorylation site on LARP1 in its affinity for RNA.

Publications arising from this work

Chapters 1 and **4** contain material published in a review article:

> **Prabhu SA***, Moussa O*, Miller Jr. WH, Del Rincón SV. The MNK1/2-eIF4E axis as a potential therapeutic target in melanoma. Int J Mol Sci. 2020;21(11):E4055. (*equal contribution)

Chapter 2 was published as an original research article

> **Prabhu SA,** Moussa O, Gonçalves C, LaPierre JH, Chou H, Huang F, Richard VR, Ferruzo PYM, Guettler EM, Soria-Bretones I, Kirby L, Gagnon N, Su J, Silvester J, Krisna SS, Rose AAN, Sheppard KE, Cescon DW, Mallette FA, Zahedi, RP, Borchers CH, Miller Jr. WH, Del Rincón SV et al. Inhibition of the MNK1/2-eIF4E axis augments palbociclib-mediated antitumor activity in melanoma and breast cancer. Mol Cancer Ther. 2023;22(2):192-204.

Chapter 3 contains material to be included in a manuscript in preparation for publication as an original research article:

> **Prabhu SA,** Goncalves C, Kajjo S, Sosa J, Arredondo N, Richard VR, Dejgaard K, Fabian M, Fonesca B, Zahedi R, Berman AJ, Miller Jr. WH, del Rincon, SV (2023) Discovery of LARP1 as a novel substrate of MNK1.

Publications that include work performed by SAP, but not included in the presentation of this dissertation:

1. Dahabieh MS*, Huang F*, Gonçalves C, Flores González R, **Prabhu SA**, Bolt A, Khoury E, Rémy-Sarrazin J, Xu ZY, Mann KK, Boisvert FM, Miller WH Jr* , Del Rincón SV* . (2021). Increasing pexophagy as an unconventional mode to kill cancer cells. Autophagy. DOI: 10.1080/15548627.2021.1936932.
2. Yang W, Khoury E, Guo Q, **Prabhu SA**, Emond A, Huang F, Gonçalves C, Zhan Y, Plourde D, Nichol JN, Dahabieh MS, Miller WH Jr, Del Rincón SV. (2020). MNK1 signaling induces an ANGPTL4-mediated gene signature to drive melanoma progression. Oncogene, 39(18), 3650-3665. DOI: 10.1038/s41388-020-1240-5.

Contribution of authors

The candidate performed the majority of the research described in this thesis under the supervision of Dr. Wilson H. Miller Jr. and Dr. Sonia del Rincón. The contribution of other authors to this work is as follows:

In **Chapter 1**, the candidate, Dr. Sonia del Rincón, and Dr. Wilson H. Miller Jr. designed the figures.

In **Chapter 2**, the candidate, Dr. Sonia del Rincón and Dr. Wilson H. Miller Jr. designed the research. The candidate performed the research. For figures 2.1G, 2.1H, 2.1I, 2.2C and 2.2D, biological replicates of the experiments were performed both by the candidate and by Omar Moussa. Data related to Figures 2.3A, 2.3B, Supplemental Figure 2.2A to 2.2L were generated by the candidate, Dr. Rene Zahedi, Dr. Vincent R. Richard, and Christophe Goncalves. Figure 2.2M and 2.2N were generated by the candidate and Hsiang Chou. Figure 2.4G was designed by the candidate and the experiments were performed by Judith LaPierre. Figure 2.5A was performed by Laura Kirby and Dr. Karen Sheppard. For *in vivo* experiments, the candidate performed majority of the measurements with help from Dr. Fan Huang, Natascha Gagnon. The *in vivo* drug dosing was performed by Jie Su and Natascha Gagnon. Data in Figure 2.6C was generated by the candidate and Judith LaPierre.

In **Chapter 3**, the candidate, Dr. Sonia del Rincón and Dr. Wilson H. Miller Jr. designed the research. The candidate performed the research. Figure 3.1A to C and Supplemental Figure 3.1A and 3.1B were performed by the candidate and Dr. Kurt

Dejgaard. For Figure 3.2A and 3.2B and Supplemental Figure 3.2A, the plasmids were generated by Dr. Bruno Fonesca and the experiments were performed by the candidate. Supplemental Figure 3.2B were performed by Elie Khoury and Omar Moussa. The phosphoproteomics experiment in Figure 3.3A to 3.3C was performed by Dr. Antoine Meant. Figures 3.3 D to G were performed by the candidate, Dr. Rene Zahedi and Dr. Vincent Richard. The T449A site-directed mutagenesis was performed by Dr. Andrea Berman at the University of Pittsburgh.

List of Figures

Chapter 1

Chapter 2

- **Supplemental Figure 2.3:** Co-targeting MNK1/2 and CDK4/6 *in vivo* improves overall survival in murine models of melanoma.

Chapter 3

- **Figure 3.1:** Proteomics based identification of LARP1 as an interacting protein of MNK1
- **Figure 3.2:** MNK1 interacts with LARP1 via the La-Module and LARP1 binds to the N-terminal region of MNK1
- **Figure 3.3:** MNK1 phosphorylates LARP1 at threonine 449
- **Figure 3.4:** Phosphodeficient T449A mutant of the La-Module has a higher affinity for RNA compared to WT
- **Supplemental Figure 3.1:** DTSSP-based immunoprecipitation optimization and MNK1:LARP1 immunoprecipitation experiments related to Figure 3.1
- **Supplemental Figure 3.2:** Interactions between FLAG-LARP1 and PABPC1 or mTOR
- **Supplemental Figure 3.3:** Expression and purification of WT and T449A La-Module; *in vitro* kinase assay of eIF4E

Abbreviations

4-HT	4-hydroxytamoxifen
AML	Acute Myeloid Leukemia
ARE	Adenylate-Uraidylate-Rich-Elements
ATP	Adenosine Triphosphate
BET	Bromodomain and Extraterminal domain
CDK1	Cyclin-Dependent Kinase 1
CDK2	Cyclin-Dependent Kinase 2
CDK4	Cyclin-Dependent Kinase 4
CDK6	Cyclin-Dependent Kinase 6
CHAPS	(3-((3-cholamidopropyl) dimethylammonio)-1-propanesulfonate)
CIP/KIP	CDK Interacting Protein/Kinase Inhibitory Protein
CML	Chronic Myelogenous Leukemia
CNV	Copy Number Variations
DFD	Aspartic acid-Phenylalanine-Aspartic acid
DFG	Aspartic acid-Phenylalanine-Glycine
DKO	Double Knockout
DMEM	Dulbecco's Modified Eagle Medium
DMSO	Dimethyl Sulfoxide
DNA	Deoxyribonucleic Acid
DTSSP	3,3'-Dithiobis (sulfosuccinimidylpropionate)
EGFR	Epidermal Growth Factor Receptor
ER	Estrogen receptor
ERK	Extracellular signal-Regulated Kinases
FBS	Fetal Bovine Serum
FDA	Food and Drug Administration
FDR	False Discovery Rate
FUCCI	Fluorescent Ubiquitination-based Cell Cycle Indicator
GST	Glutathione S-Transferase
GTP	Guanosine Triphosphate
HR	Hormone Receptor

IFN	Interferon
INK4	Inhibitors of CDK4
KO	Knockout
MAPK	Mitogen Activated Protein Kinase
MEF	Mouse Embryonic Fibroblasts
MNK1	Mitogen Activate Protein Kinase-interacting serine/threonine-protein kinases 1
MNK2	Mitogen Activate Protein Kinase-interacting serine/threonine-protein kinases 2
MPNST	Malignant Peripheral Nerve Sheath Tumor
mTOR	mammalian Target of Rapamycin
NES	Nuclear Export Signal
NLS	Nuclear Localization Signal
NOD/SCID	immunodeficient nonobese diabetic /severe combined immunodeficiency
PBS	Phosphate Buffered Saline
PD-1	Programmed cell death 1 receptor
PD-L1	Programmed death ligand 1
PI3K	phosphoinositide 3-Kinase
PMA	phorbol 12-myristate 13-acetate
RAPTOR	Regulatory-Associated Protein of mTOR
RB	Retinoblastoma protein
RIPA	Radioimmunoprecipitation Assay buffer
RNA	Ribonucleic Acid
RTK	Receptor Tyrosine Kinase
SDS	Sodium Dodecyl Sulfate
TCEP	Tris(2-carboxyethyl)phosphine
TNBC	Triple Negative Breast Cancer
TOP	Teminal Oligopyrimidine tract
WT	Wild-type

Rationale and objectives

The MNK1/2 kinases have emerged as druggable targets in cancer. The current body of literature links the expression of active MNK1/2 and phosphorylated eIF4E in cancer development and progression. However, while the MNK1/2-eIF4E axis is selectively targetable and numerous inhibitors are in the clinic or currently in development, our understanding of the biology of this pathway is inadequate. Our principal hypothesis in this body of work is that the MNK1/2-eIF4E axis is a critical and exploitable vulnerability in cancer. Improving our understanding of the inner workings of this pathway may contribute to the development of better inhibitors with the overarching objective of improving patient care. The detailed objectives of this thesis are as follows:

1. To determine the impact of combining the FDA-approved CDK4/6 inhibitor, palbociclib with preclinical and clinically available MNK1/2 inhibitors.
2. To identify the mechanism of response to the therapeutic combination.
3. To assess whether therapeutic resistance to palbociclib occurs through mechanisms involving the MNK1/2-eIF4E axis.
4. To determine the *in vivo* efficacy of the therapeutic combination in melanoma models.
5. To identify novel interactors and substrates of MNK1.
6. To characterize the binding dynamics of any identified protein:protein interactions.
7. To determine whether MNK1/2 can phosphorylate identified interacting proteins.
8. To determine the functional impact of the MNK1-dependent phosphorylation of the substrate.

Chapter 1: Literature Review

1.1 Preface

This introductory chapter focuses on the biology of MAP Kinase-interacting serine/threonine-protein kinase 1 and 2 (MNK1/2) with emphasis on the roles they play in cap-dependent mRNA translation. Furthermore, I will delve deeper into the strategies being implemented to pharmacologically target MNK1/2, and the impact of targeting MNK1/2 in combination with other small-molecule inhibitors currently being used to clinically manage melanoma and breast cancer. I will briefly elaborate on the mTOR-LARP1 axis that has recently been discovered to play an integral role in mRNA translation.

This chapter contains material published in a review article:

> **Prabhu SA***, Moussa O*, Miller Jr. WH, Del Rincón SV. The MNK1/2-eIF4E axis as a potential therapeutic target in melanoma. Int J Mol Sci. 2020;21(11):4055. (* equal contribution)

1.2 Biology of the MNK1 and MNK2 Kinases

1.2.1 Isoforms and regulation of MNK1 and MNK2

The MAP Kinase-interacting serine/threonine-protein kinase 1 and 2 (MNK1/2) are two proteins, transcribed from two distinct genes, *MKNK1* and *MKNK2* (1, 2). In humans, *MKNK1* and *MKNK2* may be alternatively spliced into “a” and “b” isoforms (Figure 1.1) (3, 4). Although, there is significant protein sequence homology between

the human and murine MNK1 and MNK2, it has been demonstrated that murine cells only possess the “a” isoforms of both kinases (Figure 1.1) (3-5). The splicing of *MKNK2* has been reported to be modulated by Serine/arginine-rich splicing factor 1 (SRSF1) (6-8). This results in reduced expression of the MNK2a isoform and an increase in expression of the MNK2b isoform (8). This study further demonstrates that, this increase in splicing, promotes resistance to gemcitabine in pancreatic ductal adenocarcinoma (PDAC), which can be overcome by silencing SRSF1, MNK2, and small-molecule inhibition of MNK1/2 (8). Furthermore, it has been demonstrated that MNK2a possesses tumor suppressive roles, while MNK2b bears oncogenic functions (7). Conversely, both isoforms of MNK1 have been demonstrated to be pro-tumorigenic (9-11).

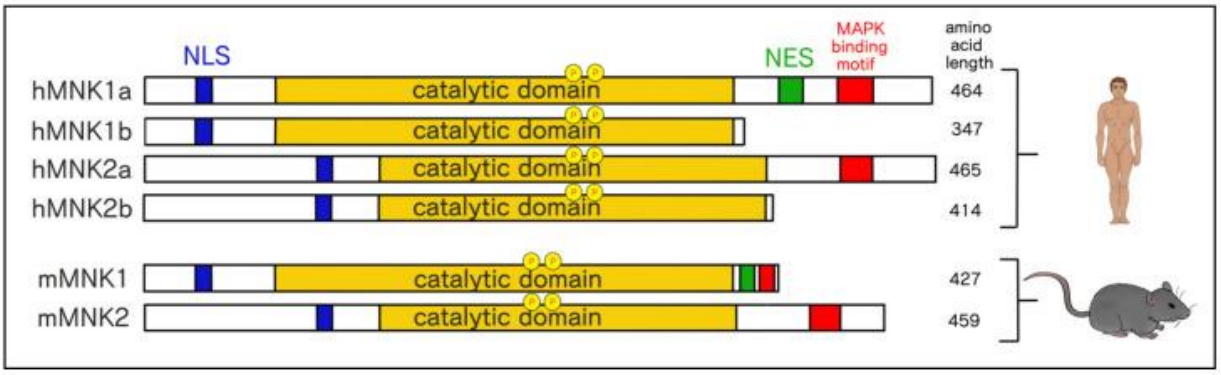

Figure 1.1: Schematic depicting the various isoforms and domains of human and murine MNK1 and MNK2: MNK1 and MNK2 mRNA are spliced into the "a" and "b" isoforms in humans. In murine cells, only the “a” isoform of both proteins are expressed. Nuclear export signal is NES; nuclear localization signal is NLS. (figure from Prabhu and Moussa et al., 2020)

1.2.2 Functional domains on MNK1 and MNK2

All isoforms of MNK1 and MNK2 possess an N-terminal poly basic sequence that allows their interaction with α-importin, and acts as a nuclear localization signal (NLS)

(Figure 1.1) (4, 12, 13). Furthermore, this region on MNK1 and MNK2 also permits their interaction with eukaryotic translation Initiation Factor 4G (eIF4G), the scaffold protein of the eukaryotic Initiation Factor 4F (eIF4F) complex (13-15). While MNK1 and MNK2 both possess a nuclear localization signal, only MNK1 possesses a nuclear export signal (NES), ensuring its cytoplasmic localization via CRM1-mediated nuclear export (Figure 1.1) (2, 4, 13). The activation of MNK1/2 occurs through phosphorylation on two threonine residues within the activation loop (209 and 214 in MNK1, and 244 and 249 in MNK2) by extracellular signal-regulated kinase (ERK1/2) and p38 Mitogen-activated protein kinase (MAPK's) (Figure 1.2) (16). Importantly, only the "a" isoforms contain a MAPK binding domain allowing for activation and regulation by ERK1/2 and p38 while the "b" isoforms possess a truncation at the C-terminus and hence lack the MAPK-binding domain (Figure 1.1) (14, 17).

The activation loop of kinases is typically conserved and may contain a DFG (Asp-Phe-Gly) motif (18). This motif on kinases permits its regulation and is frequently a target of inhibitors (18). MNK1 and MNK2 differ from other kinases in the same superfamily (Calcium-Calmodulin-Dependent Protein Kinases), in that they uniquely possess a DFD (Asp-Phe-Asp) motif in the magnesium-binding loop, instead of the DFG motif (19). As a result, the phenylalanine residue flips inwards into the ATP binding pocket, producing a unique DFD-out, auto-inhibited conformation, making the pocket less accessible to ATP (19). The exclusivity of the domain to MNK1 and MNK2 make it a desirable and highly specific target for the synthesis of small-molecule inhibitors that

could possibly maintain MNK1/2 in their auto-inhibited state and suppress their kinase activities (20).

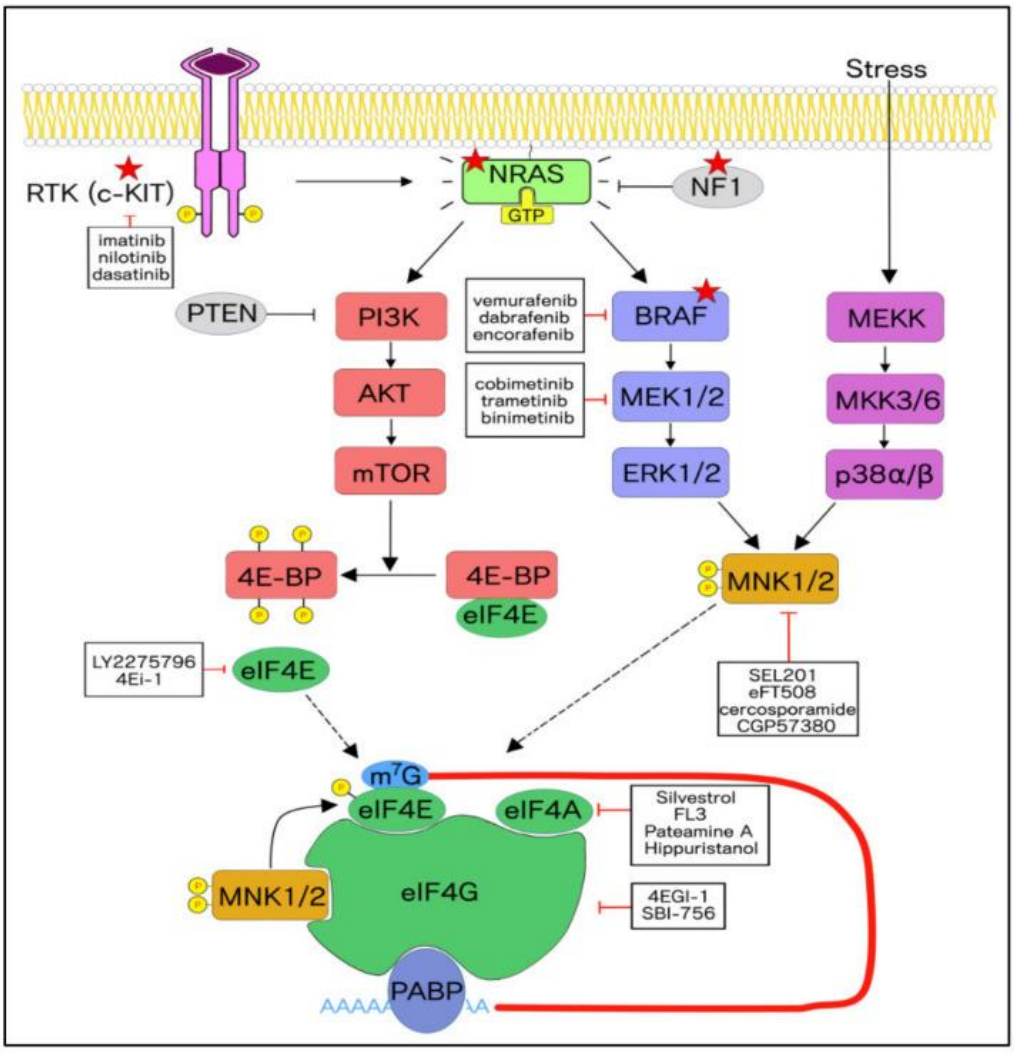

Figure 1.2: The MNK1/2-eIF4E axis is the convergence point for the two main deregulated pathways in melanoma and other malignancies. The three genetic subtypes of cutaneous melanoma are identified by the red stars on the NRAS, BRAF, and NF1. Mutations in NRAS or NF1 result in the hyperactivation of both the MAPK and PI3K pathways, whereas mutation in BRAF results in the hyperactivation of the MAPK pathway. Ras and its downstream effector pathways can be hyperactivated as a result of activating mutations in c-KIT. MNK1 and MNK2 are activated by signaling through the MAPK pathway. Signaling through the PI3K/AKT pathway results in 4E-BP hyperphosphorylation by mTOR 4E-BP releases eIF4E and allows its association with the 5'cap of mRNA and the eIF4F complex. MNK1/2 binds eIF4G and phosphorylates eIF4E at Ser209. This augments the translation of several mRNAs. Furthermore, p38 may phosphorylate MNK1 and MNK2 in response stress stimuli. (figure from Prabhu and Moussa et al., 2020)

1.2.3 Substrates of MNK1 and MNK2

The most well characterized substrate of the MNK1/2 kinases is the eukaryotic translation initiation factor 4E (eIF4E) (13, 21). MNK1 and MNK2 uniquely catalyze the phosphorylation of eIF4E on serine 209 (13, 14, 21). The exclusivity of eIF4E as a substrate of MNK1 and MNK2 has been verified in transgenic MNK1/2 double knockout mice in which eIF4E remains phospho-deficient across multiple stimuli (21). The MNK1/2-dependent regulation of eIF4E will be discussed in detail in the next section

MNK1 and MNK2 have been demonstrated to phosphorylate many downstream targets and thereby regulate numerous cellular processes. Sprouty 2 is a protein that functions as an antagonist of receptor-tyrosine kinases (RTK) and has been implicated in negatively regulating MAPK signaling (22, 23). Furthermore, *SPRY2* has been shown to be epigenetically silenced in many cancers (22, 24). The phosphorylation of SPRY2 on serines 112 and 121 by MNK1/2 stabilizes the protein and prevents its degradation (25). One of the earliest discovered substrates of the MNK1/2 kinases is the Heterogeneous nuclear ribonucleoprotein A1 (hnRNPA1) (5). This protein plays a role in promoting metastasis, cancer progression and cytokine production (5, 26, 27). MNK1 and MNK2 are able to phosphorylate hnRNPA1 on serines 192 and 310 in response to T-cell activation, resulting in increased expression of TNFα by regulating the binding of hnRNPA1 to the TNFα AU rich elements (ARE) (5). Along these lines, MNK1/2 have also been shown to phosphorylate and regulate the binding of $p54^{nrb}$ and polypyrimidine tract-binding protein (PTB)-associated splicing factor PSF to the ARE-binding domain on TNFα (28). PSF has been shown to play key roles in tumor development,

progression, and is associated with poor prognosis in estrogen receptor-positive (ER+) breast cancer (29-31). MNK1 and MNK2 have also been shown to and regulate the arachidonic acid release by Cytosolic phospholipase A2 (cPLA2) through phosphorylation at serine 727 (32). Importantly, cPLA2 has been implicated in therapy resistance and angiogenesis (33, 34). More recently, a role for MNK1 in platelet production, activation and thrombosis has been demonstrated by its ability to regulate the translation of the mRNA encoding for cPLA2 in megakaryocytes (35).

1.2.4 Role of MNK1/2-eIF4E and mTOR-4EBP1/2 axis in mRNA translation

1.2.4.1 Eukaryotic mRNA translation initiation

The process of mRNA translation into proteins can be divided into multiple critical steps. First, pools of free 40S and 60S ribosomal subunits are prepared from their previous 80S configuration primarily through competitive binding of eIF3 and eIF1A to 40S subunit, thus precluding the 60S subunit from binding the 40S subunit (36). Subsequently, the 40S binds multiple factors including eIF1, eIF3, eIF1A, eIF5, and the initiation tRNA as a ternary complex (eIF2·GTP·Met-tRNA$_i$) to form the 43S pre-initiation complex (PIC) (36-38). Next, the eIF4F complex (composed of eIF4E, eIF4G, and eIF4A) associates with the target mRNA. eIF4E binds the 5′ m^{7}G-cap of the target mRNA with high affinity (K_d of 10^{-8} to 10^{-9} M) (36). This binding, allows the helicase, eIF4A to interact with the mRNA molecule and subsequently unwinds the secondary structures of the mRNA in an ATP-dependent manner (37, 38). The formation of the eIF4F:mRNA complex results in the recruitment of the 43S PIC which binds eIF4G, the scaffold protein in the eIF4F complex (37, 38). The unwound mRNA is now able to

channel into the 40S subunit and initiate start codon scanning. Upon matching the first AUG on the mRNA molecule, the translation factors associated with the 43S PIC subunit are removed from the 40S subunit by GTP-dependent hydrolysis (36). This allows the 60S subunit to bind to the 40S subunit, thus forming the 80S ribosome to begin the elongation process of protein synthesis (36-38).

1.2.4.2 Regulation of translation by modulating eIF4E expression and availability

The translation initiation step, in which eIF4E and the eukaryotic initiation factor 4F (eIF4F) complex mediate the recruitment of ribosomes to mRNA, is the rate-limiting step in mRNA translation in eukaryotic cells (37, 38). The expression and activity of eIF4E is tightly regulated and largely dependent on multiple cellular factors such as nutrient availability, hypoxia, DNA damage, and oncogenic signals (39-41). The transcription of eIF4E has been shown to be regulated by the oncogenic protein c-MYC (42). Post-translationally, eIF4E availability is primarily regulated by the kinase mTOR (mammalian target of rapamycin) via the phosphorylation of the eukaryotic translation initiation factor 4E-binding proteins 1 and 2 (4E-BP1/2) (43, 44). In their hypophosphorylated state, 4E-BP1/2 bind and preclude eIF4E from associating with eIF4G as both eIF4G and 4E-BP1/2 interact with eIF4E on the same region (44). However, signaling downstream of the PI3K/AKT/mTOR pathway results in hyperphosphorylation of the 4E-BP1/2 thus releasing eIF4E that is now free to associate with eIF4G (43, 44).

1.2.4.3 MNK1/2-dependent regulation of cap-dependent translation

As mentioned above, MNK1 and MNK2 are the exclusive kinases for eIF4E on serine 209. While biophysical studies have demonstrated that phosphorylated eIF4E has a lower affinity for the 5′ m^7G-cap due to increased rate of dissociation (45-48), numerous other studies have shown that phosphorylation of eIF4E positively regulates the translation of oncogenic mRNAs (49-56). Although there remains some controversy around the functional consequence of phosphorylated eIF4E, studies have highlighted the pro-oncogenic potential of tumor cells with augmented levels of phosphorylated eIF4E (49-56). Specifically, studies in human and murine melanomas have shown that the increased phosphorylation of eIF4E supports tumor progression and decreases overall survival (51, 54).

1.2.4.4 Rationale for targeting the MNK1/2-eIF4E axis in cancer

Augmented levels of phosphorylated eIF4E have been detected in prostate cancer, breast cancer, colorectal adenocarcinoma, hepatocellular carcinoma, gall bladder cancer, melanoma, squamous cell carcinoma, and esophageal cancer and is frequently associated with poorer prognosis (51-63). Importantly, increased levels of active MNK1 and phosphorylated eIF4E has been demonstrated to be a predictor of poor clinical outcome in ovarian cancer (63), and associated with *KIT*-mutant acral melanoma (53), and high-grade ductal carcinoma in situ (64). Mechanistically, it has been shown that the phosphorylation of eIF4E at serine 209 engenders the increased translation of a subset of mRNAs which encode proteins responsible for cell survival, drug resistance, immune cell evasion, inflammation, invasion, and metastasis (53, 65-

69). Notably, despite eIF4E being a requisite for cap-dependent translation, haploinsufficient mice, expressing only 50% of eIF4E developed normally and, furthermore, mouse embryonic fibroblasts (MEF) cells derived from these mice were more resistant to cellular transformation by Ras and c-Myc (70). To this effect, mice expressing phospho-deficient eIF4E (S209A) or MNK1/2 double-knockout (MNK1/2-DKO) mice developed normally (21, 55). Additionally, these MNK1/2-DKO and eIF4E phospho-deficient mice were more protected from lymphoma and prostate cancer compared with their wild-type counterparts respectively (21, 55). These studies highlight the requirements of increased phosphorylated-eIF4E in cancer cells and, with the potential of limited toxicity, MNK1/2 inhibitors are a promising approach to managing malignancies. This of particular importance as the efficacy of targeted therapies is frequently marred by the undesired side effects of the inhibitor on normal cells.

1.2.5 MNK1/2 Inhibitors as a new class of therapeutic agent

Targeting mRNA translation has garnered considerable interest over the years and numerous inhibitors are being designed and implemented to either directly inhibit the function of the eIF4F complex or prevent its formation altogether (71). The major challenge in targeting the activity of the eIF4F complex itself is that non-cancerous cells require a functional eIF4F complex to effectively translate mRNA. While targeting mTOR has been shown to be promising, its long-term efficacy is limited due to multiple factors such as incomplete inhibition of 4E-BP1/2 or through activation of compensatory PI3K/AKT signaling (44, 72-75). Furthermore, the while mTOR inhibitors are able to

improve progression-free survival and overall survival in some cancer subtypes, the toxicity profile of these inhibitors have limited their clinical benefit (76, 77).

As previously mentioned, MNK1/2 and phosphorylation of eIF4E is dispensable for normal cell development (21, 55). Moreover, the reliance of cancer cells on MNK1/2 or phosphorylated eIF4E expression has prompted the rapid development and testing of selective MNK1/2 inhibitors as anti-neoplastic agents. Initial efforts to target the MNK1/2 kinases using CGP57380 and cercosporamide were effective but are insufficiently specific and thus have significant off-target effects, including potent inhibition of JAK3. More recently, highly specific inhibitors of MNK1/2 have been developed and are being tested for efficacy as single agents or in combination with other small-molecule inhibitors. Our group has demonstrated that as a single agent, the MNK1/2 inhibitors SEL201 and eFT508 can suppress *in vivo* tumor outgrowth and metastasis in human and murine models of melanoma and breast cancer (53, 54, 64, 78). *In vitro*, other research groups and our own have shown that single agent MNK1/2 inhibitors effectively inhibit oncogenic cell proliferation across solid and hematological malignancies (53, 79-81).

Importantly, the efficacy of MNK1/2 inhibitors is not limited to their anti-neoplastic activity as a single agent alone, as it synergizes well with other inhibitors. Specifically, inhibitors of MNK1/2 and mTOR effectively combine to further inhibit the proliferation of acute myeloid leukemia (AML), non-small lung cancer, and glioma, breast cancer, medulloblastoma, and T-cell lymphoma (79-85). The combination of MNK1/2 and MEK inhibitors has also demonstrated to be an effective way to promote cell death in *NF1*-

mutant malignant peripheral nerve sheath tumor (MPNST) (86). In medulloblastoma mouse xenograft models, the combined inhibition of MNK1/2 and PI3Ka was more effective in suppressing tumor outgrowth and increasing overall survival of mice (87). In chronic myelogenous leukemia (CML), MNK1/2 inhibitors have been shown to enhance the efficacy of BCR-ABL1 inhibitors (87). Additionally, in combination with paclitaxel, MNK1/2 inhibition further suppressed proliferation and migration of cervical cancer cells (88). In triple-negative breast cancer (TNBC), the combination of MNK1/2 inhibitors and adriamycin were more effective in suppressing tumor outgrowth than either single agent alone (89).

Increased expression of phosphorylated eIF4E is a well characterized resistance mechanism to many therapies (8, 65, 90). Studies have demonstrated that targeted and chemotherapeutic agents can trigger an increase in eIF4E phosphorylation (8, 90). In pancreatic ductal adenocarcinoma, cellular exposure to gemcitabine increases phosphorylation of eIF4E by promoting the splicing of *MKNK2*, thereby increasing the expression of the MNK2b isoform (8). The addition of a MNK1/2 inhibitor to the regimen effectively increased the cellular response to gemcitabine (8). Similarly, exposure of pancreatic and thyroid cancer cells to bromodomain and extra-terminal motif (BET) inhibitors have been shown to increase the expression of phosphorylated eIF4E (90). The addition of a MNK1/2 inhibitor further suppressed the proliferation of these cancer cells (90). As will be seen in chapter 3, we demonstrate that the exposure of melanoma and breast cancer cells to the CDK4/6 inhibitor, palbociclib increased the expression of phosphorylated eIF4E (91). Blocking this increase using MNK1/2 inhibitors further

suppressed *in vitro* cell proliferation and the combination of palbociclib and eFT508 significantly decreased tumor outgrowth and prolonged survival in murine models of melanoma compared to either single agent alone (91).

The efficacy of MNK1/2 inhibitors isn't restricted to their impact on tumor cells and numerous studies have demonstrated the role that MNK1/2 and phosphorylated eIF4E in generating a pro-tumor microenvironment as it has been shown that MNK1/2 activity can regulate mRNA translation in immune cells to favor an immune-suppressive microenvironment (92). Furthermore, recent work has revealed that inhibition of MNK1/2 can modulate the immune system and thereby promote anti-tumor activity. For example, in macrophages, inhibition of MNK1/2 resulted in increased production of the anti-inflammatory cytokine IL-10 (93). In another study, it was shown that MNK2 inhibition directed macrophages towards a proinflammatory phenotype and thus enhanced the activity of $CD8^+$ T cells (94). In neutrophils, MNK1/2 inhibition repressed the production of CCL-3, CCL-4, and CXCL8 with known roles in generating a pro-tumorigenic microenvironment (95). It has also been demonstrated that MNK1/2 inhibition can promote the depletion of pro-metastatic neutrophils by decreasing their expression of the anti-apoptotic proteins BCL2 and MCL1 (96).

Modulating the expression of immune suppressive markers is a method used by cancer cells to evade immune surveillance. Since cells frequently use the PD-1/PD-L1 (Programmed cell death 1 receptor/ Programmed death ligand 1) axis to evade the immune system, monoclonal antibodies to inhibit PD-1 or PD-L1 have been produced to treat a number of cancers. Importantly, inhibitors of translation have been demonstrated

to enhance the effectiveness of immunotherapy. In melanoma, it has been shown that the eIF4A inhibitor, silvestrol, represses the expression of PD-L1 on tumor cells and increases tumor infiltration in syngeneic *in vivo* models (97). This resulted in a significant delay in tumor growth, an effect that was diminished in immunocompromised mouse models (97). In MYC^{Tg};$KRAS^{G12D}$ liver cancer, it has been demonstrated that in phosphodeficient eIF4E ($eIF4E^{S209A/S209A}$) tumor cells, the expression of PD-L1 was repressed (98). This impact on PD-L1 expression was recapitulated when eIF4E-WT liver tumor cells were treated with the MNK1/2 inhibitor eFT508 (98). Our own work, has demonstrated that genetic or pharmacologic eIF4E phospho-deficiency resulted in repressed expression of PD-L1 in dendritic cells and myeloid-derived suppressor cells, thereby promoting an anti-tumor immune microenvironment (54). Furthermore, we have demonstrated that MNK1/2 inhibition can augment the efficacy of PD-1 inhibitors in murine models of melanoma (54).

Overall, these data support the development of MNK1/2 inhibitors as therapies that can inhibit the tumor cells, but also create an anti-tumor microenvironment by their direct effects on tumor supportive cells, such as fibroblasts and immune cells. (99, 100) As such, MNK1/2 inhibitors are actively being tested in clinical trials in combination with other small-molecule inhibitors or immune modulators.

1.3 Role of LARP1 axis on mRNA translation and cancer development

Recent advances have transformed our understanding of mRNA translation and have implicated a new key player in the regulation of translation of mRNAs. LARP1 belongs to a family of La-related proteins with homology in a 90 amino acid RNA-

binding region called the La-Module (101). LARP1 has been identified to bind and repress the translation of mRNA that contain a 5' TOP (Terminal Oligo Pyrimidine) motif (102-106). The TOP motif on mRNA is characterized by a cytosine followed by a 4-15 stretch of poly-pyrimidines and a subsequent GC-rich region located directly downstream (101, 103, 105, 107). These TOP mRNAs typically encode for ribosomal proteins or proteins involved in the translation machinery (101, 103, 105, 107). Similar to eIF4E, LARP1 binds to mRNA at the 5′ m^7G-cap through a domain within its C-terminal called the DM15 (103, 107). Furthermore, studies have uncovered that LARP1 also interacts with the poly (A) and the 3'end of mRNAs (107).

The activity of LARP1 has been shown to be regulated by kinases such as AKT, CDK1, CDK2, and mTOR (108-111). The most widely studied kinase of LARP1 is mTOR. It has been identified that LARP1 interacts with mTOR indirectly through RAPTOR (Regulatory-associated protein of mTOR) (111). In nutrient deficient conditions where mTOR remains inactive, 4E-BP1/2 remains hypophosphorylated, thus precluding eIF4E from associating with the eIF4G (Figure 1.2 and Figure 1.3) (101, 106, 111). Simultaneously, LARP1 tightly binds TOP mRNA and acts as a translation repressor (Figure 1.3) (101, 106, 111). When nutrients are readily available, mTOR phosphorylates LARP1 to promote the release of TOP mRNA and concurrently 4E-BP1/2 to promote the release of eIF4E, which is now free to bind the TOP mRNA and initiate protein synthesis (Figure 1.3). Recently, it has also been demonstrated that LARP1 may interact with non-canonical polyadenylases to further regulate the translation of TOP mRNA (112).

Importantly, LARP1 also functions to positively regulate the translation of oncogenic mRNA's such as *MTOR and BCL2* and its role in cancer development is gradually being revealed (113, 114). Increased expression of LARP1 has been observed in cervical cancer, hepatocellular carcinoma, non-small cell lung cancer, and colorectal cancer and is associated with disease progression and poor prognosis (113, 115-117). Studies conducted in ovarian cancer demonstrated that LARP1 binds and differentially regulates the transcripts of apoptotic regulators such as BCL-2 and BIK through binding their 3'UTR (untranslated region) (114). While LARP1 negatively regulated the expression of the pro-apoptotic *BIK* transcript, it stabilized the anti-apoptotic *BCL-2* transcript, effectively promoting cell survival (114). Another recent study has demonstrated that LARP1 may be able to sustain mRNA translation, metabolism and cell proliferation even in nutrient deficient conditions (118). While LARP1's cellular function remains elusive, overall these data indicate that the role of LARP1 requires further interrogation as a biomarker of oncogenesis and as a potential therapeutic target. In chapter 3 of this body of work, we will discuss a novel interaction between the MNK1 kinase and LARP1. We have identified that LARP1 can be phosphorylated by MNK1 at threonine 449 and using a phosphodeficient T449A mutant, we demonstrate that this mutant has a higher affinity for RNA compared with its WT counterpart. These data combined with our current knowledge of LARP1 and the MNK1/2 kinases may help us better understand the role LARP1 plays in mRNA translation, cancer development and disease progression.

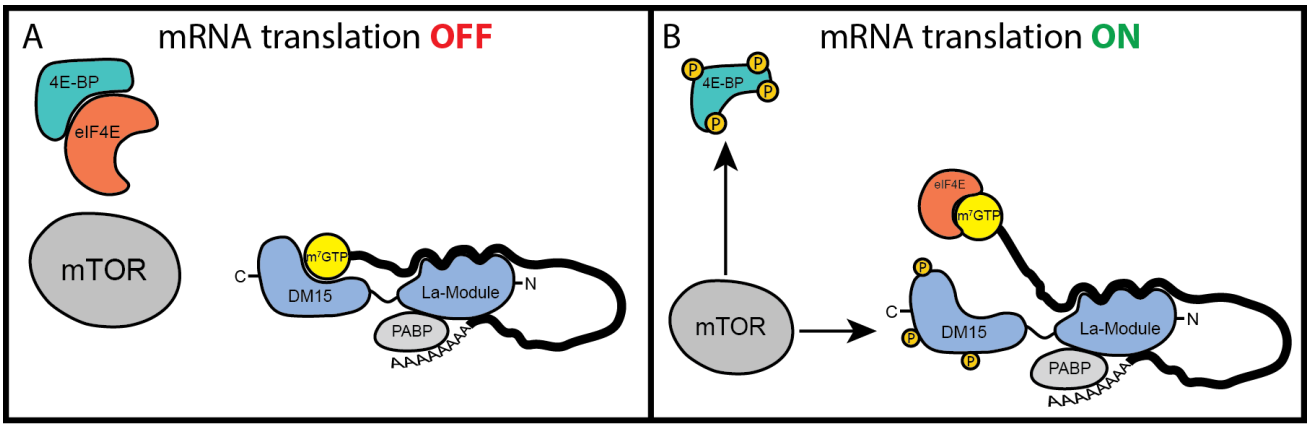

Figure 1.3: Schematic depicting the role of mTOR kinase activity on TOP mRNA translation. On the left panel (A), in translation repressive conditions, mTOR is inactive and as a result, LARP1 binds TOP mRNA and 4E-BP sequesters and inhibits eIF4E. On the right panel (B), activated mTOR, phosphorylates 4E-BP to release eIF4E. Simultaneously, mTOR phosphorylates LARP1 on the DM15 resulting in the release of 5'cap. This allows eIF4E to associate with the 5'cap of TOP mRNA and thereby initiate mRNA translation

1.4 mRNA translation and the cell cycle

Cell growth and cell cycle progression are processes highly dependent on mRNA translation (119). As cells grow, they accumulate mass in the form of proteins and additionally, as cells progress through the cell cycle, their protein requirements dynamically shift, necessitating precise regulation of mRNA translation (119). One of the key proteins involved in this process is the kinase mTOR (120, 121). As the nutrient sensing protein in the cell, mTOR regulates multiple processes that result in increased protein synthesis. As mentioned previously, mTOR phosphorylates 4E-BP1/2 promoting its dissociation from eIF4E, the 5' cap binding protein and rate limiting factor for cap-dependent mRNA translation (44). Furthermore, by phosphorylating $p70^{S6K1}$ and LARP1 in nutrient permissive conditions, mTOR is also a key regulator of ribosome biogenesis (103, 105, 106, 111, 120, 121). However, the relationship between protein synthesis and the cell cycle is still poorly understood, but recent research demonstrating a more

direct role of cell cycle dependent kinases has sparked interest in the field. It has recently been demonstrated that cyclin dependent kinases can phosphorylate the translation machinery and thereby regulate protein synthesis (109, 122, 123). The next section of my thesis will discuss the cell cycle with an emphasis on G1 to S phase transition, aberrations in this transition in cancer, and recent advances in targeting the pathway in combination with inhibitors of mRNA translation.

1.5 Phases of the cell cycle

Progression through the cell cycle in normal cells requires a well-orchestrated process composed of proliferative and anti-proliferative signals, resulting in genomic replication and the production of two identical daughter cells. Dysregulation of this process is a hallmark of malignancies. Cancer cells may hijack the cell cycle by promoting proliferative signaling cascades, blocking cellular inhibitors of the cell cycle, or by expressing a mitotic program that combines the two (124, 125). The cell cycle can be divided into two parts with four distinct phases: the interphase composed of the phases G1 (Gap 1), S (Synthesis), and G2 (Gap 2), and cell division composed of the M (Mitosis) phase. During Interphase, the cell grows (G1), replicates its genomic material (S), and continues to grow and prepare itself for mitosis (G2) (124, 125). Finally, during cell division, the duplicated genetic material and cytoplasm are divided into two new daughter cells (124, 125).

1.6 Cyclin-Dependent Kinases 4/6 and regulation of S phase entry

The progression from the G1 to the S phase of the cell cycle is regulated by the activity of the two Cyclin-Dependent Kinases 4/6 (CDK4/6) (Figure 1.4) (125, 126). CDK4 and CDK6 are serine/threonine kinases whose activity is regulated by binding to D-type cyclins (cyclin D1, cyclin D2 and cyclin D3) (125, 126). CDK4/6 bound to cyclin D, results in kinase activation and the subsequent phosphorylation of the tumor suppressor protein retinoblastoma protein 1 (RB) (Figure 1.4) (125, 126). In its unphosphorylated state, RB binds to and suppresses the transcription factor E2F, thereby preventing the expression of genes responsible for the progression of cells to the S phase (Figure 1.4) (125, 126). Intuitively, phosphorylation of RB by CDK4/6 results in the release of E2F and the transcription of genes involved in the S phase transition (Figure 1.4) (126). The expression of D-type cyclins is regulated by the MAPK and PI3K pathways (127-130). Mitogenic signals result in increased MAPK signaling and the transcription of *CCND1* (127). Additionally, PI3K/AKT/mTOR signaling promotes the expression of cyclin D through various mechanisms including increased mRNA translation, and reduced protein degradation and nuclear export (56, 129, 130). Furthermore, activation of mTOR or the MNK1/2-eIF4E axis also results in increased translation and nuclear export of *CCND1* (55, 56, 131, 132). CDK4/6 activity is also regulated by the CIP/KIP and INK4 families of cell cycle inhibitors. The INK4 family, which includes p15, p16, p18, p19, disrupts the folding and assembly of CDK4/6 and, furthermore, can induce conformational changes to weaken their association with cyclin D (133-136). While the CIP/KIP family members were previously thought to be tumor

suppressive, new research has demonstrated that their roles are more nuanced. Paradoxically, cells lacking p21 or p27 are unable to produce cyclin D1-CDK4 complexes (137). In addition to facilitating the interaction between cyclin D1 and CDK4, p21 or p27 also increase CDK4 activity by permitting the phosphorylation of CDK4's T-loop by CDK-activating kinase (CAK) (138, 139). Nevertheless, cyclin D1-CDK4 complex formation is severely inhibited by elevated levels of p21 and p27 despite these unique activation pathways (138, 140).

1.6.1 Role of the CDK4/6-CyclinD pathway in cancer

Genomic alterations in the CDK4/6 pathway have been reported in a variety of solid and hematological malignancies (141). This results in hyperactivation of the pathway and rapid progression of cells through the cell cycle. Increased expression and copy number variation (CNV) of cyclin D1 have been reported in breast cancer, pancreatic cancer, head and neck cancer, melanoma, colorectal carcinoma, mantle cell lymphoma, and multiple myeloma (142-151). Similarly, amplifications in CDK4 and CDK6 have also been described in breast cancer, melanoma, sarcomas, gliomas, and lymphomas (152-155). Mutations or loss of expression of *CDKN2A* can also result in aberrant CDK4/6 activity, contributing to the development and progression of neoplasms (156, 157). In numerous malignancies, the promoter of *CDKN2A* is hypermethylated and results in repressed expression of the gene (156-163). In up to 40% of families with a history of melanoma, germline mutations in *CDKN2A* have been reported (164). Additionally, it has been demonstrated that up to 92% of melanoma cell lines possess aberrations in *CDKN2A* or *CDK4* (165). These data are not surprising, as

the *CDKN2A* encoded protein p16 protects cells from unregulated CDK4/6 activity by binding and inhibiting the formation of CDK4/6-cyclin D complexes (157, 166, 167). As a result, RB remains hypophosphorylated and bound to E2F, thereby hindering the G1 to S cell cycle transition (157). Overall, these data strongly implicate unregulated CDK4/6 activity in development of cancer and, moreover, targeting this pathway has become a potential vulnerability of neoplasms.

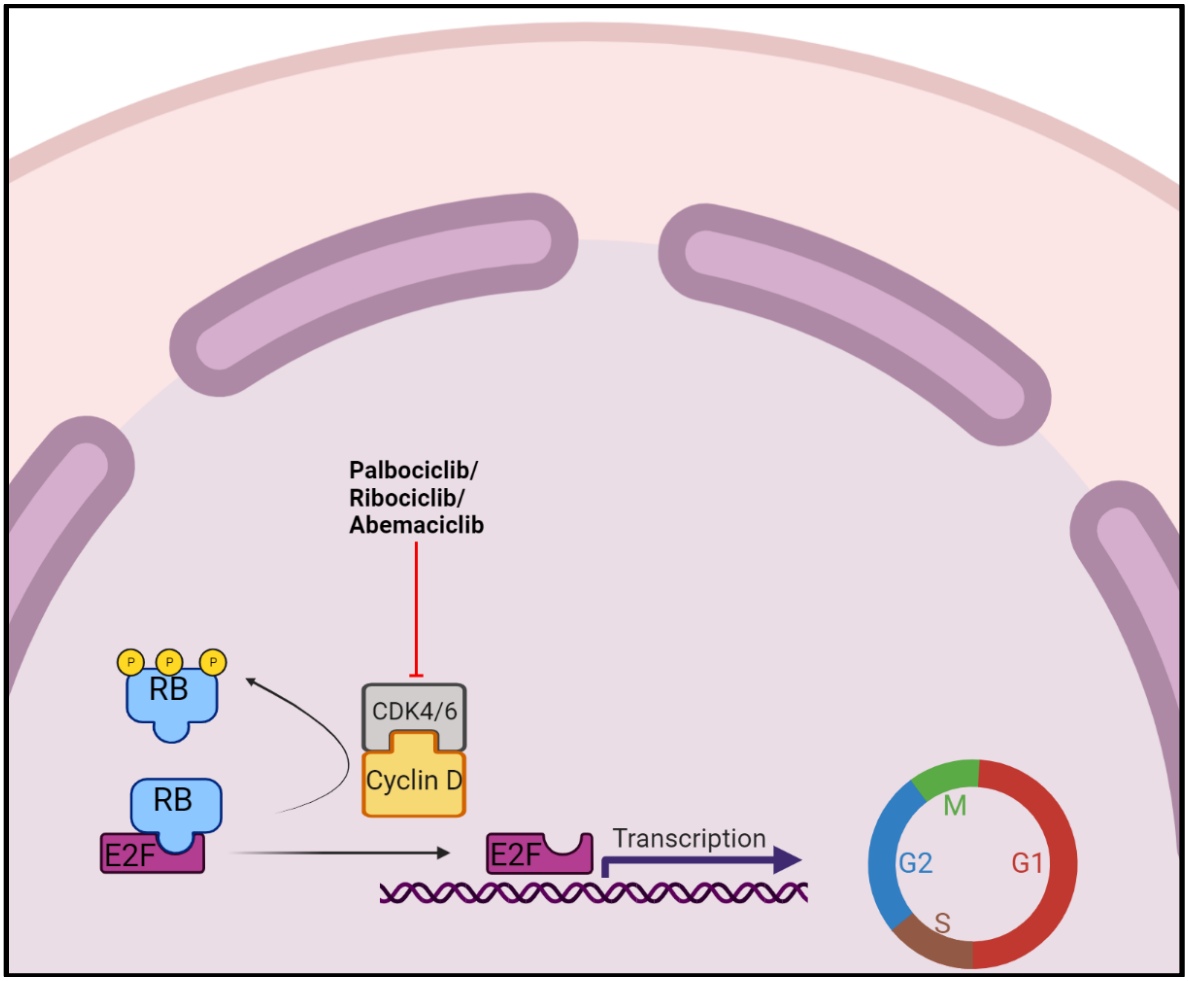

Figure 1.4: Schematic depicting the CDK4/6 pathway. CDK4/6 bound to cyclin D, phosphorylates retinoblastoma protein 1 (RB). In its unphosphorylated state, RB binds and suppresses E2F activity. Phosphorylation of RB by CDK4/6 results in the release of E2F, allowing the transcription of genes involved in the S phase transition. This process this potently inhibited by CDK4/6 inhibitors like palbociclib, ribociclib, and abemaciclib.

1.6.2 Targeting CDK4/6 in cancer

The CDK4/6 pathway has become an attractive pharmacological target, with numerous inhibitors being approved to directly target the kinases CDK4 and CDK6. The first and second generation of inhibitors targeted pan-CDK's throughout the cell cycle and hence failed clinical development due to severe toxicity (168). However, improvements in drug design with respect to target specificity resulted in the development of numerous highly selective CDK4/6 inhibitors that have recently received approval for the treatment of hormone receptor-positive (HR+) breast cancer (125). Hormone-receptor positive breast cancer makes up about 65% of all diagnosed breast cancers and is typically categorized by expressing estrogen receptor (ER+), progesterone receptor (PR+), or both (169-171). While the endocrine therapies (estrogen receptor agonists/antagonists or aromatase inhibitors) that target and inhibit the estrogen signaling pathway have proved to be effective, up to 20% of patients diagnosed with ER+ tumors recur (170). These endocrine therapy-resistant tumors are driven by signaling cascades that activate the estrogen receptor in a ligand independent manner (170). This may involve the acquisition of mutations in the ligand binding domain of ER resulting in reduced sensitivity to the ER-targeted therapies tamoxifen and fulvestrant, and enhanced hormone-independent ER transcriptional activity (170, 171). Furthermore, overexpression of epidermal growth factor receptor (EGFR) or receptor tyrosine-protein kinase erbB-2 (HER2) has been demonstrated to promote resistance to tamoxifen in ER+ breast cancers (172-174). These adaptations result in increased ERK1/2 and PI3K/AKT/mTOR signaling. Increased ER signaling has been

shown to increase the transcription and translation of cyclin D and thus and cell cycle progression (175, 176). Hence, CDK4/6 inhibitors were investigated for efficacy in both therapy naïve and therapy resistant HR+ breast cancers. Palbociclib, ribociclib, and abemaciclib were the first three CDK4/6 inhibitors to be approved by the U.S. Food and Drug Administration (FDA) for the management of HR+ breast cancer with others currently in development (Figure 1.4) (125). Importantly, CDK4/6 inhibitors have been demonstrated to overcome endocrine therapy-resistance in breast cancer, and, additionally, the combination of CDK4/6 inhibitors with endocrine therapy resulted in improved progression-free and overall survival compared with endocrine therapy alone (177-182). Moreover, CDK4/6 inhibitors have also shown promising activity in a myriad of malignancies including melanoma, non-small cell lung cancer, esophageal adenocarcinoma, pancreatic ductal adenocarcinoma, colon cancer, sarcomas (183-187). These data have demonstrated the importance of targeting the CDK4/6 kinases and have paved the way for the development of new inhibitors.

1.6.3 Mechanisms of resistance to CDK4/6 inhibitors

While CDK4/6 inhibitors have revolutionized the treatment of breast cancer and have rapidly become standard of care in combination with endocrine therapy, resistance to these therapies invariably develops; with many mechanisms gradually being revealed. Resistance mechanisms to CDK4/6 inhibition include mutation or loss of RB, amplified expression of cyclins and cyclin-dependent kinases, mutations in PI3K pathway, and amplifications in compensatory signaling pathways. These aberrations serve the central goal of reactivating the cell cycle (188-196). As CDK4/6 functions to

promote the E2F-dependent G1 to S cell cycle transition, loss of RB has been frequently observed to act as a barrier to the cellular response to CDK4/6 inhibitors in cell lines (188, 189). In patient samples, it has been demonstrated that exposure to CDK4/6 inhibitors results in acquired mutations in RB circulating tumor DNA (ctDNA) (197). Along these lines, in patient samples, it has been shown that the combination of palbociclib and fulvestrant resulted in the clonal expansion of cells harboring mutations in *RB1 (198)*. Similarly, overexpression of cyclin E or CDK2 can also promote resistance to CDK4/6 inhibition as CDK2 can phosphorylate RB and prohibit the latter from repressing E2F activity, thereby promoting cell cycle progression (194-196). As cells become resistant to CDK4/6 inhibitors, they reprogram their signaling to promote mitogenic signaling. In breast cancer, non-small lung cancer and prostate cancer, increased Fibroblast growth factor receptor 1 (FGFR1) and MAPK signaling has been observed in response to acquired CDK4/6 inhibitor resistance (199-201). Mutations and amplifications in FGFR1 has been observed in breast cancer patient samples exposed to palbociclib (199). Additionally, patients harboring mutations in FGFR1 exhibited reduced progression-free survival compared with patients with WT FGFR1 (199). Mutations in PIK3CA or hyperactivation of the PI3K/AKT/mTOR have also been observed as a resistance mechanism to CDK4/6 (202-204). Activation of this signaling cascade resulted in increased S6K signaling or increased expression of compensatory cyclins such as cyclin D and cyclin E (202-206). Recent research has demonstrated that a combination of inhibitors of mRNA translation with CDK4/6 may prove to be an effective combination strategy in melanoma and breast cancer (207-212). Along these lines, we and others have observed increased activity of the MNK1/2–eIF4E axis as

cells acquire resistance to palbociclib in models of breast cancer (91, 213). In chapter 2 of this thesis we will further discuss how the MNK1/2-eIF4E axis impacts the *in vitro* and *in vivo* efficacy of the CDK4/6 inhibitor, palbociclib in melanoma and breast cancer.

Chapter 2: Inhibition of the MNK1/2-eIF4E axis augments palbociclib-mediated anti-tumor activity in melanoma and breast cancer.

2.1 Preface

In malignancies (e.g. melanoma), deregulated MAPK signaling results in uncontrolled cell growth. It is well characterized that oncogenic MAPK signaling results in increased cell cycle progression and mRNA translation. ERK activity is fundamental to the G1 to S cell cycle transition through regulation of cyclin D1 and CDK2. Additionally, downstream of ERK are the MAP Kinase-interacting serine/threonine-protein kinase 1 and 2 (MNK1 and MNK2). These proteins are the exclusive kinases of eukaryotic translation initiation factor 4E (eIF4E). The phosphorylation of eIF4E at serine 209 results in increased translation of a subset of mRNAs involved in invasion and metastasis, including *SNAI1* and *MMP3*. Moreover, studies in human and murine melanomas have shown that the phosphorylation of eIF4E on serine 209 supports tumor progression and decreases overall survival. Increased phosphorylation of eIF4E by MNK1/2 has been observed in response to chemotherapeutic and targeted inhibitors, indicating an increased translation of pro-survival proteins. Importantly, simultaneous inhibition of MNK1/2 has been shown to enhance the activity of the targeted inhibitors.

In this chapter we identified that the CDK4/6 inhibitor, palbociclib can trigger the increase in expression of phosphorylated eIF4E in models of melanoma and breast cancer. We thus hypothesized that blocking this increase in phosphorylated eIF4E

either pharmacologically or genetically would result in increased cellular sensitivity to palbociclib.

Chapter 2 was published as an original research article:

> **Prabhu SA,** Moussa O, Gonçalves C, LaPierre JH, Chou H, Huang F, Richard VR, Ferruzo PYM, Guettler EM, Soria-Bretones I, Kirby L, Gagnon N, Su J, Silvester J, Krisna SS, Rose AAN, Sheppard KE, Cescon DW, Mallette FA, Zahedi, RP, Borchers CH, Miller Jr. WH, Del Rincón SV et al. Inhibition of the MNK1/2-eIF4E axis augments palbociclib-mediated antitumor activity in melanoma and breast cancer. Mol Cancer Ther. 2023;22(2):192-204.

Note: Supplemental Table 2.5 of this chapter is available online in the manuscript above (PMID: 36722142) and is titled: **Supplemental Table 5**: List of differentially expressed proteins annotated by cluster with pathway analysis in BLM cells

2.2 Abstract

Aberrant cell cycle progression is characteristic of melanoma, and CDK4/6 inhibitors, such as palbociclib, are currently being tested for efficacy in this disease. Despite the promising nature of CDK4/6 inhibitors, their use as single agents in melanoma has shown limited clinical benefit. Herein, we discovered that treatment of tumor cells with palbociclib induces the phosphorylation of the mRNA translation initiation factor eIF4E. When phosphorylated, eIF4E specifically engenders the translation of mRNAs that code for proteins involved in cell survival. We hypothesized that cancer cells treated with palbociclib utilize up-regulated phospho-eIF4E to escape

the anti-tumor benefits of this drug. Indeed, we found that pharmacologic or genetic disruption of MNK1/2 activity, the only known kinases for eIF4E, enhanced the ability of palbociclib to decrease clonogenic outgrowth. Moreover, a quantitative proteomics analysis of melanoma cells treated with combined MNK1/2 and CDK4/6 inhibitors showed downregulation of proteins with critical roles in cell cycle progression and mitosis, including AURKB, TPX2, and survivin. We also observed that palbociclib resistant breast cancer cells have higher basal levels of phosphorylated eIF4E and that treatment with MNK1/2 inhibitors sensitized these palbociclib-resistant cells to CDK4/6 inhibition. *In vivo* we demonstrate that the combination of MNK1/2 and CDK4/6 inhibition significantly increases the overall survival of mice compared with either monotherapy. Overall, our data support MNK1/2 inhibitors as promising drugs to potentiate the anti-neoplastic effects of palbociclib and overcome therapy-resistant disease.

2.3 Introduction

Loss of cell cycle control is a hallmark of cancer. Cyclin-dependent kinases 4 and 6 (CDK4 and CDK6) are serine-threonine kinases important for the G_1 to S phase transition of the cell cycle (1). Activation of CDK4/6 by binding to cyclin D results in phosphorylation of the tumor suppressor protein, Rb. In its unphosphorylated state, Rb binds and inhibits the transcription factor E2F, thereby maintaining the cells in the G_1 phase of the cell cycle (1). However, upon phosphorylation by CDK4/6, Rb dissociates from E2F, allowing the latter to activate the transcription of genes responsible for S phase transition (1).

The CDK4/6 inhibitor, palbociclib, has revolutionized the treatment of estrogen receptor positive (ER+) breast cancer and is currently being tested for efficacy in a myriad of malignancies including colon cancer, glioblastoma, ovarian cancer, and pancreatic cancer (2). In melanoma, palbociclib has been combined with inhibitors of MAPK signaling in preclinical studies and, more recently in clinical trials (NCT04720768) (3,4). Importantly, palbociclib is being tested in melanoma subtypes that have few effective treatment options (5,6). Furthermore, early-phase clinical trials are also underway investigating the efficacy of palbociclib as a single agent in melanomas with copy number variations of CDK4 or cyclin D1 (7). There are no targeted therapies that improve survival for patients with NRAS mutant, NF1 mutant, or triple wild type metastatic melanoma (5,6,8). Hence, CDK4/6 inhibitors may represent a promising addition to the therapeutic armamentarium for the management of BRAF wild type melanomas.

Downstream of the MAPK pathway are the MAP Kinase-interacting serine/threonine-protein kinases 1 and 2 (MNK1 and MNK2) (8). These proteins are the exclusive kinases for eukaryotic translation initiation factor 4E (eIF4E) on serine 209, the 5'cap binding protein within the eIF4F complex, which regulates mRNA translation (8). Studies in human and murine melanomas have shown that the phosphorylation of eIF4E on serine 209 supports tumor progression and decreases overall survival (9,10). Of note, increased phosphorylation of eIF4E by MNK1/2 has been observed in response to chemotherapeutics and targeted inhibitors (11,12). The latter is perhaps not entirely surprising, as feedback loops, whereby the inhibition of one pathway is

compensated for by the upregulation of other signaling pathways, are a common mechanism of acquired therapy resistance (13). The activity of eIF4E is also regulated by the PI3K/AKT/mTOR pathway (8). Activation of the PI3K-AKT/mTOR pathway results in the phosphorylation of eIF4E-binding proteins, 4EBP1/2 (8). Phosphorylation of 4EBP1/2, by mTOR, releases eIF4E and results in activated translation (8). Studies have demonstrated that inhibition of the PI3K/AKT/mTOR pathway in conjunction with palbociclib results in substantially decreased tumor growth (14-17). Furthermore, new studies have also implicated a role for CDK4 in regulating the availability of eIF4E through its phosphorylation of 4EBP1/2 (18). Herein, we present data that eIF4E phosphorylation, which is induced downstream of activated MAPK-MNK1/2 signaling, is induced in melanoma and breast cancer cell lines in response to palbociclib treatment. We thus set forth to test the hypothesis that the anti-tumor effects of palbociclib are limited by its ability to promote the downstream compensatory phosphorylation of eIF4E. Indeed, our data support that the combination of MNK1/2 inhibitors and palbociclib cooperate as a potentially important new therapeutic approach to the management of melanoma and other therapy-resistant cancers.

2.4 Results

2.4.1 Combined inhibition of CDK4/6 and MNK1/2 decrease clonogenic outgrowth of melanoma and breast cancer cell lines

Several anti-cancer therapies have been shown to trigger the activation of the MNK1/2-eIF4E axis, a well-known pro-survival pathway (11,12). We found that the CDK4/6 inhibitor, palbociclib, induced an increase in the expression of phosphorylated

eIF4E (phospho-eIF4E), compared with vehicle-control treated cells in the NRAS- and NF1-mutated melanoma cell lines BLM and MEWO, respectively (Figures 2.1A, and 2.1B). The phosphorylation of eIF4E enhances the translation of mRNAs which encode pro-survival proteins (10,20,21). Thus, we hypothesized that the therapeutic efficacy of palbociclib is limited by its ability to promote the phosphorylation of eIF4E. To test this, we blocked the activity of MNK1/2, the only known kinases for serine 209 on eIF4E, predicting that this may sensitize cancer cells to the anti-tumor effects of palbociclib. We co-treated BLM cells with palbociclib and the MNK1/2 inhibitor SEL201 and showed significantly decreased colony formation versus either single agent (Figure 2.1C). This effect is recapitulated in BLM cells exposed to a combination of palbociclib and eFT508 (22), a MNK1/2 inhibitor currently in clinical testing (NCT03616834, NCT04261218, NCT04622007). Similarly, in NF1-mutant MEWO cells combined pharmacological inhibition of CDK4/6 and MNK1/2 resulted in significantly decreased clonogenic outgrowth (Figure 2.1D). We observed suppression of phospho-Rb and phospho-eIF4E attributed to palbociclib and MNK1/2 inhibitor treatment, respectively (Figures 2.1E, 2.1F). We next assessed whether MEWO cells in which we stably silenced MNK1 and MNK2 using shRNA (MEWO shMKNK1/2) were sensitized to palbociclib. We observed that MEWO cells with MNK1/2 knocked down have significantly impaired clonogenic outgrowth when treated with palbociclib compared with their scramble counterparts (Figure 2.1G). Similarly, we used the dCas9 Clustered Regularly Interspersed Short Palindromic Repeats interference (CRISPRi) system to genetically repress the transcription of MKNK1 and MKNK2, to best recapitulate the pharmacologic inhibition of MNK1/2 in BLM cells. BLM cells that are deficient in MNK1/2 are more sensitive to

palbociclib compared with their scramble counterparts (Figure S2.1A). Repression of MKNK1 expression was measured by immunoblotting, and expression of MKNK2 was measured only by quantitative PCR, as currently available MNK2 antibodies are not specific (Figures 2.1H, 2.1I, S2.1B, S2.1C).

CDK4/6 inhibitors are clinically indicated for the treatment of ER+ metastatic breast cancer, but the majority of patients will eventually develop resistance to CDK4/6i (23). Thus we wanted to determine whether our results extended to ER+ breast cancer. Consistent with our data in melanoma, palbociclib treatment of two ER+ breast cancer cell lines, MCF7 and T47D, resulted in increased phosphorylation of eIF4E (Figures 2.2A, and 2.2B). Moreover, the combination of palbociclib and SEL201 significantly decreased the clonogenic outgrowth of MCF7 cells compared with either single agent (Figure 2.2C). Similar results were obtained in T47D, wherein the combination significantly decreased clonogenicity compared with either of the single agents alone (Figures 2.2D). Through immunoblotting, we observed suppression of phospho-Rb and phospho-eIF4E attributed to palbociclib and MNK1/2 inhibitor treatment, respectively (Figures 2.2E, and 2.2F).

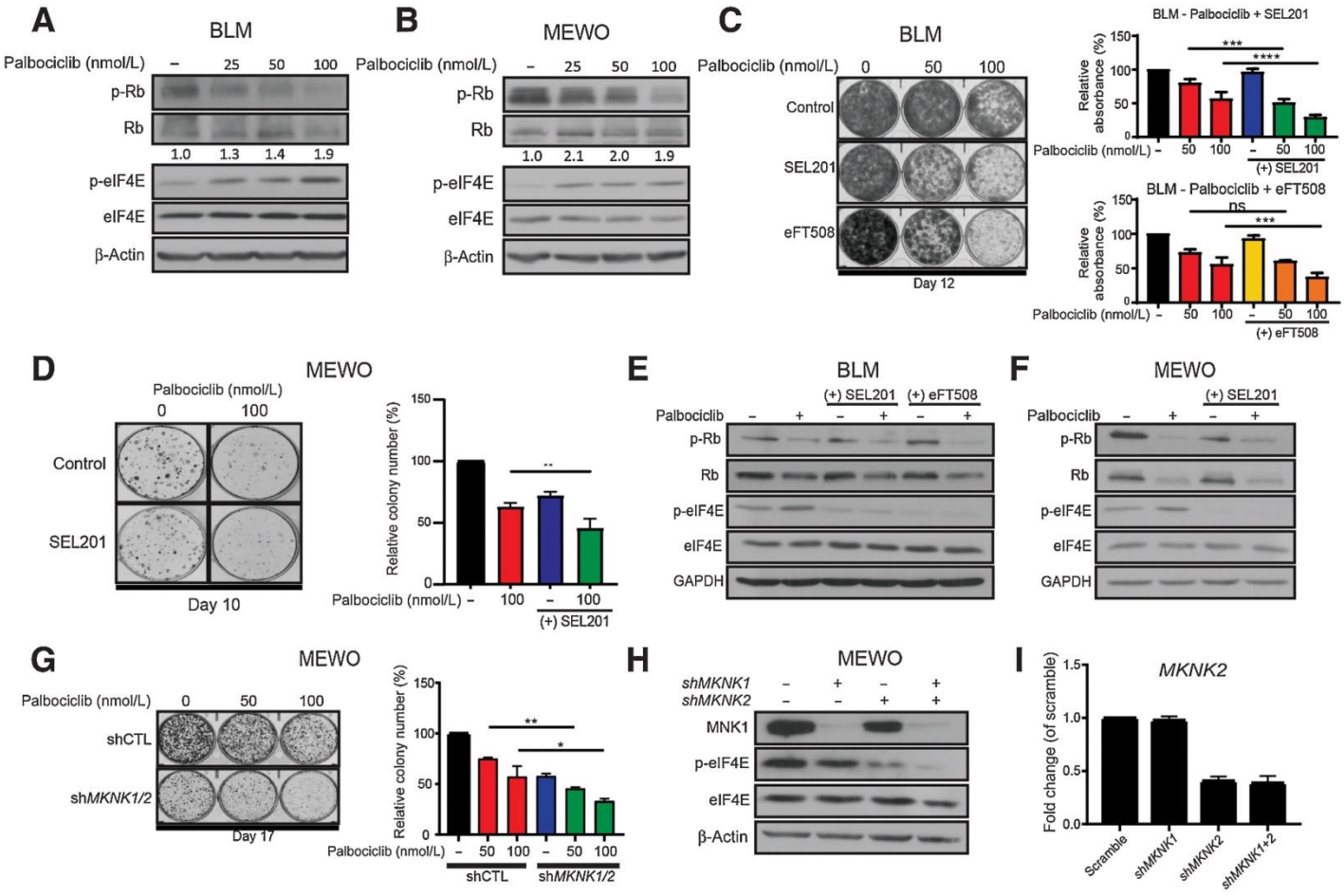

Figure 2.1: Cotargeting MNK1/2 and CDK4/6 decreases clonogenic outgrowth of melanoma cancer cell lines.

A and **B**, The phosphorylation of eIF4E is induced by palbociclib treatment in BLM and MEWO melanoma cells at 24 hours. Numbers above the p-eIF4E panels indicate the relative densitometry values for the expression of p-eIF4E/eIF4E calculated from the values of 3 biological replicates per cell line. **C**, Clonogenic assay demonstrating the effects of palbociclib in combination with 2.5 μmol/L SEL201 or 0.5 μmol/L eFT508 in BLM melanoma cells across 3 (P+S) or 4 (P+E) biological replicates. (one-way ANOVA P50 vs. P50+S, P = 0.0009; P100 vs. P100+S, P = 0.0011) (one-way ANOVA P50 vs. P50+E, P = 0.0638; P100 vs. P100+E, P = 0.002). **D**, Clonogenic assay demonstrating the effect of palbociclib in combination with 2.5 μmol/L SEL201 in MEWO melanoma cells across 3 biological replicates. (one-way ANOVA P100 vs. P100+S, P = 0.0058). **E** and **F**, Phosphorylation of Rb and eIF4E is repressed upon palbociclib and SEL201 exposure at 48 hours in BLM and MEWO, respectively. **G**, Representative clonogenic assay demonstrating that MEWO cells deficient in MKNK1 and MKNK2 are sensitive to palbociclib across 2 biological replicates (one-way ANOVA shCTL P50 vs. shMNK1/2 P50, P = 0.0037; shCTL P100 vs. shMNK1/2 P100, P = 0.0101). **H**, Immunoblot demonstrating MNK1 knockdown in MEWO-modified cells. **I**, qPCR data demonstrating MKNK2 knockdown in MEWO-modified cells.

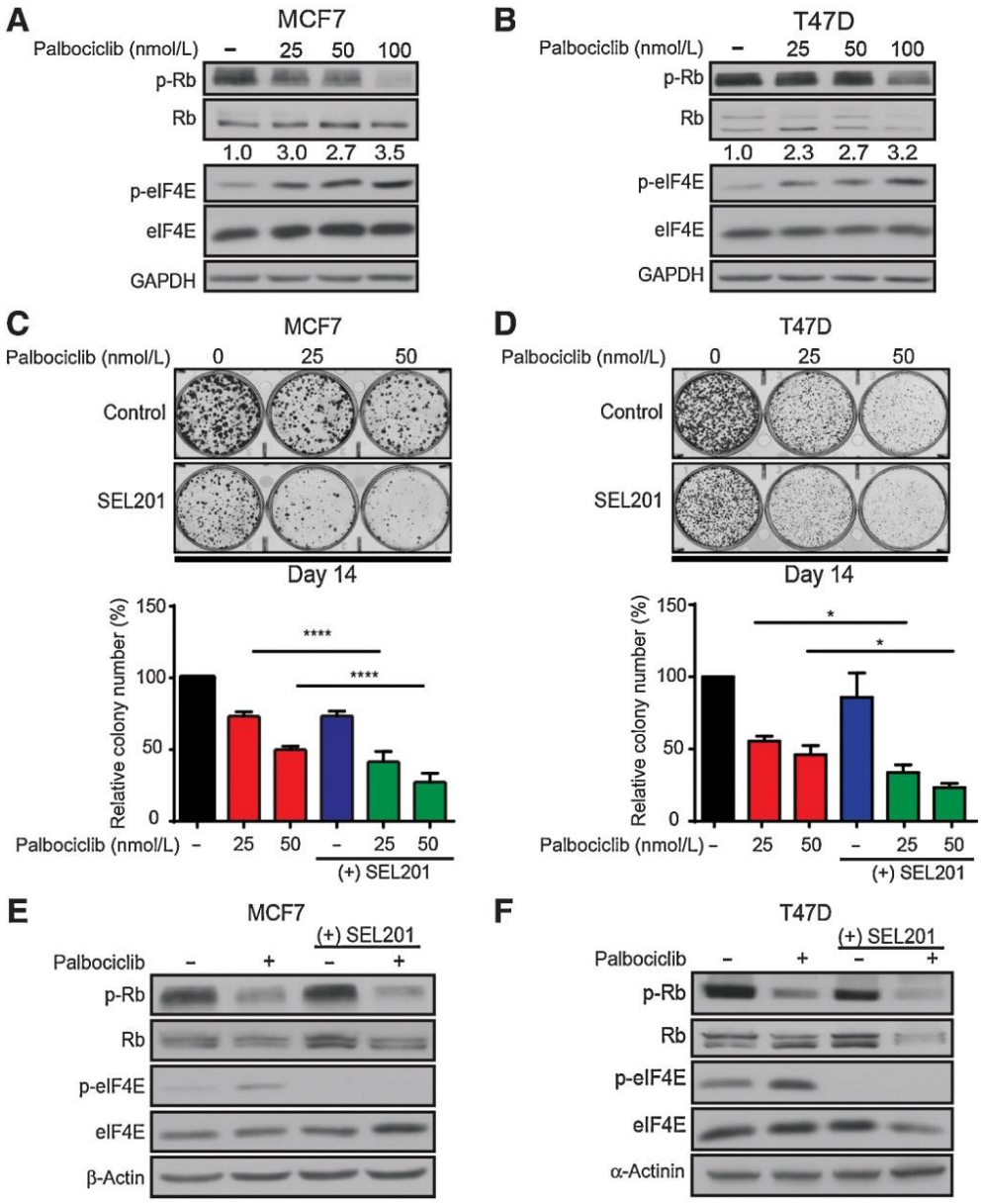

Figure 2.2: Combined inhibition of MNK1/2 and CDK4/6 represses clonogenic outgrowth in breast cancer cell lines.

A and **B**, The phosphorylation of eIF4E is induced by palbociclib treatment in MCF7 and T47D breast cancer cells at 24 hours. Numbers above the p-eIF4E panels indicate the relative densitometry values for the expression of p-eIF4E/eIF4E calculated from the values of three biological replicates per cell line. **C**, Clonogenic assay demonstrating the effects of palbociclib in combination with 2.5 µmol/L SEL201 in MCF7 across three biological replicates (one-way ANOVA P25 vs. P25+S, P = < 0.0001; P50 vs. P50+S, P = < 0.0001). **D**, Clonogenic assay demonstrating the effects of palbociclib in combination with SEL201 in T47D across three biological replicates (one-way ANOVA P25 vs. P25+S, P = 0.0483; P50 vs. P50+S, P = 0.0379). **E** and **F**, Phosphorylation of Rb and phosphorylation of eIF4E is repressed upon palbociclib and SEL201 exposure, respectively, at 48 hours in MCF7 and T47D.

2.4.2 Combined inhibition of CDK4/6 and MNK1/2 results in decreased expression of proteins involved in DNA replication, cell cycle and mitosis

We next sought to determine the mechanism by which SEL201 and palbociclib cooperate to inhibit clonogenic outgrowth of cancer cells. MNK1/2 inhibitors are well known to repress the synthesis of a subset of proteins with roles in cell cycle regulation and cell survival (20,24). Therefore, we used mass spectrometry-based quantitative proteomics to identify differentially expressed proteins upon combined SEL201 and palbociclib. Hierarchical clustering of differentially expressed proteins revealed a unique protein expression signature in cells treated with the combination of palbociclib and SEL201, compared with single agents alone (Figure 2.3A). Moreover, we observed a large cluster (cluster 9) of proteins that have uniquely decreased expression in the combination therapy compared with SEL201 or palbociclib alone (Figures 2.3B, and Supplemental Table 2.5). Pathway analysis of cluster 9 revealed multiple enriched pathways involved in cell cycle dynamics including hallmark E2F targets (M5925), cell cycle (R-HSA-1640170), and chromosome segregation (GO:0007059) in cells treated with the combination therapy (Figure 2.3B, and Supplemental Table 2.5). Upon closer inspection, we observed that the cells treated with the combination had a repressed E2F protein expression signature (Figure S2.2A). In depth analysis identified that the combination repressed the protein expression of critical cell cycle regulators that are frequently associated with poor prognosis in multiple malignancies including TOP2a (25), AURKB (26), KIF4A (27), RRM2 (28) (Figure 2.3C), TPX2 (29), and INCENP (30). Network analysis of cluster 9 further demonstrated that proteins frequently associated

with AURKB were near collectively repressed in the combination (Figure S2.2B; red solid circles), resulting in deficiencies in resolution of sister chromatid cohesion (R-HSA-2500257), separation of sister chromatids (R-HSA-2467813), and chromosome, centromeric region (GO:0000775). Pathway analysis of other clusters represented in the heatmap of differentially expressed proteins identified other potentially relevant clusters which appeared to be driven by the single agent treatments (Figures S2.2C to S2.2I).

Next, we validated the identified changes in proteins that are required for mitosis by immunoblot. Consistently, in BLM, MCF7 and T47D, expression of proteins critical for chromosome segregation, such as AURKB, survivin, and TPX2, were further reduced in cells treated with the combination, compared with single agents (Figures 2.3D to 2.3F). Moreover, qPCR analysis of BLM and MCF7 cells treated with the combination demonstrated that the repressed expression of these proteins was also detected at the mRNA level (Figures S2.2M and S2.2N). To further validate these effects, we treated the MNK1/2 deficient BLM cells with palbociclib. MNK1/2 deficient BLM cells treated with palbociclib for 48 hours showed a further decrease in AURKB, survivin, and TPX2 expression compared with scramble control and MNK1/2 knockdown alone (Figure 2.3G). These results suggest that dual inhibition of MNK1/2 and CDK4/6 repress the expression of key mitotic proteins that are commonly associated with poor prognosis.

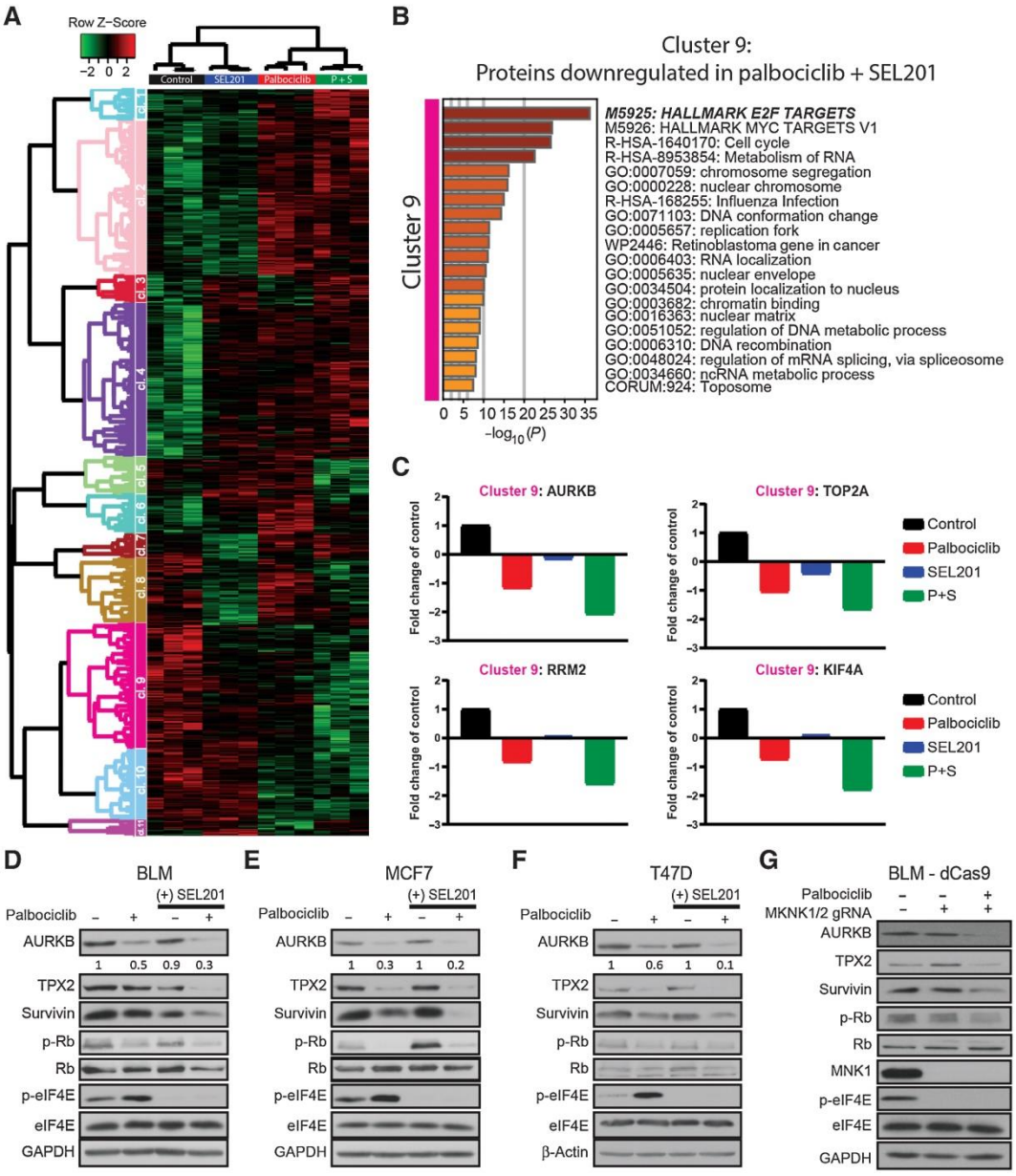

Figure 2.3: Combined inhibition of MNK1/2 and CDK4/6 results in repression of critical mitotic regulators.

A, Heatmap showing differential protein expression between BLM cells treated with vehicle, SEL201, palbociclib, or the combination therapy at 48 hours. **B**, Pathway analysis of proteins in cluster 9 shows repression of key mitotic proteins in the combination. **C**, Combined inhibition of MNK1/2 and CDK4/6 further decreases the expression of E2F target proteins associated with mitosis. **D–F**, Immunoblot validating that the combination of SEL201 plus palbociclib further represses the expression of critical mitotic enhancers in BLM, MCF7, and T47D at 48 hours. Numbers below the AURKB panels indicate the relative densitometry values for the expression of AURKB/loading control calculated from the values of 2 biological replicates per cell line. **G**, Immunoblot demonstrating that palbociclib represses the expression of critical mitotic enhancers in MNK1/2-deficient BLM-dCas9 cells at 48 hours.

2.4.3 Combined inhibition of CDK4/6 and MNK1/2 results in G_1 cell cycle arrest, suppression of cyclin A expression and increased cellular senescence

Palbociclib and SEL201 are both able to repress the expression of critical cell cycle regulators (2, 21, 24, 31). Moreover, based on the pathway analysis from cluster 9 in our quantitative proteomics, we examined the impact of combined palbociclib and SEL201 treatment on progression through the cell cycle. The FUCCI (Fluorescence Ubiquitination Cell Cycle Indicator) system employs two fluorescent proteins (mKusabira-Orange, and Clover), each fused to different regulators of the cell cycle, (cdt1, and geminin) respectively (32). During G_1, cells fluoresce orange due to the proteasomal degradation of clover-geminin, while mKO-cdt1 expression is sustained. In subsequent phases of the cell cycle, mKO-cdt1 is degraded while clover-geminin expression increases, resulting in cells that fluoresce green in G_2 (32). When we treated FUCCI stable-BLM cells with palbociclib and SEL201 we observed that the cells treated with the combination therapy had an increased accumulation in the G_1 phase of the cell cycle, compared with either single agent alone (Figure 2.4A).

It is possible that anti-cancer agents that deregulate cell cycle progression can induce unwanted fluorescence kinetics in the FUCCI system, which are not consistent with actual changes in the phases of the cell cycle (33). Using traditional flow cytometry and propidium iodide staining, BLM cells showed increased accumulation of cells in the G_1 phase of the cell cycle with combined SEL201 and palbociclib treatment compared with either single agent (Figure 2.4B). Similarly, in MCF7, the combined treatment with palbociclib and SEL201 increased the proportion of cells in G_1, compared with either

single agent (Figures 2.4C). Cyclin A is an E2F target gene whose overexpression has been associated with poor patient outcomes (34). Although palbociclib represses cyclin A expression, palbociclib resistant cells fail to maintain repressed cyclin A levels (16, 35). Through immunoblotting, we observed that the expression of cyclin A is further repressed in BLM, and MCF7 cells treated with combined SEL201 and palbociclib, compared with either of the single agents (Figures 2.4D to 2.4F).

In our proteomics analysis, we observed that BLM cells treated with the combination of palbociclib and SEL201 had elevated levels of p27 compared to either monotherapy. Recent studies have shed light on the dual roles p27 plays in cell cycle control. Cells devoid of p21 or p27, paradoxically, cannot form cyclin D1-CDK4 complexes (36). Not only does p27 facilitate the interaction between cyclin D1 and CDK4, but, p21 or p27 also enhance CDK4 activity by enabling CDK-activating kinase (CAK)-mediated phosphorylation of the T-loop in CDK4 (37,38). However, despite these distinct activating mechanisms, increased levels of p21 and p27 strongly inhibit cyclin D1-CDK4 complex formation (37, 39). We observed that the treatment of BLM and BLM-FUCCI cells with combined palbociclib and SEL201 led to increased p27 levels, compared with either single agent alone (Figure 2.4D, 2.4E). Similarly, MCF7 cells treated with SEL201 have an increased expression of p27 (Figure 2.4F). Cellular accumulation of the cell cycle inhibitor p27 is an established marker of senescence (40). We observed that our cells treated with the combination were enlarged and flattened; a phenotype characteristic of cells undergoing senescence (Figure 2.4G) (41). Palbociclib has been demonstrated to induce senescence (3, 4, 42), and in our BLM model this

effect was mild (Figure 2.4G). However, the combination of palbociclib with SEL201 resulted in a significant increase in senescence compared with either single agent as measured by β–galactosidase activity (Figure 2.4G). An initial pathway analysis of cluster 2 from our proteomics data (Figure 2.3A) revealed an enrichment of proteins related to Senescence and autophagy in cancer (WP615) (Figure S2.2D, and Supplemental table 2.5). The latter prompted a more focused analysis of the proteomics data, revealing an augmented expression of proteins frequently implicated in senescence, including proteins among the senescence-associated secretory phenotype (SASP) (Supplemental table 2.6). In support of the proteomics data, immunoblotting of BLM cells treated for 48 hours with the combination of palbociclib and SEL201 revealed an increased expression of pro-senescence markers ATG7, ISG15, Fibronectin, and PDCD4 (Figure 2.4H and Supplemental table 2.6). Similarly, MCF7 cells treated with the combination resulted in significantly increased β–galactosidase activity compared to either monotherapy at 7 days (Figure 2.4I). Overall, these data indicate that the combined inhibition of MNK1/2 and CDK4/6 results in an accumulation of cells in G_1 during short-term exposure, and prolonged exposure results in cells becoming senescent.

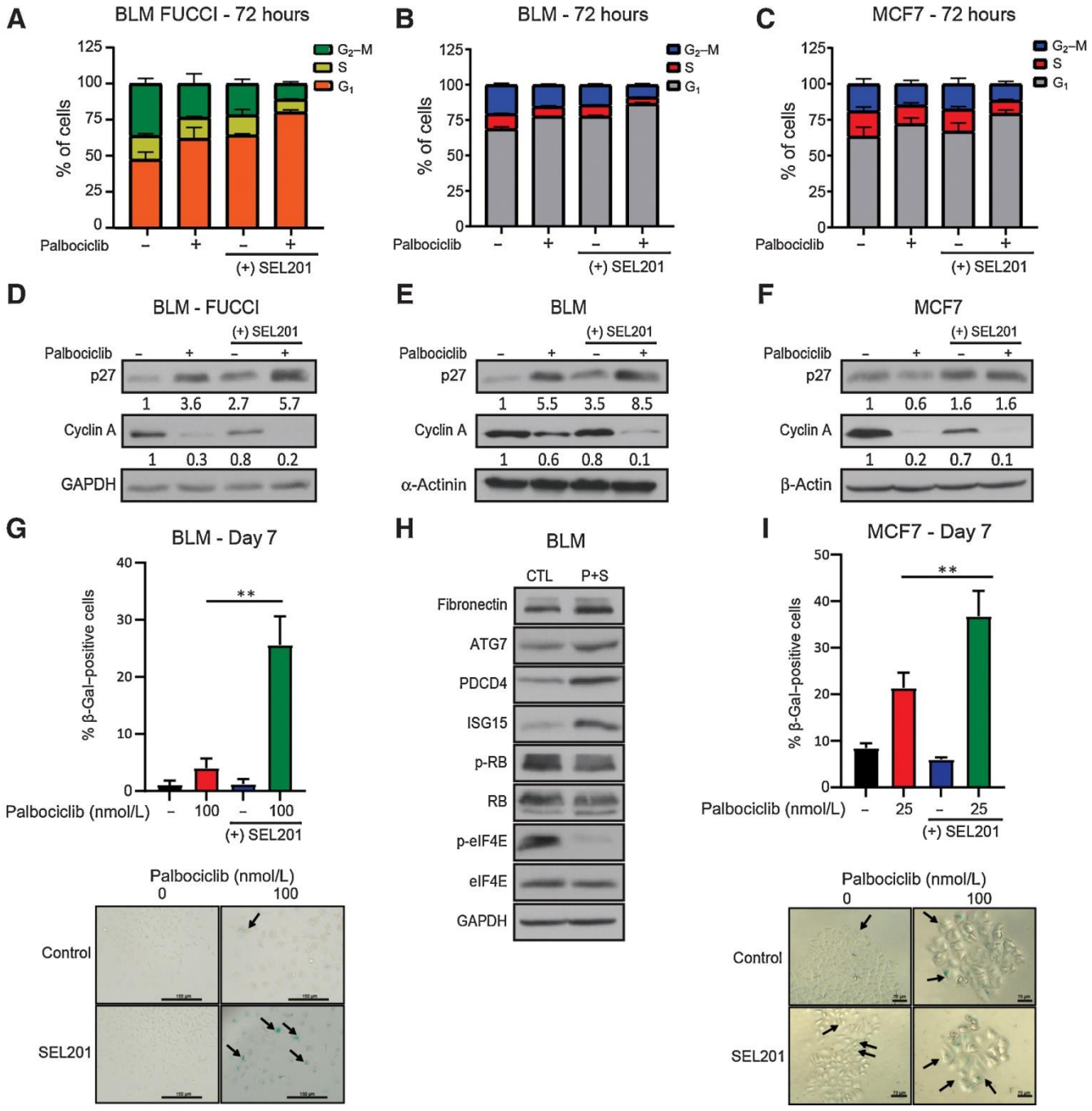

Figure 2.4: Inhibition of MNK1/2 and CDK4/6 results in G_1 cell-cycle arrest, suppression of cyclin A expression, and increased cellular senescence.

A, The combination of palbociclib and SEL201 induces G_1 cell-cycle arrest as measured by the FUCCI-tagged BLM melanoma cells (bar graph represents the average ± SD of 2 biological replicates). **B**, The combination of palbociclib and SEL201 induces G_1 cell-cycle arrest as measured by Propidium Iodide-stained BLM melanoma cells (bar graph represents the average ± SD of 2 biological replicates). **C**, Cell-cycle analysis demonstrated that the combination induces G_1 cell-cycle arrest in MCF7 cells (bar graph represents the average ± SD of 2 biological replicates). **D**, Immunoblot demonstrating increased

expression of endogenous cell-cycle inhibitor p27 and decreased expression in cyclin A in BLM-FUCCI cells treated with the combination at 48 hours. Numbers below p27 and cyclin A blots indicate average relative densitometry values of target protein/loading control across 3 biological replicates. **E and F**, Immunoblot demonstrating increased expression of endogenous cell-cycle inhibitor p27 and decreased expression of cyclin A in BLM, MCF7 cells treated with the combination at 48 hours. Numbers below the p27 and cyclin A panels indicate the relative densitometry values for the expression of target protein/loading control across 3 biological replicates per cell line. **G**, BLM cells treated with palbociclib and SEL201 have significantly more senescent cells compared with either monotherapy across 2 biological replicates. Scale bar, 150 μm; (one-way ANOVA; palbociclib vs. palbociclib+SEL201, P = 0.0047; SEL201 vs. palbociclib+SEL201, P = 0.003). **H**, BLM cells treated with palbociclib and SEL201 express higher levels of senescence markers at 48 hours. **I**, MCF7 cells treated with palbociclib and SEL201 have significantly more senescent cells compared with either monotherapy across 3 biological replicates. Scale bar, 75 μm; (one-way ANOVA; palbociclib vs. palbociclib+SEL201, P = 0.0017; SEL201 vs. palbociclib+SEL201, P = <0.0001).

2.4.4 Inhibition of MNK1/2 overcomes resistance to palbociclib

Multiple mechanisms lead to the acquisition of resistance to palbociclib, including loss of RB, loss of PRMT5 regulation, increased cyclin E expression, or activating mutations in the PI3K pathway (14, 23, 31). Several studies have also demonstrated that aberrant mRNA translation may be a mode of acquired resistance to therapies, including palbociclib (16, 43). To understand whether inhibitors of MNK1/2 hold promise in CDK4/6 inhibitor resistant disease, we tested previously described palbociclib-resistant CHL-1 (CHL-1-PalboR) melanoma cells (31). CHL-1 cells harbor no mutations in BRAF, NF1, and NRAS (triple-WT) (31). We observed that the combined inhibition of MNK1/2 and CDK4/6 significantly repressed clonogenic outgrowth of CHL-1 parental melanoma cells (Figure 2.5A). Moreover, CHL-1-PalboR cells treated with MNK1/2 inhibition were resensitized to palbociclib (Figure 2.5A).

As therapeutic resistance to CDK4/6 inhibition is an emerging clinical problem in patients with breast cancer, we next tested the response of palbociclib-resistant breast cancer cells to MNK1/2 inhibition. For this, we treated a previously described MCF7 model of acquired resistance to palbociclib (MCF7-PalboR) (43) with SEL201. Similar to

our melanoma model of palbociclib-resistance, treatment of MCF7-PalboR cells with SEL201 resensitized them to palbociclib (Figure 2.5B). In agreement with the results obtained in CHL-1 and MCF7, SEL201 also resensitized T47D palbociclib-resistant breast cancer cells (T47D-PalboR) to palbociclib (Figure 2.5D). Importantly, we observed that MCF7-PalboR and T47D-PalboR cells expressed higher levels of phosphorylated eIF4E compared with their parental counterparts (Figures 2.5C and 2.5F). qPCR analysis of these cells revealed that the palbociclib-resistant MCF7 and T47D cells express higher levels of MKNK2 (Figures 2.5D and 2.5G). These data support our hypothesis that activation of the MNK1/2-eIF4E axis may be a novel mechanism associated with resistance to palbociclib. In concordance with these data, Pancholi et al. recently demonstrated that palbociclib-resistant MCF7 cells express higher levels of MKNK2 and increased ERK/MAPK signaling (44). Overall, these data suggest that palbociclib-resistant cells may have a higher reliance on the MNK1/2-eIF4E axis for survival, and that MNK1/2 inhibition may be a therapeutic vulnerability in palbociclib-resistant cancer cells.

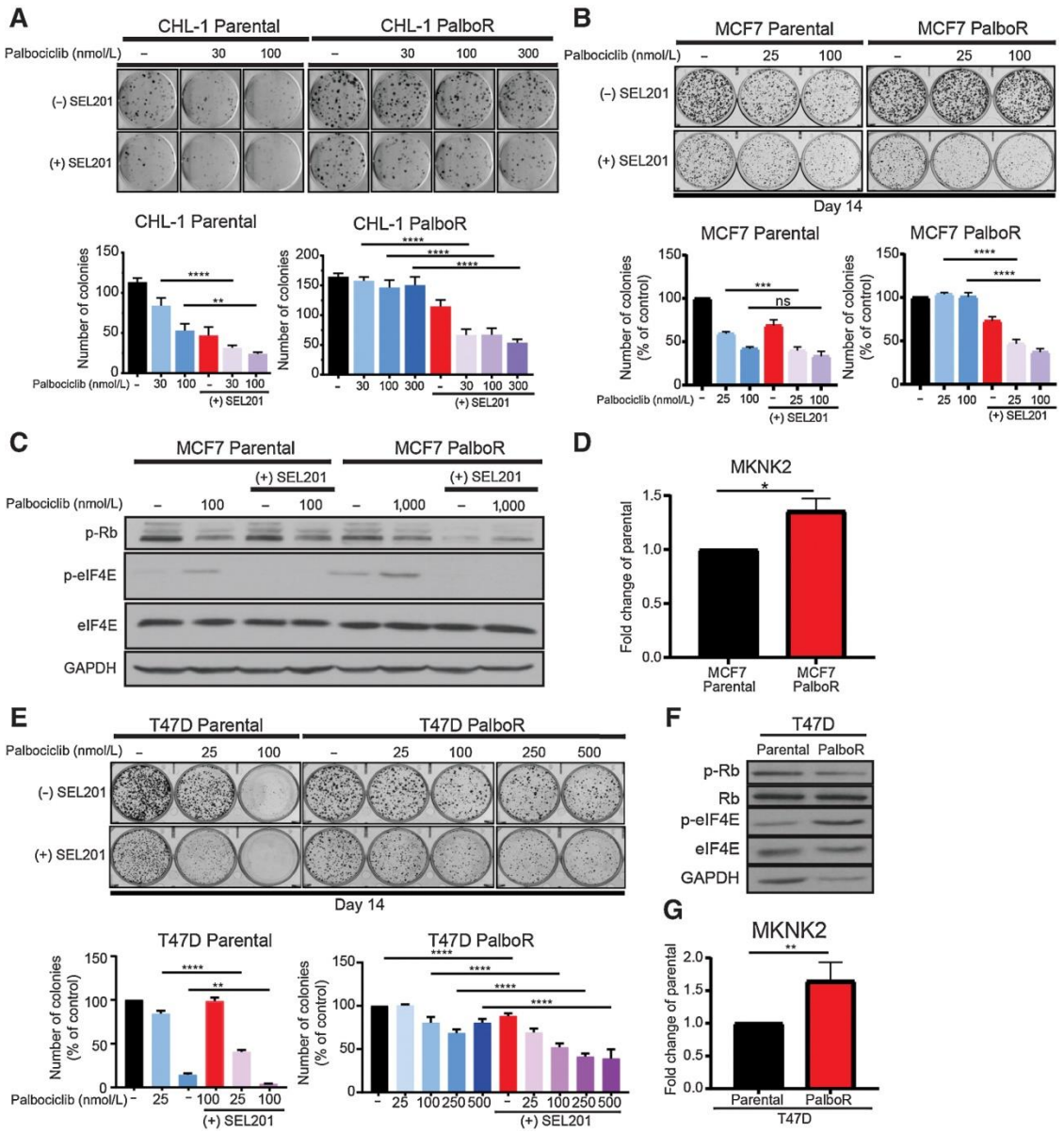

Figure 2.5: Pharmacologic inhibition of MNK1/2 overcomes palbociclib resistance in models of melanoma and breast cancer.

A, Clonogenic outgrowth of CHL-1 palbociclib-resistant melanoma cells is repressed upon exposure to 2.5 μmol/L SEL201 across 3 biological replicates (CHL-1 Parental: one-way ANOVA P30 vs. P30+S, P = <0.0001; P100 vs. P100+S, P = 0.0037; CHL-1 PalboR: one-way ANOVA P30 vs. P30+S, P = <0.0001; P100 vs. P100+S P = <0.0001; P300 vs. P300+S P = <0.0001). **B**, Clonogenic outgrowth of MCF7 palbociclib-resistant breast cancer cells is repressed upon exposure to 2.5 μmol/L SEL201 across 3 biological replicates (MCF7 Parental: one-way ANOVA P25 vs. P25+S P = 0.001; P100 vs. P100+S P = 0.1864; MCF7 PalboR: one-way ANOVA P25 vs. P25+S P = <0.0001; P100 vs. P100+S P = < 0.0001). **C**, MCF7 palbociclib-resistant breast cancer cells have a higher basal level of phospho-eIF4E compared with their parental counterpart at 48 hours. **D**, Palbociclib-resistant MCF7 cells express higher levels of MKNK2 compared with MCF7 parental cells across 2 biological replicates (unpaired t test P = 0.046). **E**, T47D palbociclib-resistant breast cancer cells are resensitized to palbociclib upon exposure to 2.5 μmol/L SEL201 exposure across 3 biological replicates (T47D Parental: one-way ANOVA P25 vs. P25+S P = <

0.0001; P100 vs. P100+S P = 0.0016; T47D PalboR: one-way ANOVA P25 vs. P25+S P = < 0.0001; P100 vs. P100+S P = < 0.0001; P250 vs. P250+S P = < 0.0001; P500 vs. P500+S P = < 0.0001). **F**, T47D palbociclib-resistant breast cancer cells have a higher basal level of phospho-eIF4E compared with their parental counterpart. **G**, Palbociclib-resistant T47D cells express higher levels of MKNK2 compared with T47D parental cells across 4 biological replicates (unpaired t test P = 0.0036).

2.4.5 Targeting MNK1/2 and CDK4/6 delays tumor progression and increases overall survival in vivo in murine models of melanoma

Loss of PTEN has been demonstrated to promote resistance to MAPK therapy (45). Moreover, there are conflicting studies as to whether PTEN loss alters sensitivity to CDK4/6 inhibitors. Recent work has demonstrated that PTEN-loss promotes resistance to palbociclib (46), while others have shown that PTEN-loss confers sensitivity to palbociclib (47). With this in mind, we next sought to test the in vivo efficacy of the MNK1/2 inhibitor eFT508, which is currently being tested in clinical trials, in combination with palbociclib using the well described Tyr::CreER/BRaf$^{CA/+}$/Pten$^{lox/lox}$ conditional melanoma model. This melanoma model allows for 4-hydroxytamoxifen (4-HT) inducible, melanocyte-targeted BRAF^{V600E} expression, and simultaneous PTEN inactivation. 12 to 15 days post 4-HT treatment, hyperpigmented lesions were observed and treatments were initiated (10). We observed a significant inhibition of tumor outgrowth in the combination treatment arm compared with the palbociclib monotherapy arm at day 54, when tumor volume was assessed at approximately 1000 mm3 (Figure 2.6A). Maintaining this tumor volume threshold, we observed that the mice in the combination arm had a median overall survival of 75 days compared with mice in the palbociclib-single agent arm, which achieved a median overall survival of 70.5 days. Additionally, assessing survival when tumor volumes reached 1500 mm3, we observed a significant overall survival advantage in the mice treated with the combination therapy,

compared with either monotherapy (Figure 2.6B). Median overall survival was as follows for each cohort: combination (83 days) > palbociclib (74 days) > eFT508 (67.5 days) > Vehicle (54 days). No overt toxicity was observed in the combination compared with single agents, as measured by mouse body weight (Figure S2.3E). eFT508 administration in mice demonstrated on target-engagement, as shown by the repression of phosphorylated eIF4E expression in the tumors (Figures 2.6C and 2.6D). Furthermore, we observed that murine tumors treated with the combination exhibited decreased expression of AURKB and survivin (Figure 2.6D), recapitulating our in vitro immunoblotting results in figure 3. Similar results, tumor growth delay and increased overall survival with no overt toxicity, were obtained in a BLM xenograft mouse model (Figures 2.6E, 2.6F, and S2.3J). In toto, our data support the use of MNK1/2 inhibitors to augment the therapeutic benefit of palbociclib in melanoma.

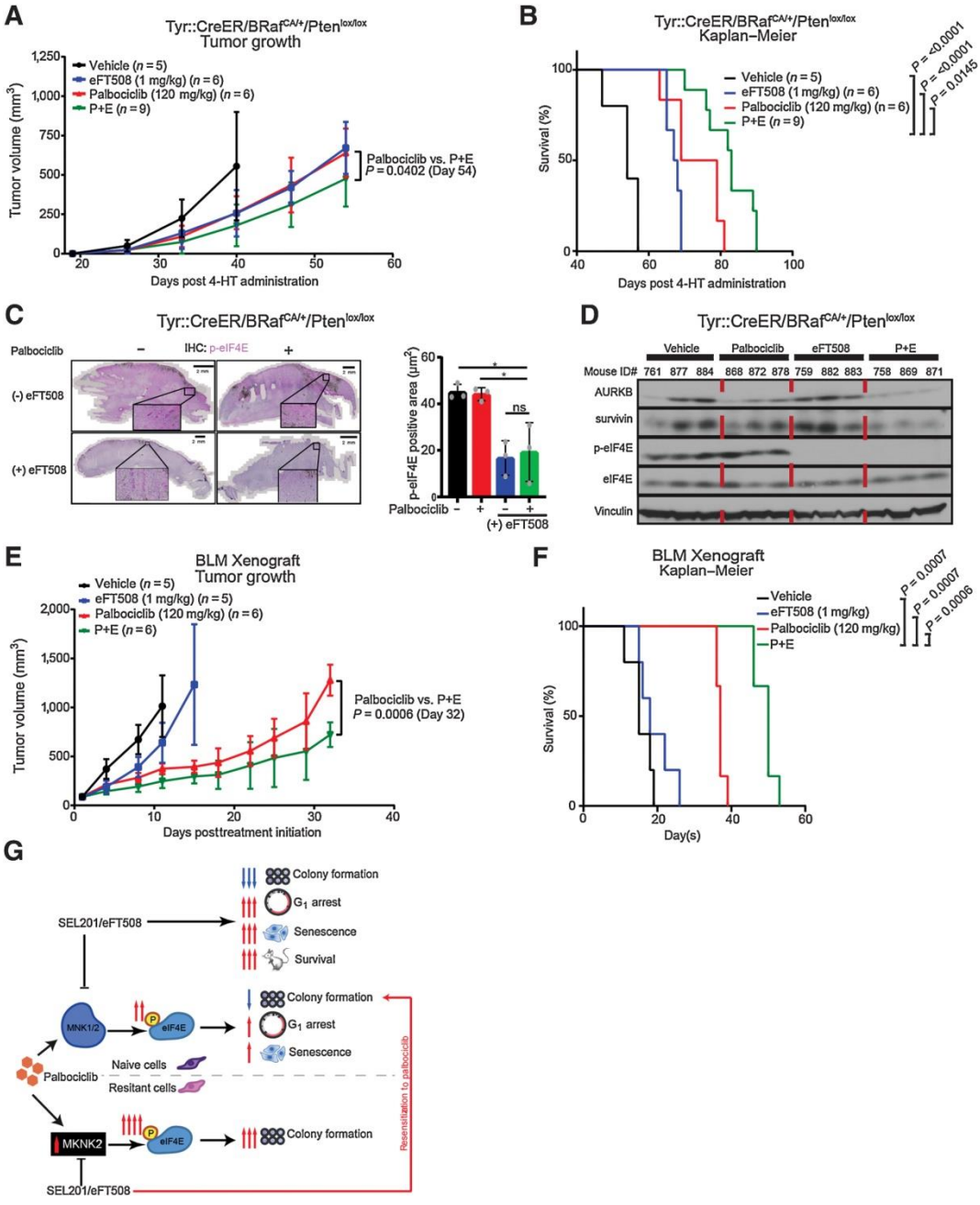

Figure 2.6: Cotargeting MNK1/2 and CDK4/6 in vivo improves overall survival in murine models of melanoma.

A, Tumor growth curves of Tyr::CreER/BRaf$^{CA/+}$/Pten$^{lox/lox}$ mice treated with vehicle, single-agent palbociclib, eFT508, or a combination of the two. **B**, Kaplan–Meier demonstrates significant survival advantage of Tyr::CreER/BRaf$^{CA/+}$/Pten$^{lox/lox}$ murine melanomas treated with the combination compared with vehicle or either monotherapy (log-rank test). **C**, Phosphorylation of eIF4E is repressed in vivo in response to eFT508 treatment. Scale bar, 2 mm; (one-way ANOVA; veh vs. P+E, P = 0.0140; P vs. P+E, P = 0.0171). **D**, Representative immunoblots of Tyr::CreER/BRaf$^{CA/+}$/Pten$^{lox/lox}$ tumors demonstrating repressed expression of AURKB and survivin in the combination compared with palbociclib. **E**, Tumor growth curves of BLM xenografts in NOD/SCID mice treated with vehicle, single-agent palbociclib,

eFT508, or a combination of the two. **F**, Kaplan–Meier demonstrates significant survival advantage of NOD/SCID mice engrafted with BLM melanoma cells and treated with the combination compared with vehicle or either monotherapy. (log-rank test). **G**, Model depicting the impact of MNK1/2-eIF4E inhibition in combination with palbociclib in melanoma and breast cancer cells. Our data suggest that the efficacy of palbociclib is limited by its ability to promote the phosphorylation of eIF4E. Blocking the increase in palbociclib-mediated phosphorylation of eIF4E results in augmented antitumor activity in therapy-naïve or palbociclib-resistant cells.

2.5 Discussion

Our data show that simultaneous inhibition of MNK1/2 and CDK4/6 work together to repress clonogenic outgrowth, increase G_1 cell cycle arrest, senescence and prolong the survival of melanoma bearing mice. Pathway analysis of the proteome of cells treated with the combination showed an overrepresentation of markers associated with cell cycle and chromosome segregation. Notably, we observed that the combination further repressed the expression of numerous mitotic regulators, including TOP2a, AURKB, KIF4A, RRM2, TPX2, and INCENP, compared with either single agent alone. This is of particular importance as increased expressions of these markers have been associated with poor prognosis in multiple cancers (25-30).

The combination of palbociclib with hormone therapy has significantly improved clinical outcome of ER-positive breast cancer (23). Furthermore, MNK1/2 inhibitors are actively being tested for efficacy in advanced breast cancer (NCT04261218). Similar to our data in melanoma, MCF7 breast cancer cells treated with the combination of MNK1/2 and CDK4/6 inhibitors have decreased clonogenic outgrowth compared with single agents. Melanoma and breast cancer cells exposed to the combination demonstrate increased G_1 accumulation, and reduced expression of cyclin A. Additionally, we observed increased expression of p27 and senescence in cell treated with the combination. Similar to BLM, we observe that breast cancer cells treated with the combination have reduced levels of critical mitotic regulators, such as TPX2,

AURKB, and survivin. Strikingly, we observed no evidence of G_2/M cell cycle arrest in melanoma or breast cancer cells treated with the combination. Interestingly, repression of AURKB activity has also been demonstrated to induce a G_1 arrest in non-small cell lung cancer cells (48). It would be very interesting to test whether the repression of AURKB through combined inhibition of CDK4/6 and MNK1/2 directly impacts accumulation of cells in G_1/S phase of the cell cycle.

Of clinical relevance, our data demonstrate that breast cancer cells that acquire resistance to palbociclib have increased levels of phosphorylated-eIF4E. Although we are continuing to explore the mechanism via which the phosphorylation of eIF4E increases, our data and that of others (44), suggest it may be due to increased expression of *MKNK2* (Figure 2.6G). Pharmacologic inhibition of MNK1/2 in palbociclib-resistant cells results in re-sensitization to palbociclib. Given that CDK4/6 inhibitors are being clinically investigated as single agents in melanoma (NCT02465060, NCT02857270, and NCT02791334), we tested whether palbociclib-resistant melanoma cells were sensitive to MNK1/2 inhibitors. Similar to breast cancer, CHL1 palbociclib-resistant melanoma cells are resensitized to palbociclib upon MNK1/2 inhibition.

In therapy naïve cells, increased levels of phospho-eIF4E in response to chemotherapeutic and targeted agents have been previously reported. One study demonstrated that treatment of pancreatic ductal adenocarcinoma cells with gemcitabine results in increased SRSF1-mediated MNK2b splicing that results in increased phosphorylated eIF4E (13). Furthermore, blocking this increase in phospho-eIF4E results in increased apoptosis in gemcitabine treated cells (13). Other studies have also implicated a role for increased phosphorylated eIF4E in resistance to stress

and DNA damaging agents through the selective translation of cyclin D1, HuR, and Mcl-1 mRNA's (49). Our future work will be aimed at identifying the subset of mRNAs which are most efficiently translated in response to CDK4/6 inhibitors.

Overall, our data demonstrate the MNK1/2-eIF4E axis to be an exploitable salvage pathway in treatment naïve and palbociclib-resistant models (Figure 2.6G). Palbociclib has recently demonstrated modest anti-tumor activity in acral lentiginous melanoma (ALM) (50). Additionally, we have previously shown that the oncogenicity of *KIT*-mutant acral melanomas are highly reliant on the MNK1/2-eIF4E axis, and, by blocking MNK1/2 we are able to repress the oncogenicity of these melanomas (20). Albeit the single-efficacy of MNK1/2 inhibitors are mild, we would predict that the addition of MNK1/2 inhibitors would potently augment the efficacy of palbociclib, and perhaps that of other CDK4/6 inhibitors, in melanoma subtypes with limited treatment options. Furthermore, although speculative, one might envision the use of phospho-eIF4E as a potential biomarker to predict the onset of resistance to palbociclib.

2.6 Materials and Methods

Cell lines and reagents

BLM cells were a generous gift from Ghanem Ghanem (Institut Jules Bordet, Bruxelles). MEWO cells were a generous gift from Ian Watson (McGill University). BLM, MEWO, MCF7, T47D, CHL-1 and HEK293T cell lines were cultured in DMEM (Wisent bioproducts #319-005-CL) containing 10% FBS and 100 I.U/mL penicillin and 100 I.U/mL streptomycin at 37°C and 5% CO_2. HEK293T and palbociclib-resistant MCF7 cells were a generous gift from Dr. Sidong Huang. T47D-parental and matched

palbociclib-resistant cell lines were a generous gift from Dr. David Cescon (19). All experiments were initiated within 5 passages of thawing a master stock of cells. Cell lines were routinely tested for Mycoplasma using the e-Myco™ VALID Mycoplasma PCR Detection Kit. Identity of cell lines was verified by short tandem repeat (STR) profiling. Palbociclib (#S1116) was purchased from Selleck Chemicals and dissolved according to manufacturer's instructions to a stock concentration of 10 mM. During experiments, cells were exposed to palbociclib at concentrations ranging from 25 nM to 250 nM. For *in vivo* experiments, palbociclib monhohydrochloride was purchased from MedChemExpress (#HY-50767A). SEL201 (20) was provided by RYVU therapeutics. eFT508 was purchased from Selleckchem (#S8275). Unless specified otherwise, SEL201 and eFT508 drug treatments were performed at 2.5 μM and 0.5 μM respectively.

Colony formation assay

Cells were seeded in 6-well plates at densities of 2,000 to 5,000 cells per well and allowed to adhere overnight. Media was changed the next day and drug was added. At experimental endpoint, the cells were stained with 0.5% crystal violet in 70% ethanol for 1 hour. The plates were scanned and clonogenic outgrowth was quantified manually using ImageJ, or were dissolved using 1mL of 10% glacial acetic acid per well for 1 hour on a shaker. Subsequently, absorbance was measured at 590 nm and relative differences were graphed. Clonogenic assays on CHL1 were performed at The Peter MacCallum Cancer Centre, Victoria, Australia.

Immunoblotting

500,000 to 1,000,000 cells were treated for 48 hours. Lysates were prepared using RIPA containing 50mM Tris HCl pH8.0, 150mM NaCl, 1% NP-40, 0.5% deoxycholate, 0.1% SDS, 5mM EDTA, protease (Roche #11697498001), and phosphatase inhibitors (Roche #4906845001). Cells were lysed using 50µl of complete RIPA per 1 million cells and sonicated before centrifuging at max speed for 15 minutes. Protein concentration was measured by Bradford assay. 50µg of protein lysate were PAGE-separated (40% Acrylamide/Bis Solution, 37.5:1 Bio-Rad #1610148) and transferred onto PVDF membranes (Roche #0301004001), blocked for one hour in 5% non-fat milk, and incubated with primary antibody overnight at 4°C. The following day, the membranes were washed and incubated with secondary antibody for 1 hour. The membranes were developed using Amersham ECL Western Blotting Reagent (#RPN2106) or Immobilon Western Chemiluminescent HRP Substrate (#WBKLS0500). Antibody details can be found in Supplemental Table 2.1.

Quantitative PCR

RNA was prepared using E.Z.N.A. Total RNA Kit (Omega Bio-tek). cDNA was prepared from 1 µg of total RNA using iScript cDNA Synthesis Kit (Bio-Rad). Gene expression was quantified using the Applied Biosystems 7500 Fast Real-Time PCR System using GoTaq Green Master Mix (Promega). Primer details can be found in Supplemental Table 2.2.

Lentivirus production and transduction

Lentiviral plasmids were co-transfected with the packaging plasmids Pax2 and MD2G into HEK293T cells using calcium phosphate precipitation. Viral supernatant was

harvested 72 hours post transfection, spun down at 500xg for 5 minutes, and filtered through a 0.45 µm filter. 500 µl of viral supernatant were used to transduce 100,000 cells in the presence of 8 µg/mL polybrene for 24 hours. The following day, media was changed, and transduced cells were selected using 2 µg/mL of puromycin.

Cell-cycle analysis

20,000 to 50,000 cells were treated with inhibitors for 3 days and then washed twice with ice-cold PBS containing 1% FBS. Cells were stained with 50 µg/mL propidium iodide solution in hypotonic buffer (0.1% Triton X-100 and 0.1% sodium citrate) for at least 20 minutes in the dark. At least 10,000 cycling cells were analyzed using BD LSR Fortessa II. Data was analyzed using FlowJo VX (RRID:SCR_008520).

dCas9 cell line generation

BLM cells were transduced with vectors encoding dCas9 (Addgene #46911) Infected cells were single-cell sorted and clones were expanded and selected for proliferation rates that matched the parental cell lines. sgRNA's were cloned in to pU6-sgRNA EF1Alpha-puro-T2A-BFP (Addgene #60955). sgRNA sequences can be found in Supplemental Table 2.3.

FUCCI cell line generation

Cells were virally transduced with FUCCI vector expressing mKO-CDT1 and clover-Geminin. Populations of cells expressing medium to high levels of mKO and clover were sorted into culture and used for further experiments.

Senescence assay

One hundred cells were seeded in 12-well plates and subsequently treated with indicated concentrations of SEL201, palbociclib, or their combination for 7 days.

Senescence staining was performed using Senescence β-Galactosidase Staining Kit (Cell Signaling Technology, #9860) according to manufacturer's protocol. After the incubation period, images were taken and approximately equal numbers of total cells were quantified across treatments. Total and β-gal positive cells were manually counted using ImageJ software (RRID:SCR_003070).

***In vivo* experiments**

Animal experiments were conducted according to the regulations established by the Canadian Council of Animal Care, and protocols approved by the McGill University Animal Care and Use Committee (2015-7672). Tyr::CreER/BRaf$^{CA/+}$/Pten$^{lox/lox}$ mice were treated topically with 4-hydroxytamoxifen (4-HT) for 3 consecutive days. 15 days post 4-HT exposure, mice were randomized into 4 cohorts and treated independently with vehicle, palbociclib (120 mg/kg), eFT508 (1 mg/kg), or the combination of both drugs by oral gavage (P.O). Endpoint was determined when the tumors ulcerated or reached a volume of approximately 1500 mm^3. BLM cells were injected into the right flank of immunodeficient nonobese diabetic (NOD)/severe combined immunodeficiency (SCID) mice. When tumor volumes reached around 80 to 100mm^3, the mice were randomized into 4 cohorts and treated independently with vehicle, palbociclib (120 mg/kg), eFT508 (1 mg/kg), or the combination of both drugs. Endpoint was determined when the tumor volume reached approximately 2000 mm^3. All *in vivo* drug treatments were administered on a 5-day-on and 2-day-off schedule.

Mass Spectrometry-based proteomics

BLM cells were treated with either monotherapy or the combination of the two for 48 hours. At end point the cells were washed with PBS, harvested by scraping, flash

frozen in liquid nitrogen and stored at -80°C before processing. Detailed methods for sample preparation, acquisition and subsequent data analysis can be found in the supplemental methods.

Immunohistochemistry

Briefly, tumor sections were stained for phospho-eIF4E, and counterstained with 20% Harris-modified hematoxylin (Thermo Fisher Scientific). Slides were scanned and phosphorylated eIF4E levels were assessed by calculating the area of positive and negative cells using the pixel classification feature on QuPath software (threshold score range: negative >0.9<positive). Antibody details can be found in Supplemental Table 2.1.

Statistical Analysis

Unless otherwise specified, all experiments were performed in a minimum of 3 biological replicates. All *in vitro* and *in vivo* data are represented as mean ± SD. Student t-test or one-Way ANOVA (Tukey's post-hoc test) were applied for statistical tests presented, using GraphPad Prism Version 9.0.0 (RRID:SCR_002798). The specific statistical analysis for each figure is listed in Supplemental Table 2.4. *P* values < 0.05 were considered significant. Log-Rank test was applied to Kaplan Meier analyses in *in vivo* experiments. p-values are specified in the figure itself, the figure legend, or in Supplemental Table 2.4

Data Availability

Proteomics data from our mass spectrometry experiments have been deposited to the PRIDE database (RRID:SCR_012052) with the dataset accession PXD033390.

2.7 Acknowledgments

This research was funded by the Canadian Institutes of Health Research (CIHR) (grant PJT-162260 to SVDR and grant PJT-156269 to WHM and SVDR. SAP and SSK hold FRQS studentships. OM holds an FRQS scholarship and was awarded the Andy-Lena Chabot award by the Cancer Research Society. FH was sponsored by a McGill Faculty of Medicine graduate studentship and received a McGill Integrated Cancer Research Training Program graduate studentship. We are grateful to Genome Canada for financial support through the Genomics Technology Platform (GTP: 264PRO). We are also grateful for financial support from the Terry Fox Research Institute. CHB is grateful for support from the Segal McGill Chair in Molecular Oncology at McGill University (Montreal, Quebec, Canada), and for support from the Warren Y. Soper Charitable Trust and the Alvin Segal Family Foundation to the Jewish General Hospital (Montreal, Quebec, Canada). We thank Christian Young for valuable expertise in designing and executing flow cytometry experiments. We thank Dr. Josie Ursini-Siegel for providing the NOD-SCID mice and Dr. Luc Furic for providing reagents. Special thanks to Dr. Henry Yu for invaluable discussions. Current affiliations: ISB is currently affiliated with Repare Therapeutics; RZ is currently affiliated with University of Manitoba.

2.8 References

1. Sheppard KE, McArthur GA. The cell-cycle regulator CDK4: an emerging therapeutic target in melanoma. Clinical cancer research : an official journal of the American Association for Cancer Research 2013;19:5320-8
2. Schettini F, De Santo I, Rea CG, De Placido P, Formisano L, Giuliano M, et al. CDK 4/6 Inhibitors as Single Agent in Advanced Solid Tumors. Frontiers in oncology 2018;8:608
3. Martin CA, Cullinane C, Kirby L, Abuhammad S, Lelliott EJ, Waldeck K, et al. Palbociclib synergizes with BRAF and MEK inhibitors in treatment naïve melanoma but not after the development of BRAF inhibitor resistance. International journal of cancer 2018;142:2139-52
4. Yoshida A, Lee EK, Diehl JA. Induction of Therapeutic Senescence in Vemurafenib-Resistant Melanoma by Extended Inhibition of CDK4/6. Cancer research 2016;76:2990-3002
5. Johnson DB, Puzanov I. Treatment of NRAS-mutant melanoma. Current treatment options in oncology 2015;16:15
6. Siegel RL, Miller KD, Jemal A. Cancer statistics, 2018. CA: a cancer journal for clinicians 2018;68:7-30
7. Tang B, Sheng X, Kong Y, Chi Z, Si L, Cui C, et al. Palbociclib for treatment of metastatic melanoma with copy number variations of CDK4 pathway: case report. Chinese clinical oncology 2018;7:62
8. Prabhu SA, Moussa O, Miller WH, Jr., Del Rincón SV. The MNK1/2-eIF4E Axis as a Potential Therapeutic Target in Melanoma. International journal of molecular sciences 2020;21
9. Carter JH, Deddens JA, Spaulding NI, Lucas D, Colligan BM, Lewis TG, et al. Phosphorylation of eIF4E serine 209 is associated with tumour progression and reduced survival in malignant melanoma. British journal of cancer 2016;114:444-53
10. Huang F, Gonçalves C, Bartish M, Rémy-Sarrazin J, Issa ME, Cordeiro B, et al. Inhibiting the MNK1/2-eIF4E axis impairs melanoma phenotype switching and potentiates antitumor immune responses. The Journal of clinical investigation 2021;131
11. Adesso L, Calabretta S, Barbagallo F, Capurso G, Pilozzi E, Geremia R, et al. Gemcitabine triggers a pro-survival response in pancreatic cancer cells through activation of the MNK2/eIF4E pathway. Oncogene 2013;32:2848-57
12. Geter PA, Ernlund AW, Bakogianni S, Alard A, Arju R, Giashuddin S, et al. Hyperactive mTOR and MNK1 phosphorylation of eIF4E confer tamoxifen resistance and estrogen independence through selective mRNA translation reprogramming. Genes & development 2017;31:2235-49
13. Vasan N, Baselga J, Hyman DM. A view on drug resistance in cancer. Nature 2019;575:299-309
14. O'Brien NA, McDermott MSJ, Conklin D, Luo T, Ayala R, Salgar S, et al. Targeting activated PI3K/mTOR signaling overcomes acquired resistance to CDK4/6-based therapies in preclinical models of hormone receptor-positive breast cancer. Breast cancer research : BCR 2020;22:89
15. Yamamoto T, Kanaya N, Somlo G, Chen S. Synergistic anti-cancer activity of CDK4/6 inhibitor palbociclib and dual mTOR kinase inhibitor MLN0128 in pRb-expressing ER-negative breast cancer. Breast cancer research and treatment 2019;174:615-25
16. Yoshida A, Bu Y, Qie S, Wrangle J, Camp ER, Hazard ES, et al. SLC36A1-mTORC1 signaling drives acquired resistance to CDK4/6 inhibitors. Science advances 2019;5:eaax6352
17. Michaloglou C, Crafter C, Siersbaek R, Delpuech O, Curwen JO, Carnevalli LS, et al. Combined Inhibition of mTOR and CDK4/6 Is Required for Optimal Blockade of E2F Function and Long-term Growth Inhibition in Estrogen Receptor-positive Breast Cancer. Molecular cancer therapeutics 2018;17:908-20
18. Mitchell DC, Menon A, Garner AL. Cyclin-dependent kinase 4 inhibits the translational repressor 4E-BP1 to promote cap-dependent translation during mitosis-G1 transition. FEBS letters 2020;594:1307-18
19. Soria-Bretones I, Thu KL, Silvester J, Cruickshank J, El Ghamrasni S, Ba-Alawi W, et al. The spindle assembly checkpoint is a therapeutic vulnerability of CDK4/6 inhibitor-resistant ER(+) breast cancer with mitotic aberrations. Science advances 2022;8:eabq4293
20. Zhan Y, Guo J, Yang W, Goncalves C, Rzymski T, Dreas A, et al. MNK1/2 inhibition limits oncogenicity and metastasis of KIT-mutant melanoma. The Journal of clinical investigation 2017;127:4179-92
21. Robichaud N, del Rincon SV, Huor B, Alain T, Petruccelli LA, Hearnden J, et al. Phosphorylation of eIF4E promotes EMT and metastasis via translational control of SNAIL and MMP-3. Oncogene 2015;34:2032-42

22. Ke XY, Chen Y, Tham VY, Lin RY, Dakle P, Nacro K, et al. MNK1 and MNK2 enforce expression of E2F1, FOXM1, and WEE1 to drive soft tissue sarcoma. Oncogene 2021;40:1851-67
23. McCartney A, Migliaccio I, Bonechi M, Biagioni C, Romagnoli D, De Luca F, et al. Mechanisms of Resistance to CDK4/6 Inhibitors: Potential Implications and Biomarkers for Clinical Practice. Frontiers in oncology 2019;9:666
24. Robichaud N, Hsu BE, Istomine R, Alvarez F, Blagih J, Ma EH, et al. Translational control in the tumor microenvironment promotes lung metastasis: Phosphorylation of eIF4E in neutrophils. Proceedings of the National Academy of Sciences of the United States of America 2018;115:E2202-e9
25. Heestand GM, Schwaederle M, Gatalica Z, Arguello D, Kurzrock R. Topoisomerase expression and amplification in solid tumours: Analysis of 24,262 patients. European journal of cancer (Oxford, England : 1990) 2017;83:80-7
26. Zhang Y, Jiang C, Li H, Lv F, Li X, Qian X, et al. Elevated Aurora B expression contributes to chemoresistance and poor prognosis in breast cancer. International journal of clinical and experimental pathology 2015;8:751-7
27. Hou G, Dong C, Dong Z, Liu G, Xu H, Chen L, et al. Upregulate KIF4A Enhances Proliferation, Invasion of Hepatocellular Carcinoma and Indicates poor prognosis Across Human Cancer Types. Scientific reports 2017;7:4148
28. Abdel-Rahman MA, Mahfouz M, Habashy HO. RRM2 expression in different molecular subtypes of breast cancer and its prognostic significance. Diagnostic pathology 2022;17:1
29. Zou J, Huang RY, Jiang FN, Chen DX, Wang C, Han ZD, et al. Overexpression of TPX2 is associated with progression and prognosis of prostate cancer. Oncology letters 2018;16:2823-32
30. Adams RR, Eckley DM, Vagnarelli P, Wheatley SP, Gerloff DL, Mackay AM, et al. Human INCENP colocalizes with the Aurora-B/AIRK2 kinase on chromosomes and is overexpressed in tumour cells. Chromosoma 2001;110:65-74
31. AbuHammad S, Cullinane C, Martin C, Bacolas Z, Ward T, Chen H, et al. Regulation of PRMT5-MDM4 axis is critical in the response to CDK4/6 inhibitors in melanoma. Proceedings of the National Academy of Sciences of the United States of America 2019;116:17990-8000
32. Sakaue-Sawano A, Kurokawa H, Morimura T, Hanyu A, Hama H, Osawa H, et al. Visualizing spatiotemporal dynamics of multicellular cell-cycle progression. Cell 2008;132:487-98
33. Kaida A, Sawai N, Sakaguchi K, Miura M. Fluorescence kinetics in HeLa cells after treatment with cell cycle arrest inducers visualized with Fucci (fluorescent ubiquitination-based cell cycle indicator). Cell biology international 2011;35:359-63
34. Michalides R, van Tinteren H, Balkenende A, Vermorken JB, Benraadt J, Huldij J, et al. Cyclin A is a prognostic indicator in early stage breast cancer with and without tamoxifen treatment. British journal of cancer 2002;86:402-8
35. Xue Z, Lui VWY, Li Y, Jia L, You C, Li X, et al. Therapeutic evaluation of palbociclib and its compatibility with other chemotherapies for primary and recurrent nasopharyngeal carcinoma. Journal of Experimental & Clinical Cancer Research 2020;39:262
36. Cerqueira A, Martín A, Symonds CE, Odajima J, Dubus P, Barbacid M, et al. Genetic characterization of the role of the Cip/Kip family of proteins as cyclin-dependent kinase inhibitors and assembly factors. Molecular and cellular biology 2014;34:1452-9
37. Guiley KZ, Stevenson JW, Lou K, Barkovich KJ, Kumarasamy V, Wijeratne TU, et al. p27 allosterically activates cyclin-dependent kinase 4 and antagonizes palbociclib inhibition. Science (New York, NY) 2019;366
38. Schachter MM, Merrick KA, Larochelle S, Hirschi A, Zhang C, Shokat KM, et al. A Cdk7-Cdk4 T-loop phosphorylation cascade promotes G1 progression. Molecular cell 2013;50:250-60
39. Ray A, James MK, Larochelle S, Fisher RP, Blain SW. p27Kip1 inhibits cyclin D-cyclin-dependent kinase 4 by two independent modes. Molecular and cellular biology 2009;29:986-99
40. Calcinotto A, Alimonti A. Aging tumour cells to cure cancer: "pro-senescence" therapy for cancer. Swiss medical weekly 2017;147:w14367
41. Zhao H, Darzynkiewicz Z. Biomarkers of cell senescence assessed by imaging cytometry. Methods in molecular biology (Clifton, NJ) 2013;965:83-92

42. Jost T, Heinzerling L, Fietkau R, Hecht M, Distel LV. Palbociclib Induces Senescence in Melanoma and Breast Cancer Cells and Leads to Additive Growth Arrest in Combination With Irradiation. Frontiers in oncology 2021;11:740002
43. Kong T, Xue Y, Cencic R, Zhu X, Monast A, Fu Z, et al. eIF4A Inhibitors Suppress Cell-Cycle Feedback Response and Acquired Resistance to CDK4/6 Inhibition in Cancer. Molecular cancer therapeutics 2019;18:2158-70
44. Pancholi S, Ribas R, Simigdala N, Schuster E, Nikitorowicz-Buniak J, Ressa A, et al. Tumour kinome re-wiring governs resistance to palbociclib in oestrogen receptor positive breast cancers, highlighting new therapeutic modalities. Oncogene 2020;39:4781-97
45. Paraiso KH, Xiang Y, Rebecca VW, Abel EV, Chen YA, Munko AC, et al. PTEN loss confers BRAF inhibitor resistance to melanoma cells through the suppression of BIM expression. Cancer research 2011;71:2750-60
46. Costa C, Wang Y, Ly A, Hosono Y, Murchie E, Walmsley CS, et al. PTEN Loss Mediates Clinical Cross-Resistance to CDK4/6 and PI3Kα Inhibitors in Breast Cancer. Cancer discovery 2020;10:72-85
47. Dosil MA, Mirantes C, Eritja N, Felip I, Navaridas R, Gatius S, et al. Palbociclib has antitumour effects on Pten-deficient endometrial neoplasias. The Journal of pathology 2017;242:152-64
48. Bertran-Alamillo J, Cattan V, Schoumacher M, Codony-Servat J, Giménez-Capitán A, Cantero F, et al. AURKB as a target in non-small cell lung cancer with acquired resistance to anti-EGFR therapy. Nature communications 2019;10:1812
49. Martínez A, Sesé M, Losa JH, Robichaud N, Sonenberg N, Aasen T, et al. Phosphorylation of eIF4E Confers Resistance to Cellular Stress and DNA-Damaging Agents through an Interaction with 4E-T: A Rationale for Novel Therapeutic Approaches. PloS one 2015;10:e0123352
50. Mao L, Dai J, Cao Y, Bai X, Sheng X, Chi Z, et al. Palbociclib in advanced acral melanoma with genetic aberrations in the cyclin-dependent kinase 4 pathway. European journal of cancer (Oxford, England : 1990) 2021;148:297-306

2.9 Supplemental Data

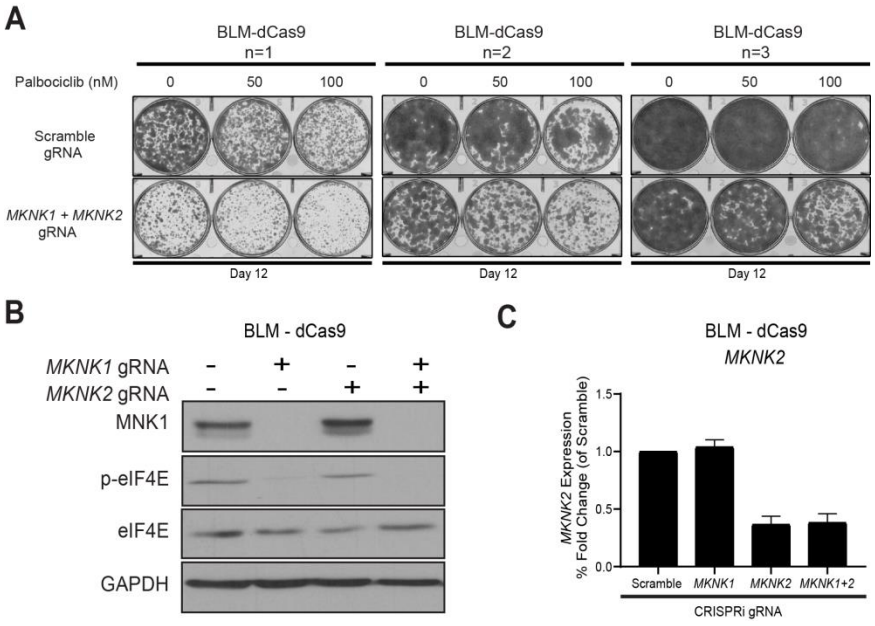

Supplemental Figure 2.1: Clonogenic assays and MKNK1 and MKNK2 knockdown validation in BLM-dCas9 cells.
A. Clonogenic assays from three independent biological experiments demonstrating that BLMdCas9 cells deficient in MKNK1/2 are more sensitive to palbociclib than Scramble control cells. **B.** Immunoblot demonstrating MNK1 knockdown in BLM-dCas9 cells. **C.** qPCR analysis demonstrating MKNK2 knockdown in BLM-dCas9 cells.

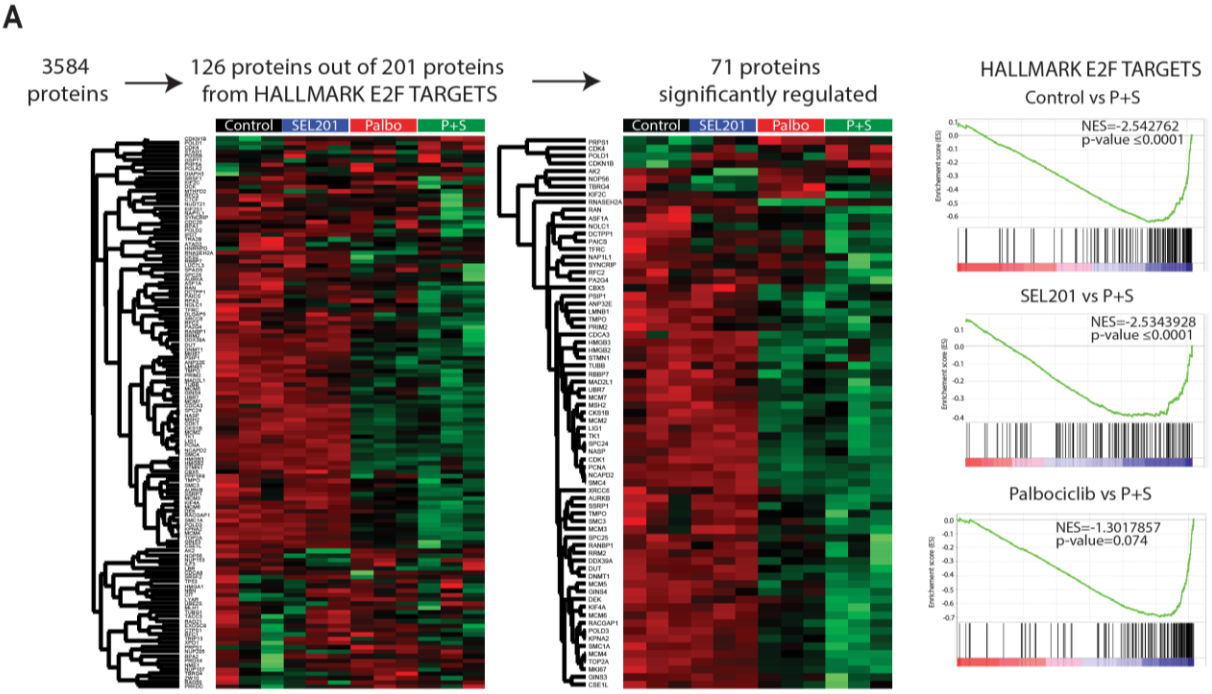

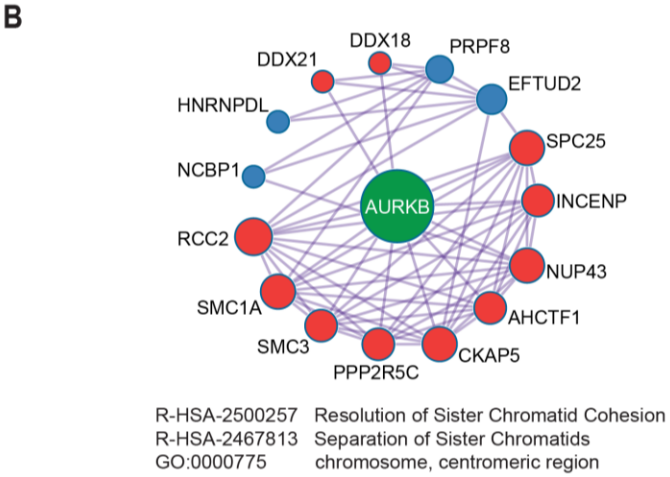

R-HSA-2500257 Resolution of Sister Chromatid Cohesion
R-HSA-2467813 Separation of Sister Chromatids
GO:0000775 chromosome, centromeric region

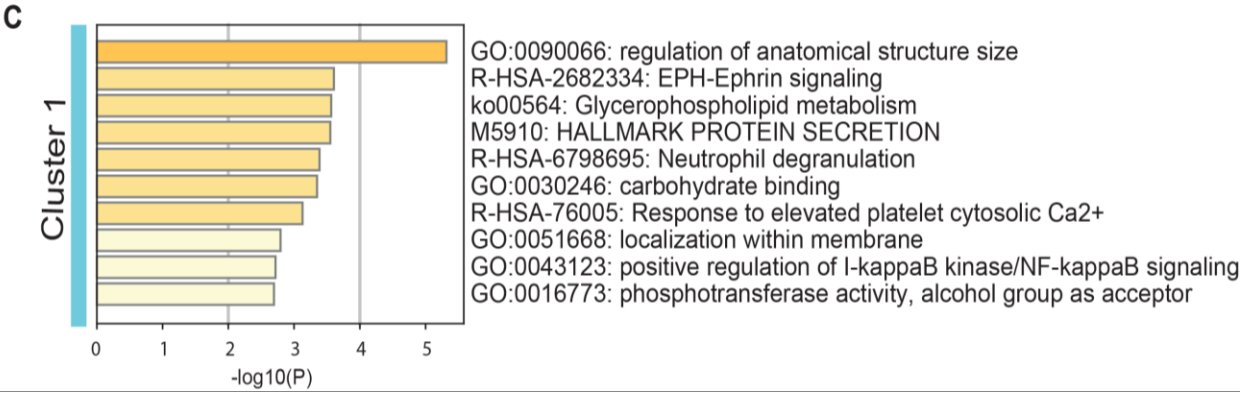

D

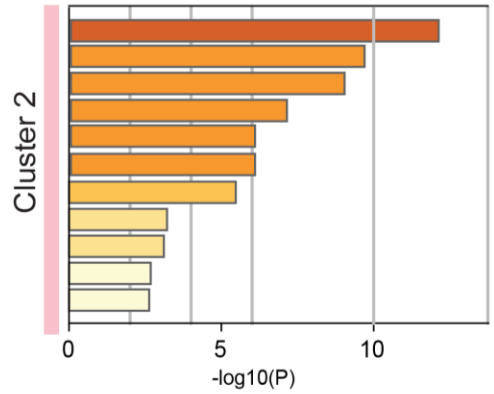

GO:0009150: purine ribonucleotide metabolic process
GO:0034976: response to endoplasmic reticulum stress
GO:0034976: response to endoplasmic reticulum stress
ko00280: Valine, leucine and isoleucine degradation
GO:0009205: purine ribonucleoside triphosphate metabolic process
R-HSA-2262752: Cellular responses to stress
GO:0062197: cellular response to chemical stress
M5902: HALLMARK APOPTOSIS
WP615: Senescence and autophagy in cancer
R-HSA-111465: Apoptotic cleavage of cellular proteins
M5939: HALLMARK P53 PATHWAY

E

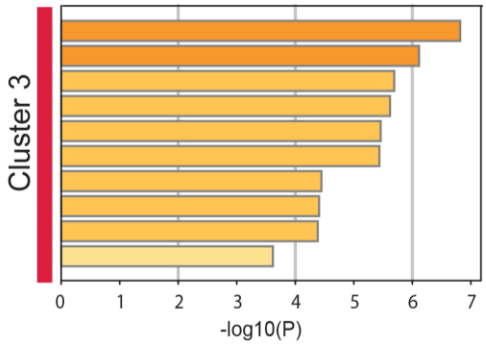

R-HSA-6798695: Neutrophil degranulation
GO:1904724: tertiary granule lumen
R-HSA-71387: Metabolism of carbohydrates
GO:1901699: cellular response to nitrogen compound
R-HSA-1169410: Antiviral mechanism by IFN-stimulated genes
hsa00230: Purine metabolism
GO:0060485: mesenchyme development
GO:0048471: perinuclear region of cytoplasm
GO:0006913: nucleocytoplasmic transport
WP3888: VEGFA-VEGFR2 signaling pathway

F

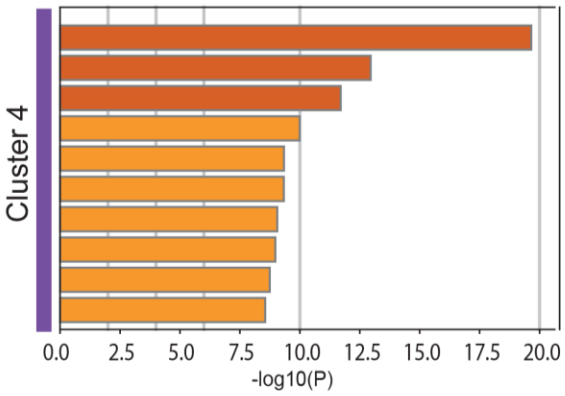

GO:0030117: membrane coat
GO:1904813: ficolin-1-rich granule lumen
WP3888: VEGFA-VEGFR2 signaling pathway
GO:0045296: cadherin binding
GO:0030118: clathrin coat
GO:0051668: localization within membrane
GO:0048471: perinuclear region of cytoplasm
GO:0042803: protein homodimerization activity
GO:0006897: endocytosis
GO:0006914: autophagy

G

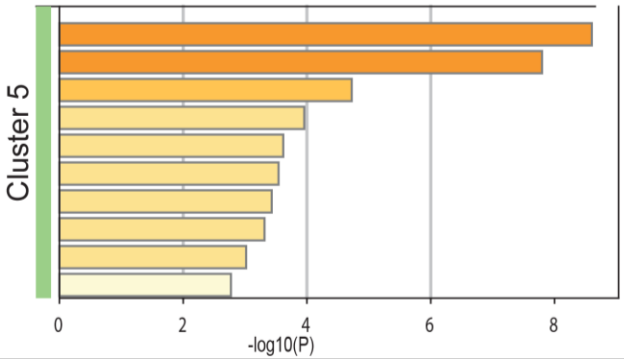

GO:0022613: ribonucleoprotein complex biogenesis
GO:1990904: ribonucleoprotein complex
GO:0006412: translation
GO:0042254: ribosome biogenesis
R-HSA-2467813: Separation of Sister Chromatids
M5926: HALLMARK MYC TARGETS V1
GO:0006457: protein folding
GO:0016607: nuclear speck
GO:0005759: mitochondrial matrix
GO:0043484: regulation of RNA splicing

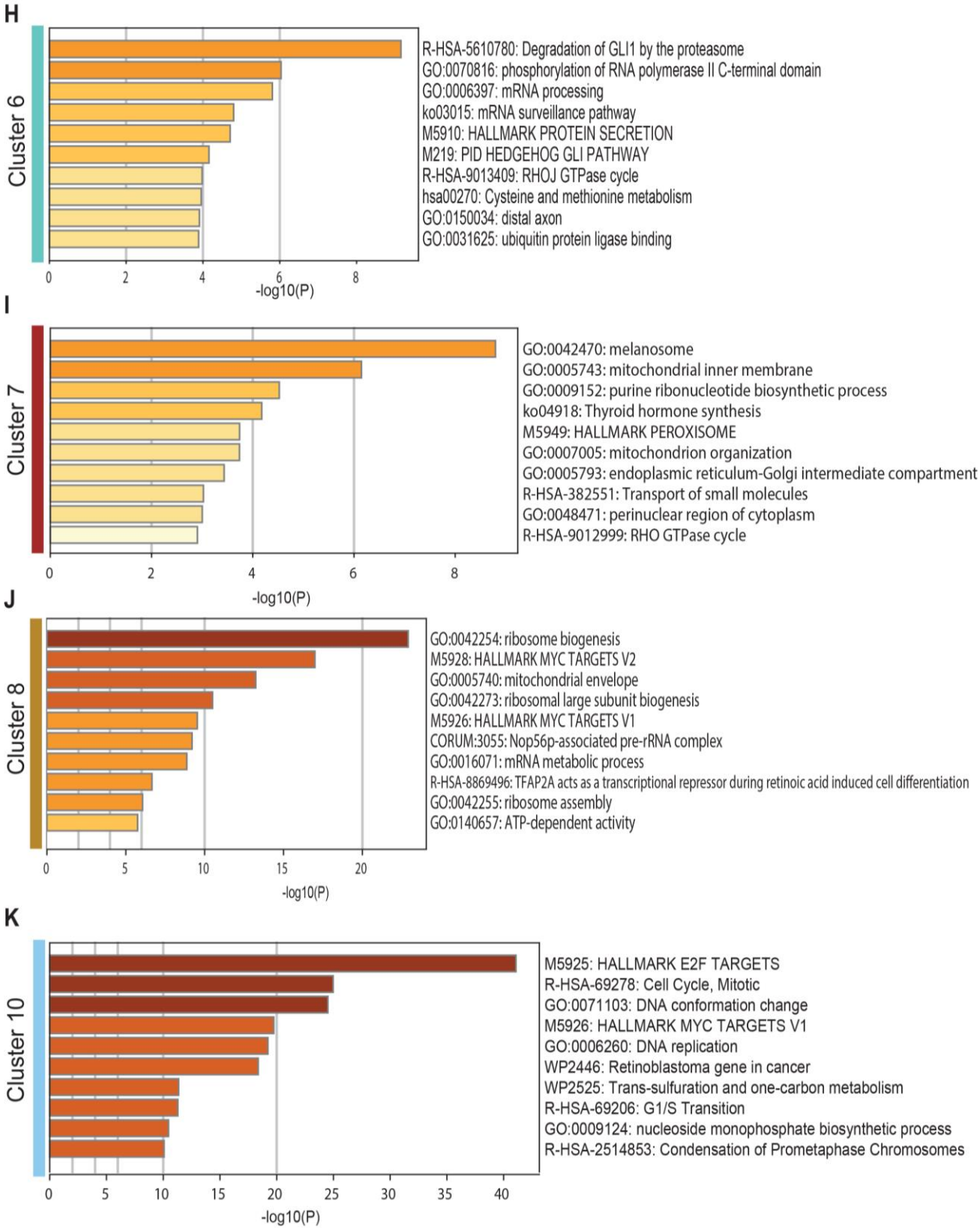
H
Cluster 6
R-HSA-5610780: Degradation of GLI1 by the proteasome
GO:0070816: phosphorylation of RNA polymerase II C-terminal domain
GO:0006397: mRNA processing
ko03015: mRNA surveillance pathway
M5910: HALLMARK PROTEIN SECRETION
M219: PID HEDGEHOG GLI PATHWAY
R-HSA-9013409: RHOJ GTPase cycle
hsa00270: Cysteine and methionine metabolism
GO:0150034: distal axon
GO:0031625: ubiquitin protein ligase binding
0 2 4 6 8
-log10(P)
I
Cluster 7
GO:0042470: melanosome
GO:0005743: mitochondrial inner membrane
GO:0009152: purine ribonucleotide biosynthetic process
ko04918: Thyroid hormone synthesis
M5949: HALLMARK PEROXISOME
GO:0007005: mitochondrion organization
GO:0005793: endoplasmic reticulum-Golgi intermediate compartment
R-HSA-382551: Transport of small molecules
GO:0048471: perinuclear region of cytoplasm
R-HSA-9012999: RHO GTPase cycle
0 2 4 6 8
-log10(P)
J
Cluster 8
GO:0042254: ribosome biogenesis
M5928: HALLMARK MYC TARGETS V2
GO:0005740: mitochondrial envelope
GO:0042273: ribosomal large subunit biogenesis
M5926: HALLMARK MYC TARGETS V1
CORUM:3055: Nop56p-associated pre-rRNA complex
GO:0016071: mRNA metabolic process
R-HSA-8869496: TFAP2A acts as a transcriptional repressor during retinoic acid induced cell differentiation
GO:0042255: ribosome assembly
GO:0140657: ATP-dependent activity
0 5 10 15 20
-log10(P)
K
Cluster 10
M5925: HALLMARK E2F TARGETS
R-HSA-69278: Cell Cycle, Mitotic
GO:0071103: DNA conformation change
M5926: HALLMARK MYC TARGETS V1
GO:0006260: DNA replication
WP2446: Retinoblastoma gene in cancer
WP2525: Trans-sulfuration and one-carbon metabolism
R-HSA-69206: G1/S Transition
GO:0009124: nucleoside monophosphate biosynthetic process
R-HSA-2514853: Condensation of Prometaphase Chromosomes
0 5 10 15 20 25 30 35 40
-log10(P)

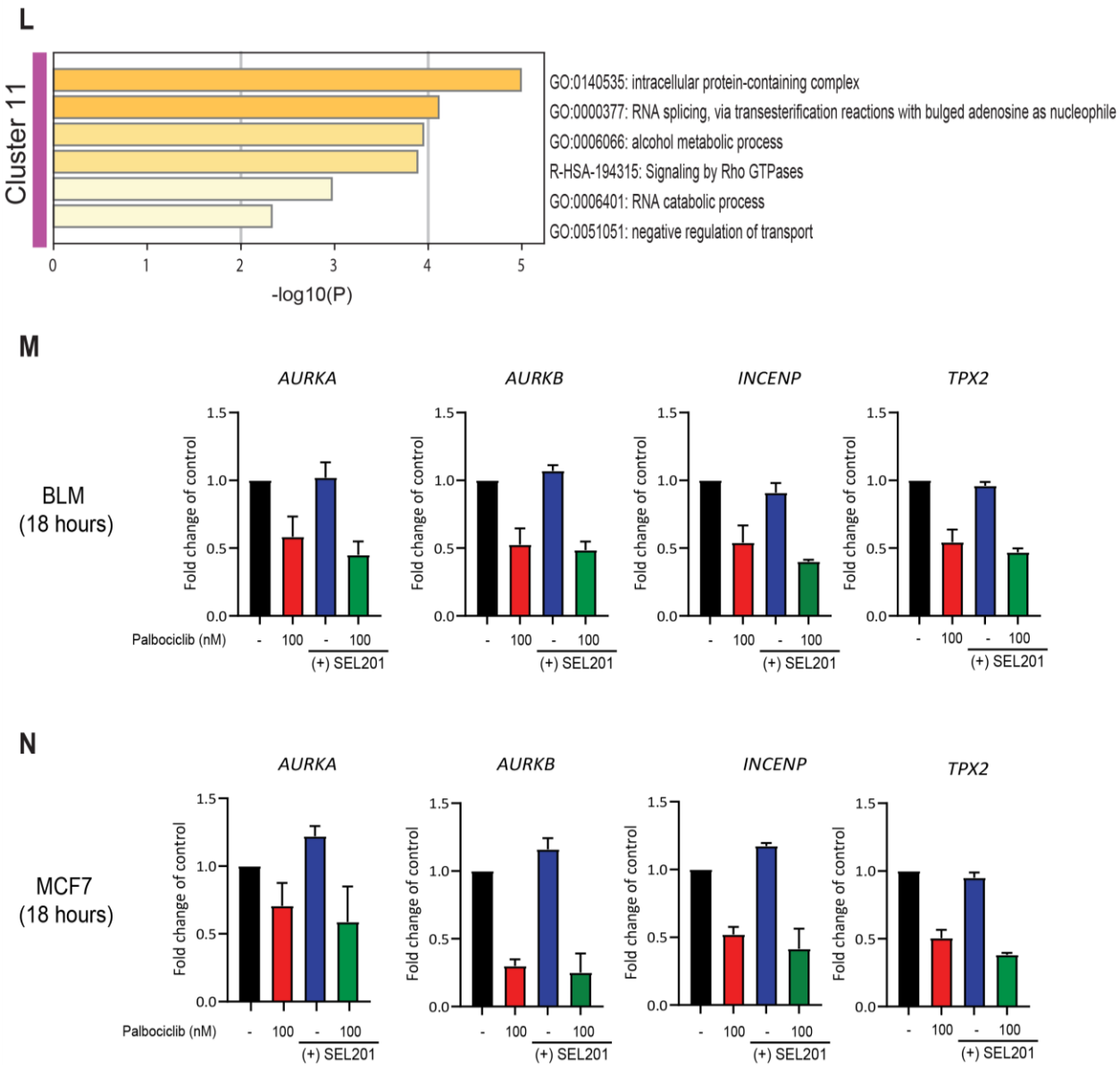

Supplemental Figure 2.2: Pathway analysis of all clusters from the differential protein expression analysis.

A. Differential expression heatmap and gene set enrichment analysis of hallmark E2F targets (M5925) detected in our dataset. **B**. AURKB network of protein-protein interactions whose expression are repressed in the combination (see supplemental methods for details) **C**. Pathway analysis of cluster 1. **D**. Pathway analysis of cluster 2. **E**. Pathway analysis of cluster 3. **F**. Pathway analysis of cluster 4. **G**. Pathway analysis of cluster 5. **H**. Pathway analysis of cluster 6. **I**. Pathway analysis of cluster 7. **J**. Pathway analysis of cluster 8. **K**. Pathway analysis of cluster 10. **L**. Pathway analysis of cluster 11. **M**. qPCR analysis of BLM melanoma cells treated with either monotherapy or the combination demonstrating transcriptional repression of critical genes involved in mitosis. **N**. qPCR analysis of MCF7 breast cancer cells treated with either monotherapy or the combination demonstrating transcriptional repression of critical genes involved in mitosis.

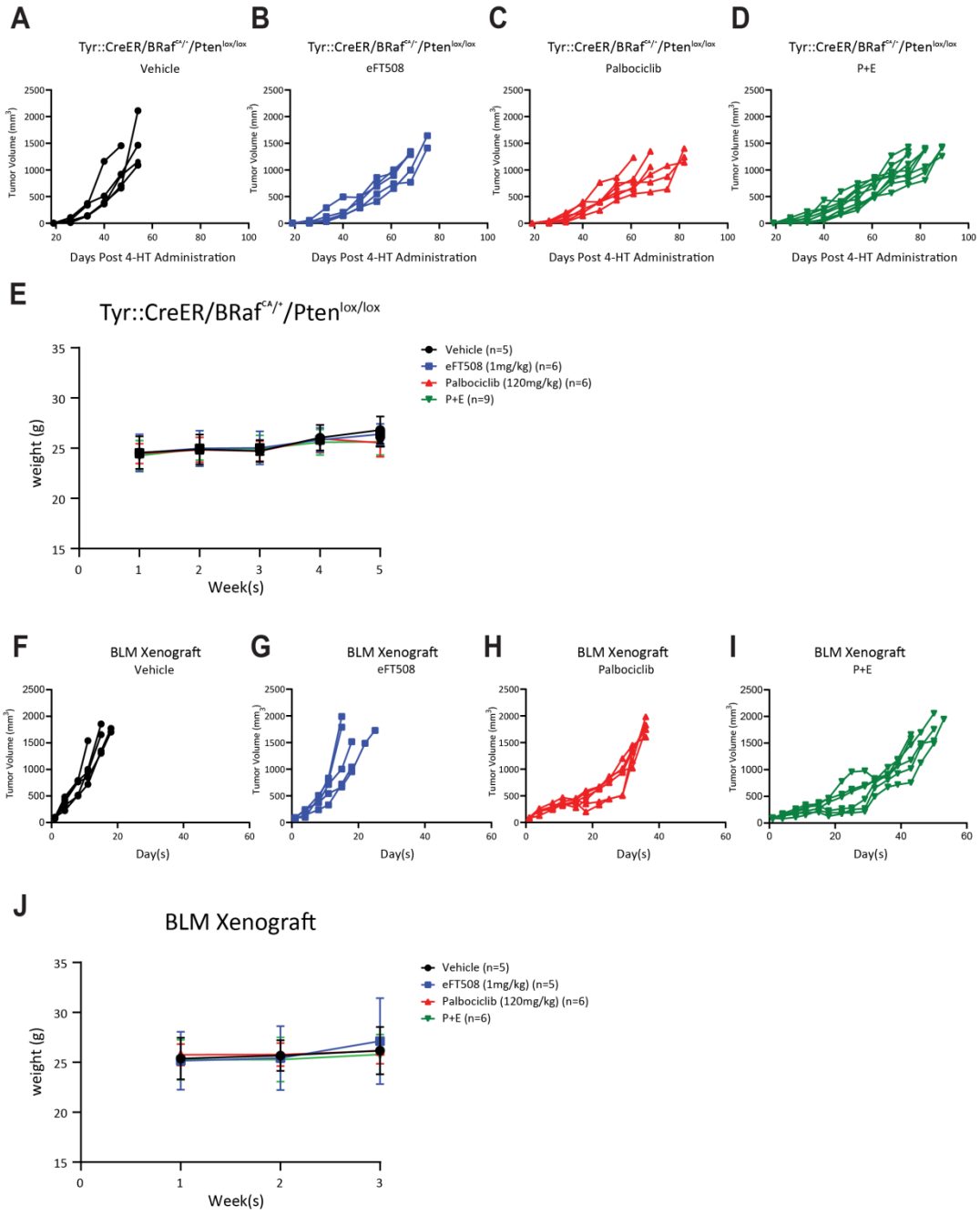

Supplemental Figure 2.3: Co-targeting MNK1/2 and CDK4/6 in vivo improves overall survival in murine models of melanoma.

A-D. Tumor volume graphs depicting the tumor growth of individual mice upon 4-HT administration and treatment with either monotherapy or the combination. **E**. Graph depicting the average body weight of all mice in each cohort over the duration of 5 weeks. **F-I**. Tumor volume graphs depicting the tumor growth of individual mice upon subcutaneous injection of BLM cells and treatment with either monotherapy or the combination. **J**. Graph depicting the average body weight of all mice in each cohort over the duration of 3 weeks

Supplemental Method

Sample preparation for mass spectrometry

Proteins from BLM cells were extracted in lysis buffer containing 5% sodium dodecyl sulfate (SDS) and 100 mM TRIS pH 7.8. Samples were subsequently heated to 99°C for 10 minutes and subjected to probe based ultrasonication with 3 x 5s rounds at 26% amplitude, using a Sonic Dismembrator (Thermo Fisher Scientific). The lysate underwent centrifugation at 20,000 x g for 2 minutes to remove insoluble debris. After dilution of an aliquot of the lysate to <1% SDS, the protein content was assessed by bicinchoninic acid assay (BCA) (Pierce/Thermo). In the remaining sample, protein disulfide bonds were reduced by addition of tris(2-carboxyethyl)phosphine (TCEP) to a final concentration of 20 mM and incubation at 60°C for 30 minutes. Free cysteines were alkylated by incubation with iodoacetamide at a final concentration of 30 mM and incubated for 30 minutes at 37°C in the dark. An equivalent of 20 µg of total protein (at 1 mg/mL in lysis buffer) was used for proteolytic digestion using suspension trapping (S-TRAP) (PMID: 24678027). In brief, proteins were acidified by adding phosphoric acid to a final concentration of 1.3% v/v. The sample was then diluted in 165 µL of S-TRAP loading buffer (9:1 methanol:water in 100 mM TRIS, pH 7.8) and loaded onto an S-TRAP Micro cartridge (Protifi LLC, Huntington NY) and spun at 4,000 x g for 2 minutes. Samples were washed with 150 µL of STRAP loading buffer three times. Proteins were then digested using trypsin (Promega) at a 1:10 enzyme to substrate ratio for 2 hours at 47°C. Peptides were eluted with 40 µL of 50 mM ammonium bicarbonate, 0.1% formic acid in water, and 50% acetonitrile. Peptides were then desalted using self-made R3-

STAGE tips. Desalted peptides were vacuum concentrated and reconstituted in 0.1% trifluoroacetic acid (TFA) prior to analysis by LC-MS/MS.

LC-MS/MS acquisition and data analysis

Samples were analyzed by data dependent acquisition (DDA) using an Easy-nLC 1200 online coupled to a Q Exactive Plus (both Thermo Fisher Scientific). After loading onto a precolumn (Acclaim PepMap 100 C18, 3 µm particle size, 75 µm inner diameter x 2 cm length) in 0.1% formic acid (buffer A), peptides were separated using a 100-min binary gradient from 3-40% of buffer B (84% acetonitrile, 0.1% formic acid) on the main column (Acclaim PepMap 100 C18, 2 µm particle size, 75 µm inner diameter x 25 cm length) at a flow rate of 300 nL/min. Full MS scans were acquired from m/z 350-1,500 at a resolution of 70,000, with an automatic gain control (AGC) target of 1×10^6 ions and a maximum injection time of 50 ms. The 15 most intense ions (charge states +2 to +4) were isolated with a window of m/z 1.2, an AGC target of 2×10^4 and a maximum injection time of 64 ms and were fragmented using a normalized higher-energy collisional dissociation (HCD) energy of 28. MS/MS were acquired at a resolution of 17,500 and the dynamic exclusion was set to 40 s. DDA MS raw data was processed with Proteome Discoverer 2.5 (Thermo Scientific; RRID:SCR_014477) and searched using Sequest HT against a human UniProt FASTA database (downloaded October 10th 2019, 20,360 target sequences). The enzyme specificity was set to trypsin with a maximum of 2 missed cleavages. Carbamidomethylation of cysteine was set as a fixed modification and oxidation of methionine as a variable modification. The precursor ion mass tolerance was set to 10 ppm, and the product ion mass tolerance was set to 0.02 Da. Percolator was used to assess posterior error probabilities and the data was filtered

using a false discovery rate (FDR) <1% on peptide and protein level. The Minora feature detector node of Proteome Discoverer was used for label free quantitation (LFQ) based on precursor areas. In instances where proteins were quantified in 2 of 3 samples from one sample group, missing values were imputed using low abundance resampling in the precursor ions quantifier node. LFQ abundances were normalized based on the total peptide amount per sample. Only proteins quantified with at least 2 protein-unique peptides were retained in the study.

Pathway and protein interaction analysis

Differential expression of proteins was determined with Perseus software using an FDR of 0.05. The list of proteins detected in at least 2 groups was retained and clustered using unbiased hierarchical clustering. Proteins in the clusters were input and analyzed for pathway enrichment and protein-protein interaction into Metascape using default settings. The top 100 pathway were maintained (Supplemental Table 2.5). Visualization of protein –protein interaction was processed on Cytoscape (RRID:SCR_003032). For Gene-Set Enrichment Analysis, pre-ranked list of proteins based on differential expression in cluster 9 were run against Hallmark E2F Targets (M5925) from MSigDB in GSEA tool (RRID:SCR_005724).

Supplemental Tables

Supplemental Table 2.1: Detailed information of the primary antibodies used for western blotting, and immunohistochemistry.

Target	Antibody Source and Catalog #	Application	Dilution
p-Rb	Cell Signaling #8516	Western Blot	1:500
Rb	Santa Cruz Biotechnology #sc-50	Western Blot	1:1000
Rb	BD Biosciences #554136	Western Blot	1:500
ISG15	Abcam #ab14374	Western Blot	1:1000
ATG7	Santa Cruz Biotechnology #sc8668	Western Blot	1:1000
PDCD4	Fortis Life Sciences #A301-107A	Western Blot	1:1000
Fibronectin	BD Biosciences #610077	Western Blot	1:1000
p-eIF4E	Cell Signaling #9741	Western Blot	1:1000
eIF4E	BD Biosciences #610270	Western Blot	1:1000
AURKB	Cell Signaling #3094	Western Blot	1:1000
TPX2	Cell Signaling #12245	Western Blot	1:1000
Survivin	Cell Signaling #2808	Western Blot	1:1000
Cyclin A	Santa Cruz Biotechnology #sc-271682	Western Blot	1:1000
p27	Santa Cruz Biotechnology #sc-528	Western Blot	1:1000
GAPDH	Cell Signaling #2118	Western Blot	1:5000
α-actinin	Santa Cruz Biotechnology #sc-17829	Western Blot	1:1000
β-actin	Sigma Aldrich #A5441	Western Blot	1:5000
MNK1	Cell Signaling #2195	Western Blot	1:1000
Vinculin	Cell Signaling #13901	Western Blot	1:1000
p-eIF4E	Abcam #ab76256	IHC	1:50

Supplemental Table 2.2: Detailed information of the primers used for qPCR analysis.

Gene	Forward sequence 5'-3'	Reverse sequence 5'-3'
MKNK1 (NM_001135553)	GAGGTTCCATCTTAGCCCACAT	ACGATGAGCAATGCCTTTGGT
MKNK2 (NM_199054)	CGCCTTGGACTTTCTGCATAA	TCACAGATCTTCACGGGGGA
INCENP (NM_020238)	AGGCTCCTGAATGTTGAGGTGC	GTGTGCTGTTGGCAATCTCCGT
TPX2 (NM_012112)	TTCAAGGCTCGTCCAAACACCG	GCTCTCTTCTCAGTAGCCAGCT
AURKA (NM_198433)	GCAACCAGTGTACCTCATCCTG	AAGTCTTCCAAAGCCCACTGCC
AURKB (NM_004217)	GGAGTGCTTTGCTATGAGCTGC	GAGCAGTTTGGAGATGAGGTCC
RPLP0 NM_001002.4	TCCTCGTGGAAGTGACATCGT	CTGTCTTCCCTGGGCATCA
ACTB (NM_001101)	AGGCACCAGGGCGTGAT	GCCCACATAGGAATCCTTCTGAC

Supplemental Table 2.3: Detailed information of the gRNA and shRNA used for knockdown experiments.

Gene	**Sequence 5'-3'**
MKNK1 gRNA	GGGAGGAGCGATCTGCAGGT
MKNK2 gRNA	GCAGGAGAAAGGCGATCCTG
Scramble gRNA	GTCCACCCTTATCTAGGCTA
MKNK1 shRNA TRCN0000314803	CCTATGCCAAAGTTCAAGGTG
MKNK2 shRNA TRCN0000199855	GAGGCTAGCATCTACGACAAG

Supplemental Table 2.4: Statistical analysis

NB: within the table, P indicates palbociclib, S indicates SEL201 and E indicates eFT508

Figure # and Description	Number of Samples	Statistical Test	p-value
1c BLM colony forming assay (Palbociclib + SEL201)	3 independent experiments for P+S (6 data points per condition)	One-way ANOVA	P50 vs. P50+S p=0.0009; P100 vs. P100+S p=0.0011
1c BLM colony forming assay (Palbociclib + eFT508)	4 independent experiments for P+E (8 data points per condition)	One-way ANOVA	one-way ANOVA P50 vs. P50+E p=0.0638; P100 vs. P100+E p=0.002
1d MEWO colony forming assay	3 independent experiments (6 data points per condition)	One-way ANOVA	P100 vs P100+S p=0.0058
1g (MEWO shRNA colony forming assay	2 independent experiments (4 data points per condition)	One-way ANOVA	shCTL P50 vs shMNK1/2 P50 p=0.0037; shCTL P100 vs shMNK1/2 P100 p=0.0101
2c MCF7 colony forming assay	3 independent experiments (6 data points per condition)	One-way ANOVA	P25 vs. P25+S p=<0.0001; P50 vs P50+S p=<0.0001
2d T47D colony forming assay)	3 independent experiments (6 data points per condition)	One-way ANOVA	P25 vs.P25+S p=0.0483; P50 vs P50+s p=0.0379
4g BLM senescence assay	2 independent experiments	One-way ANOVA	P vs. P+S p=0.0047; S vs. PS p=0.003
4h MCF7 senescence assay	3 independent experiments	One-way ANOVA	P vs. P+S p=0.0017; S vs. PS p=<0.0001
5a CHL-1 Parental colony forming assay	3 independent experiments	One-way ANOVA	P30 vs. P30+S p=<0.0001; P100 vs. P100+S p=0.0037
5a CHL-1 PalboR colony forming assay	3 independent experiments	One-way ANOVA	P30 vs. P30+S p=<0.0001; P100 vs. P100+S p=<0.0001; P300 vs. P300+S p=<0.0001
5b MCF7 Parental colony forming assay	3 independent experiments	One-way ANOVA	P25 vs. P25+S p=0.001; P100 vs. P100+S p=0.1864
5b MCF7 PalboR colony forming assay	3 independent experiments	One-way ANOVA	P25 vs. P25+S p=<0.0001; P100 vs. P100+S p=<0.0001
5d MCF7 Parental vs. PalboR *MKNK2* qPCR	2 independent experiments	t-test (unpaired)	Parental vs. PalboR p=0.0460
5e T47D Parental	3 independent experiments	One-way	P25 vs. P25+S

colony forming assay		ANOVA	p=<0.0001; P100 vs. P100+S p=0.0016
5e T47D PalboR colony forming assay	3 independent experiments	One-way ANOVA	P25 vs. P25+S p=<0.0001; P100 vs. P100+S p=<0.0001; P250 vs. P250+S p=<0.0001; P500 vs. P500+S p=<0.0001
5g T47D Parental vs. PalboR *MKNK2* qPCR	4 independent experiments	t-test (unpaired)	Parental vs. PalboR p=0.0036
6a BRAF/PTEN Tumor growth curve (Day 54)	6 mice in Palbociclib cohort vs. 9 mice in P+E cohort	Two-way ANOVA	P vs. P+E p=0.0402
6b BRAF/PTEN Kaplan-Meier	5 mice in Vehicle cohort 6 mice in eFT508 cohort 6 mice in Palbociclib cohort vs. 9 mice in P+E cohort	Log-rank Test	Veh vs. P+E p=<0.0001 E vs. P+E p=<0.0001 P vs. P+E p=0.0145
6c p-eIF4E IHC staining	3 mice per cohort stained for p-eIF4E	One-way ANOVA	Veh vs. P+E p=0.0140; P vs. P+E p=0.0171
6d BLM Xenograft Tumor growth curve (Day 32)	6 mice in Palbociclib cohort vs. 6 mice in P+E cohort	Two-way ANOVA	P vs. P+E p=0.0006
6f BLM Xenograft Kaplan-Meier	5 mice in Vehicle cohort 5 mice in eFT508 cohort 6 mice in Palbociclib cohort 6 mice in P+E cohort	Log-rank Test	Veh vs. P+E p=0.007; E vs. P+E p=0.007; P vs. P+E p=0.0006

Supplemental Table 2.6: List of senescence markers modulated in BLM melanoma cells by the palbociclib (P)+ SEL201 (S) combination therapy compared to vehicle control.

Protein	Log2 Fold Change P+S vs. Control	Reference PMID	Status and role during senescence
PDCD4	1.89	12054647	Increased
GLB1	1.54	16626397	Increased; key marker protein responsible for SA-b-gal activity
IGFBP7	1.32	18267069	Increased; part of SASP
		24201810	
FN1	1.31	20078217	Increased; part of SASP
ISG15	1.2	19802007	Increased
MVP	0.89	18600231	Increased; confers apoptosis resistance
ATG7	0.8	31931659	Increased; Key player in senescence induction
VAT1	0.72	34637314	Increased
LMNB1	-0.54	22496421	Decreased; Lamin B1 loss is a general marker of senescence
HMGB2	-0.71	29706538	HMGB2 is decreased during senescence allowing CTCF clustering
HIST1H1B	-0.64	17158953	Decreased; Decreased H1 during senescence
HIST1H1C	-0.87		
HIST1H1D	-1.11		
HIST1H1E	-0.7		
MCM2	-0.7	12809602, 24351540, 31092751, 15377661, 15716376, and 21205865	Decreased; E2F gene targets are downregulated during cell senescence
MCM4	-0.96		Decreased; E2F gene targets are downregulated during cell senescence
MCM5	-1.02		Decreased; E2F gene targets are downregulated during cell senescence
MCM6	-0.7		Decreased; E2F gene targets are downregulated during cell senescence
MCM7	-0.84		Decreased; E2F gene targets are downregulated during cell senescence
RFC4	-0.85		Decreased; E2F gene targets are downregulated during cell senescence
PCNA	-0.58		Decreased; E2F gene targets are downregulated during cell senescence
MSH6	-0.73		Decreased; E2F gene targets are downregulated during cell senescence
SMC4	-0.62		Decreased; E2F gene targets are downregulated during cell senescence
SMC1A	-0.65		Decreased; E2F gene targets are downregulated during cell senescence
GINS3	-2.09		Decreased; E2F gene targets are downregulated during cell senescence

In chapter 2 of this body of work, we have demonstrated a role for the MNK1/2-eIF4E axis in impacting the anti-neoplastic effectiveness of the CDK4/6 inhibitor, palbociclib in therapy naïve and therapy-resistant cancer models.

However, independent of phosphorylating eIF4E, the cellular functions of the MNK1/2 kinases remain elusive. Other substrates of MNK1 and MNK2 have been identified. However, there have been limited subsequent studies verifying the impact of their interaction in *in vivo* models.

Therefore, in the next chapter, we set forth, and used a proteomics-based approach to determine whether there are other interactors of the MNK1/2 kinases. In doing so, we hoped to uncover additional functions of MNK1 and MNK2 that are uncoupled from phosphorylating eIF4E.

The MNK1/2 kinases have been implicated in numerous cellular processes including cell cycle and senescence. Identifying novel substrates of MNK1/2 would allow us to understand the impact of the kinases in cell growth, cancer development and progression. This is important because MNK1/2 inhibitors are being extensively tested for efficacy in malignancies. While MNK1/2 expression is dispensable for normal development, we don't understand how far-reaching the functions of these kinases are.

Overall, we aimed to identify a novel interactor and substrate, which could improve our understanding as to roles MNK1/2 play in cells. Additionally, it could provide us with insight as to how these kinases play a role in tumorigenesis and further determine the impact of their pharmacologic inhibition.

Chapter 3: Discovery of LARP1 as a novel substrate of MNK1

3.1 Preface

Despite having been identified more than two decades ago, our understanding of the breadth of biological functions that MNK1 regulates remains largely uncharacterized. Therefore, we performed mass spectrometry to identify novel interacting proteins of MNK1. Our data revealed proteins whose interaction with MNK1 has been previously reported, and included in our list of putative interacting proteins was the RNA-binding protein LARP1. Similar to eIF4E, LARP1 binds to mRNA at the 5'cap; and moreover, comparable to eIF4E, the activity of LARP1 has been demonstrated to be dependent on mTOR. However, the processes by which varied kinases regulate LARP1 activity is currently being debated. We know that MNK1 promotes mRNA translation by phosphorylating eIF4E on serine 209. We also know that LARP1 can repress the translation of mRNA. What remains unknown is whether MNK1 has additional roles in regulating mRNA translation through its interaction with LARP1. In this chapter, we describe the studies used to confirm the interaction between MNK1 and LARP1 and further investigate whether MNK1 activity alters RNA-binding activity of LARP1 to RPS6 TOP motif and poly (A_{25}).

Chapter 3 contains material to be included in a manuscript in preparation for publication as an original research article:

> **Prabhu SA,** Goncalves C, Méant A, Kajjo S, Sosa J, Arredondo N, Richard VR, Dejgaard K, Fabian M, Fonesca B, Zahedi R, Berman AJ, Miller Jr. WH, del Rincón, SV (2023) Discovery of LARP1 as a novel substrate of MNK1.

3.2 Abstract

The MAP Kinase-interacting serine/threonine-protein kinases 1 and 2 (MNK1/2) are downstream of the highly deregulated MAP kinase pathway, and their activity has been associated with disease progression in numerous malignancies. However, our knowledge of the extent of MNK1/2 activity in cells is limited. MNK1/2 play a critical role in regulating mRNA translation by phosphorylating their most well characterized substrate, the translation initiation factor eIF4E on serine 209. While other substrates of MNK1/2 have been identified, they have proved challenging to validate *in vivo*. We thus employed a proteomics-based approach to identify novel interactors and substrates of the MNK1/2 kinases. Using this method, we identified numerous candidate proteins that may interact with MNK1, including the RNA-binding protein LARP1. Investigation of this interaction revealed that LARP1 specifically interacts with MNK1 but not MNK2, in an RNA-independent manner. We discovered that MNK1 interacts with the La-Module of LARP1 and that LARP1 interacts with the N-terminal polybasic region of MNK1. Furthermore, using phosphoproteomics and *in vitro* kinase assays, we discovered that MNK1 phosphorylates LARP1 on threonine 449. Mechanistically, we demonstrate that substituting threonine for alanine on 449 on LARP1 increases the affinity of the La-Module to RNA compared with the WT counterpart. Overall, these data identify LARP1 as a novel interactor of MNK1 and, moreover, reveal a novel mechanism by which the MNK1 kinase may regulate mRNA translation.

3.3 Introduction

Despite efforts to understand the process of cellular protein synthesis, the regulation of mRNA translation has been shown to be complex, with numerous key components. Cap-dependent mRNA translation initiates through the successful formation of the heterotrimeric protein complex Eukaryotic initiation factor 4F (eIF4F), with the ultimate goal of bringing mRNA to the 40S ribosome, facilitating the formation of the 80S ribosome complex [1, 2]. The eIF4F complex is comprised of the translation initiation factor eIF4E, which binds the m^7GTP cap structure on mRNA, the helicase eIF4A that unwinds secondary structures on mRNA, and the scaffold protein eIF4G, which recruits the 40S ribosome to initiate start codon scanning [1-3]. The availability of eIF4E to bind the 5'cap is controlled by the kinase activity of the mammalian target of rapamycin (mTOR) [3, 4]. Signaling through the PI3K-AKT/mTOR pathway causes the phosphorylation of eIF4E-binding proteins, 4EBP1/2 [4]. Phosphorylation of 4EBP1/2 results in the release of eIF4E, which is available to bind eIF4G, and ultimately results in mRNA translation. While the availability of the translation initiation factor eIF4E critically regulates cap-dependent mRNA translation, recent research has demonstrated that this process is more nuanced than previously thought. Similar to eIF4E, another protein, LARP1 was discovered to regulate translation via binding to the 5'cap of mRNA [5 – 7]. Furthermore, the activity of LARP1 has been demonstrated to be reliant on the kinase activity of mTOR [6, 8]. The phosphorylation of LARP1 by mTOR results in the dissociation of mRNA from LARP1, allowing eIF4E to bind the cap and initiate translation [5 – 9].

In addition to mTOR-mediated regulation of eIF4E availability, the activity of eIF4E is also regulated by the MAP Kinase-interacting serine/threonine-protein kinases 1 and 2 (MNK1 and MNK2) [3, 4]. The phosphorylation of eIF4E by MNK1 and MNK2 has been shown to increase the translation of a subset of mRNA's with oncogenic properties [3, 10-14]. Aside from eIF4E, only a handful of MNK1/2 substrates have been described and their *in vivo* relevance remains to be verified. Herein, we used a proteomics-based approach to identify novel interacting proteins, and thus potential phosphorylation substrates, of MNK1/2 kinases. Interestingly, we have discovered that MNK1 can interact with LARP1. Thus, we hypothesized that MNK1 may interact with LARP1 to regulate mRNA translation. Indeed, we discovered that MNK1 phosphorylates LARP1 on threonine 449. We further demonstrate that a T449A phosphodeficient La-Module on LARP1 binds RNA with a higher affinity than its WT counterpart.

3.4 Results

3.4.1 Proteomics-based identification of LARP1 as a novel interactor of MNK1

To identify novel interactors and potential substrates of MNK1, we used a proteomics approach. Using our previously published human A375 and murine D4M.3a melanoma models wherein we knocked out MNK1 (A375-KO and D4M.3a-KO) [14], we created isogenic model systems wherein we re-introduced WT-MNK1 in these cell lines (A375-MNK1 and D4M.3a-MNK1); Supplemental Figure 3.1A). Next, after brief exposure of the protein lysate to the crosslinker 3,3'-Dithiobis (sulfosuccinimidylpropionate) (DTSSP), we immunoprecipitated MNK1 and after washes and elution, we analyzed all proteins co-immunoprecipitated with MNK1 by mass

spectrometry (Figure 3.1A). Crosslinking immunoprecipitation with DTSSP has been used to identify numerous novel protein-protein interactions [15-18]. In an effort to avoid concentrations of DTSSP that would result in precluded co-immunoprecipitation or false positive interactions, we optimized the concentration of DTSSP in our experiment by performing a DTSSP-dose-dependent immunoprecipitation of MNK1 in A375-MNK1 and D4M.3a-MNK1 cells (Supplemental Figure 3.1B). We observed that at 50 µM and 100 µM of DTSSP, we co-immunoprecipitated higher amounts of eIF4G1, eIF4E1, and ERK2 compared with no DTSSP (Supplemental Figure 3.1B). Notably, we observed that at concentrations of DTSSP higher than 100 µM, the interactions between MNK1 and its canonical binding partners were hindered (Supplemental Figure 3.1B). Thus, we proceeded with using 50 µM DTSSP for our MNK1-interactome discovery assays. Analysis of the co-immunoprecipitated proteins in A375-MNK1 compared with A375-KO yielded 172 proteins that were found to bind to MNK1 (Figure 3.1B). Similarly, in D4M.3a-MNK1 cells compared with their knockout counterparts, we identified 70 proteins that bound to MNK1 (Figure 3.1B). When the lists from both cell lines were compared with each other, we observed 34 proteins that commonly co-immunoprecipitated with MNK1 (Figure 3.1B). Pathway analysis revealed an enrichment for proteins associated with the translation machinery (CORUM:742: eIF3 complex), translation initiation (GO:0006446), and regulation of translation (GO:0006417 and GO:0045727) (Figure 3.1C). As expected, we observed some of the canonical binding partners of MNK1, including eIF4G1, eIF4G2 and eIF4E [19 – 21] (Figure 3.1C). Importantly, we observed that LARP1 co-immunoprecipitated with MNK1 in both cell lines (Figure 3.1C). Similar to eIF4E, LARP1 binds the 5'cap of mRNA and has been

demonstrated to be a critical regulator of mRNA translation [5-8, 22]. Furthermore, comparable to eIF4E, the activity of LARP1 has been demonstrated to be dependent on mTOR [5-8]. Taking these data together, we proposed to prioritize the validation and characterization of a possible MNK1 interaction with LARP1.

In order to verify the mass spectrometry results above, we transiently overexpressed GST-MNK1 and GST-MNK2 independently in HEK293T cells. In the absence of DTSSP, we observed that LARP1 interacts with GST-MNK1, but not with GST-MNK2 (Figure 3.1D). Similarly, we observed that endogenous LARP1 co-immunoprecipitates with MNK1 in the BLM melanoma cells stably overexpressing MNK1 (Supplemental Figure 3.1B). Next, we wanted to verify that the interaction between MNK1 and LARP1 observed was not due to overexpression artifact. We performed immunoprecipitation in cells expressing endogenous levels of MNK1 and LARP1, and we observed that endogenous LARP1 co-immunoprecipitated with MNK1 in A375 and MCF7 (Figure 3.1E and Supplemental Figure 3.1C). Finally, we wanted to assess whether the interaction between MNK1 and LARP1 is a direct interaction or perhaps the co-immunoprecipitation was due to a proximity-based interaction with RNA. As some protein-protein interactions may be mediated by RNA [23, 24], we performed endogenous immunoprecipitation of MNK1 in the presence of the ribonuclease, RNAse A. In A375, we observed that the interaction between MNK1 and LARP1 was enhanced in conditions with depleted RNA compared with their control counterparts (Figure 3.1F). We observed similar results in HEK293T cells, where the depletion of RNA enhanced the binding of endogenous LARP1 to endogenous MNK1 (Supplemental Figure 3.1E).

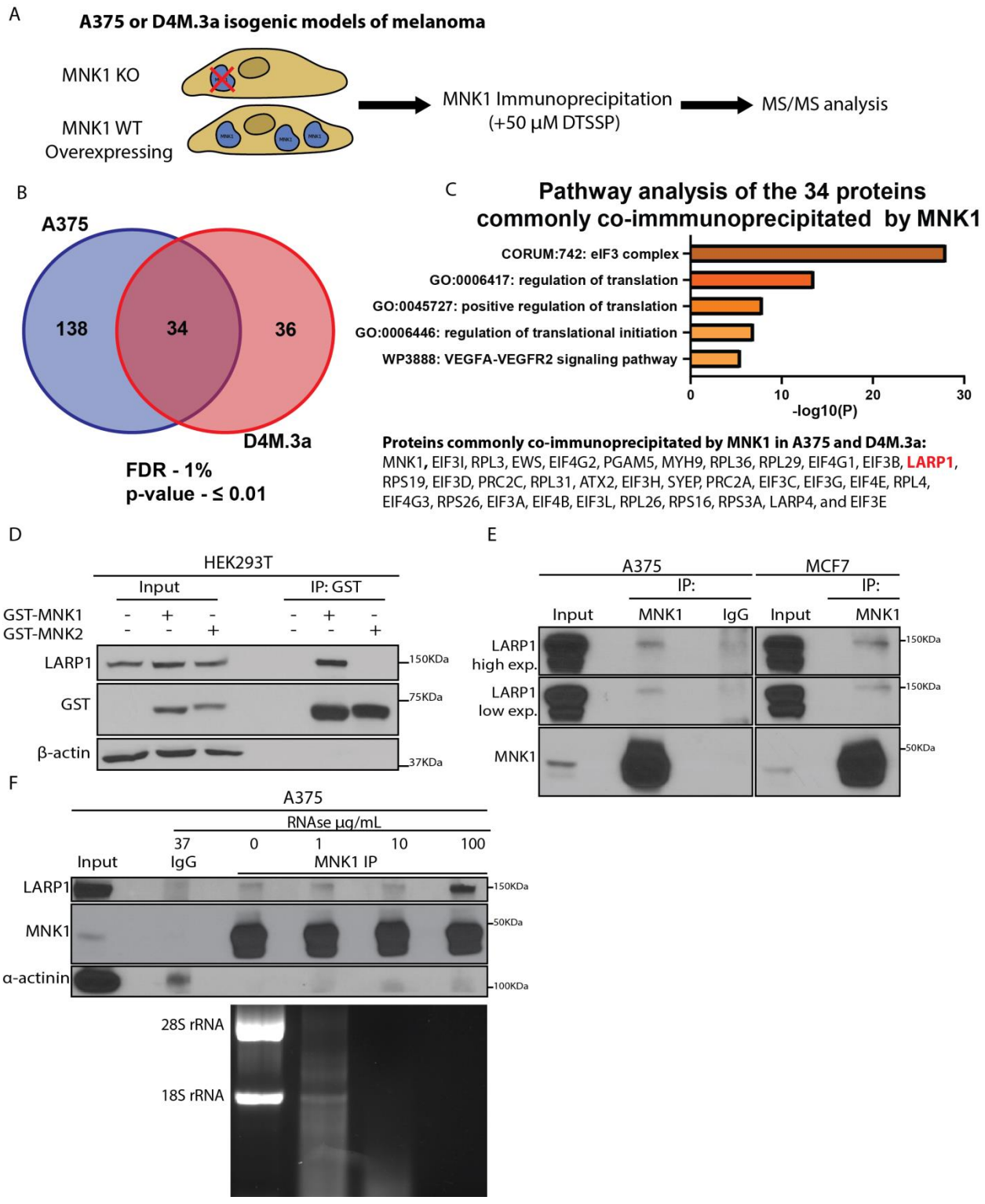

Figure 3.1: Proteomics based identification of LARP1 as an interacting protein of MNK1.
A: Schematic of the proteomics experiment to identify novel interactors of MNK1.**B:** Venn diagram of the overlapping co-immunoprecipitated proteins in A375 and D4M.3a melanoma cells. FDR – 1%; p-value - 0.01 **C:** Metascape pathway analysis and complete list of proteins that commonly co-immunoprecipitated

with MNK1 in A375 and D4M.3a cells. **D:** Immunoblot demonstrating that endogenous LARP1 co-immunoprecipitates with GST-MNK1 but not GST-MNK2 in HEK293T cells transiently overexpressing GST-tagged MNK1 or MNK2. **E:** Immunoblot demonstrating that endogenous LARP1 co-immunoprecipitates with endogenous MNK1 in A375 and MCF7 cells. **F:** Top panel: Immunoblot demonstrating that endogenous LARP1 co-immunoprecipitates with endogenous MNK1 in A375 cells in an RNA-independent manner. Bottom panel: agarose gel validation of RNA degradation by RNAse A in lysates used for immunoprecipitation in top panel.

3.4.2 MNK1 interacts with the La-Module of LARP1 and LARP1 interacts with the N-terminal region of MNK1

Prior work using full-length or deletion constructs of LARP1 has demonstrated that mTOR, via RAPTOR, interacts with the C-terminal region of LARP1 comprising the DM15 domain, while Poly(A) Binding Protein Cytoplasmic 1 (PABPC1) binds LARP1 on the La-Module (Supplemental Figure 3.2A) [7]. Using some of these previously published LARP1 deletion constructs, we next mapped the domains of LARP1 that are essential for MNK1 binding (Figure 3.2A) [7]. As we have shown that the MNK1:LARP1 interaction is enhanced in RNAse A treated samples (Figure 3.1F and Supplemental Figure 3.1E), we immunoprecipitated endogenous MNK1 from lysates derived from HEK293T cells transfected to express FLAG-LARP1 fragments in the presence of RNAse A. Western blotting of the immunoprecipitates revealed that endogenous MNK1 co-immunoprecipitates full-length LARP1 and interacts with the La-Module (FLAG-LARP1 205-509) in an RNA-independent manner (Figure 3.2B). Interestingly, we observed that the La-Module (205-509) of LARP1 co-immunoprecipitated with MNK1.

Similarly, we wanted to investigate the regions on MNK1 that are required for its interaction with LARP1. To test this, we generated a MNK1 mutant with substitution mutations at the nuclear localization sequence (NLS) by substituting R26/27/28A (Figure 3.2C Supplemental Figure 3.2B). It has been previously demonstrated that the

N-terminal, particularly the NLS region, on MNK1 is critical for its interaction with the scaffolding protein eIF4G1 [19, 20, and 25-27]. Consistent with prior literature, we observed that eIF4G1 was unable to co-immunoprecipitate with MNK1 harboring the mutated NLS (26-28 R-A) (Figure 3.2C). Interestingly, this MNK1 mutant was also unable to co-immunoprecipitate LARP1 (Figure 3.2C). However, we observed that LARP1 does interact with a different MNK1 mutant, containing a mutation at the nuclear export signal (MNK1 - L390S). (Figure 3.2C and Supplemental Figure 3.2B). Together, these data suggest that LARP1 directly binds MNK1 through the hydrophilic residues on the N-terminal of MNK1.

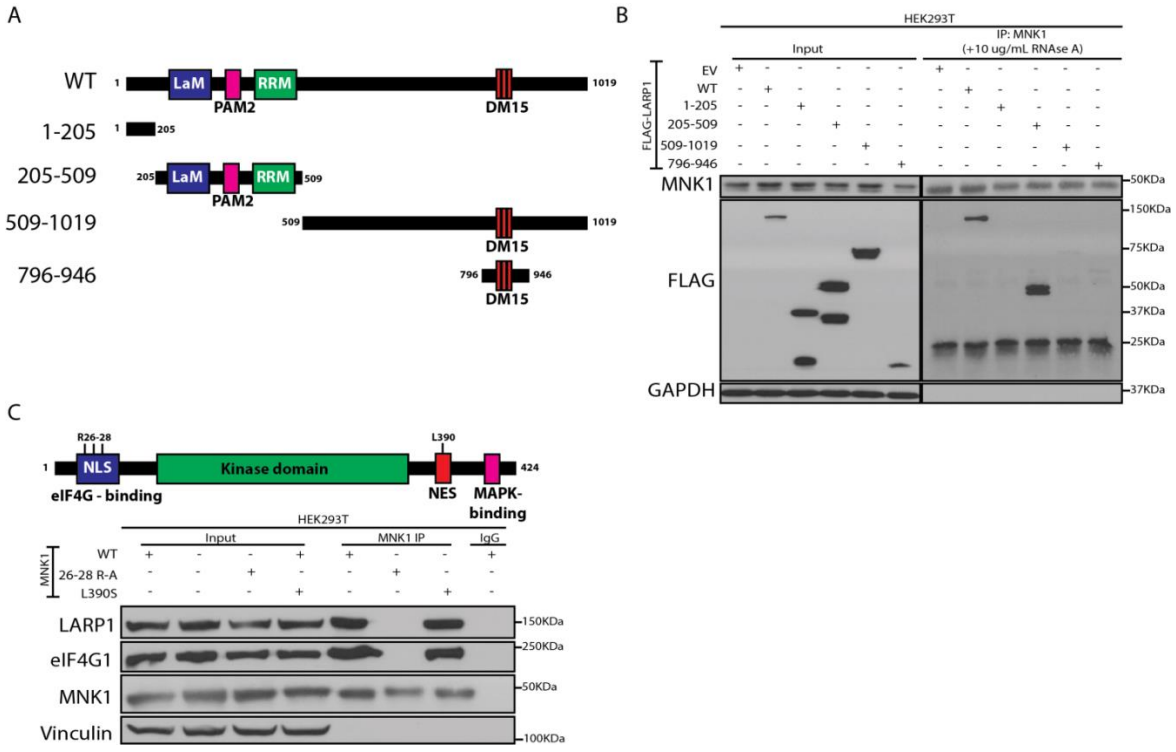

Figure 3.2 MNK1 interacts with LARP1 via the La-Module and LARP1 binds to the N-terminal region of MNK1.
A: Schematic of the domains on LARP1 and the various fragments utilized in downstream experiments. **B:** Immunoblot demonstrating that FLAG-tagged LARP1 WT and fragment 205-509 co-immunoprecipitates with MNK1 in HEK293T cells in an RNA-independent manner. **C:** Immunoblot demonstrating that the mutation of arginine residues at positions 26-28 on MNK1 precludes its interaction from LARP1 in HEK293T cells.

3.4.3 MNK1 phosphorylates LARP1 on the La-Module at Threonine 449

Considering that MNK1 regulates mRNA translation by phosphorylating eIF4E, a logical next step was to assess whether MNK1 can phosphorylate LARP1. To test this, overnight serum starved HEK293 cells were pre-treated with DMSO or the MNK1/2 inhibitor SEL201 for 1 hour followed by a 30-minute stimulation with Phorbol 12-Myristate 13-Acetate (PMA), a well-known MNK1/2-eIF4E activator (Figure 3.3A). The samples were then harvested and, after phosphopeptide enrichment, were analyzed by mass spectrometry (Figure 3.3A). As expected, PMA stimulated the phosphorylation of eIF4E and ERK1/2 in HEK293 cells. Moreover, the pre-treatment of HEK293 cells with SEL201 inhibited the phosphorylation of eIF4E (Figure 3.3B). Analysis of the mass spectrometric data indicated that the phosphorylation of threonine 449 on LARP1 was significantly diminished in cells treated with SEL201+PMA compared with DMSO+PMA (Figure 3.3C). This was particularly interesting as we have shown that MNK1 interacts with the La-Module of LARP1, which contains T449 (Figure 3.2B-construct containing amino acids 205-509). To further interrogate this, HEK293T cells transfected to express full-length FLAG-LARP1 were treated with SEL201 for 3 hours (Figure 3.3D). We then immunoprecipitated FLAG-LARP1 and following phosphopeptide enrichment, the sample was analyzed by mass spectrometry (Figure 3.3D). Analysis of the mass spectrometry data once again showed that the phosphorylation of LARP1 at threonine 449 was significantly repressed in cells treated with the MNK1/2 inhibitor compared with DMSO control (Figure 3.3E).

We next sought to verify that MNK1 could phosphorylate LARP1 on T449 using *in vitro* radioactive ATP kinase assays. We purified either the WT-La-Module (310 to 540) (Supplemental Figure 3.3 A-C) or the mutant La-Module (T449A) (Supplemental Figure 3.3 D-F) from BL21 (BE3) *E. coli* cells. Additionally, we used purified DM15 (796-946) as a negative control because we showed that MNK1 does not interact with this fragment (Figure 3.2B). We discovered that MNK1 is indeed able to phosphorylate the WT-La-Module, but not the DM15 region on LARP1 (Figure 3.3F). Consistent with T449A being a putative phosphorylation site of MNK1, we observed that the La-Module-T449A mutant is not phosphorylated as robustly as the unmutated La-Module. The latter suggests that MNK1 potentially phosphorylates additional serine or threonine site(s) within the La-Module. We verified the specificity of the GST-MNK1 recombinant protein using GST-eIF4E, whereby we performed kinase assays in the absence of radioactive ATP and detected the phosphorylation of eIF4E by immunoblotting with an eIF4E^{S209} phosphorylation specific antibody (Supplemental Figure 3.3G).

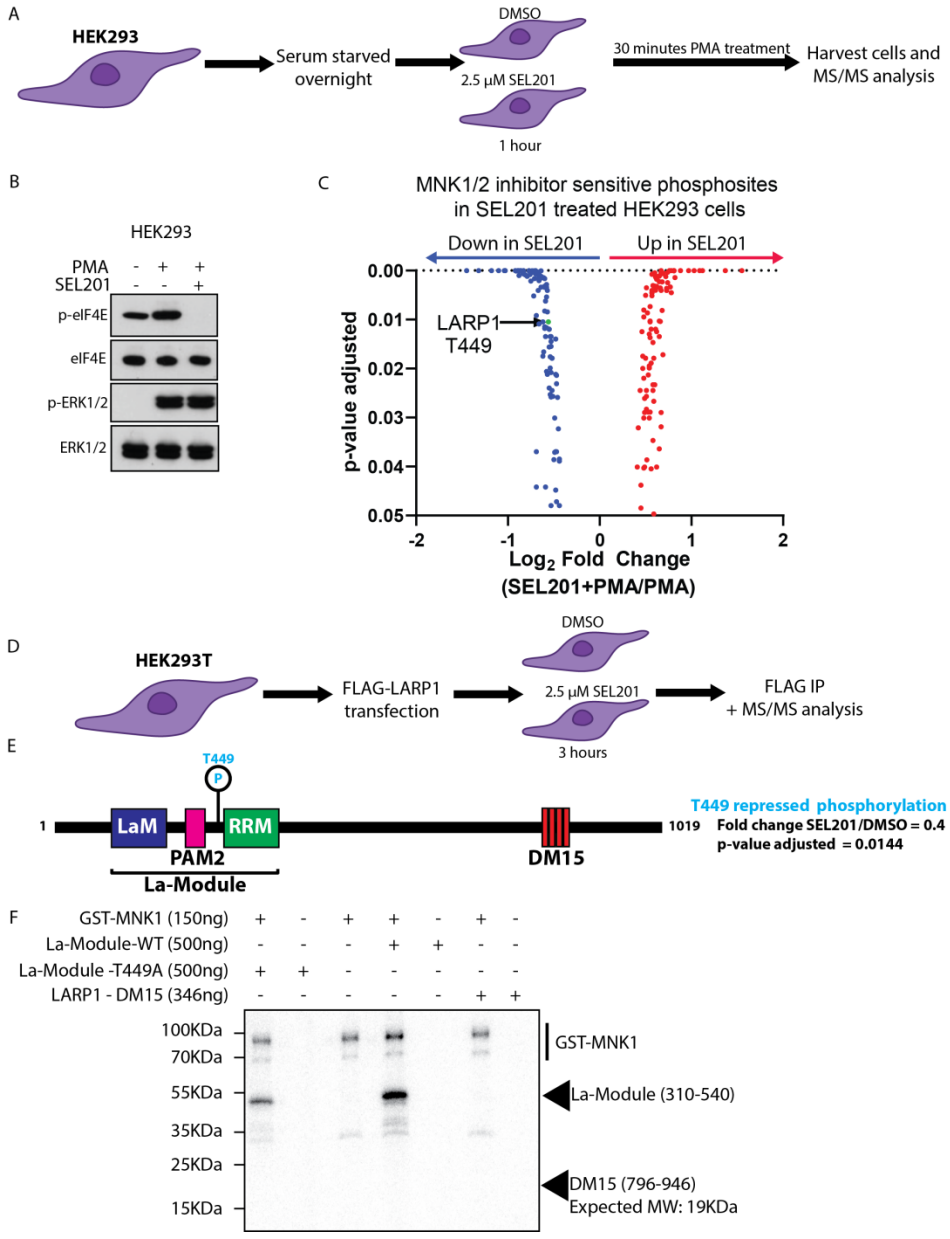

Figure 3.3: MNK1 phosphorylates LARP1 at threonine 449.
A: Schematic depicting the shotgun phosphoproteomics experiment used to identify possible substrates of MNK1/2 using the MNK1/2 inhibitor SEL201 in HEK293 cells. **B:** Immunoblot demonstrating the eIF4E and ERK1/2 phosphorylation status in overnight starved, 30 minutes PMA stimulated and 1 hour SEL201 pre-treated followed by 30 minute PMA stimulation in HEK293 cells. **C:** Volcano plot demonstrating that the phosphorylation of threonine at 449 on LARP1 is significantly repressed in HEK293 cells treated with SEL201+PMA compared with PMA stimulated cells alone. **D:** Schematic depicting the targeted phosphoproteomics experiment using full-length FLAG-tagged LARP1 immunoprecipitation to verify that the threonine residue at position 449 on LARP1 is a MNK1/2 inhibitor sensitive residue. **E:** Lollipop plot of LARP1 protein demonstrating that phosphorylation of T449 is significantly repressed in HEK293T cells treated with SEL201 for 3 hours compared with DMSO. **F:** In vitro radioactivity kinase assay demonstrated that GST-MNK1 phosphorylates the La-Module but not the DM15 on LARP1

3.4.4 The T449A mutant La-Module of LARP1 has a higher affinity for RNA compared to WT

It has been demonstrated that the La-Module on LARP1 can interact with the TOP motif and poly (A) RNA [28]. Using the purified recombinant WT and T449A La-Module protein, we performed electrophoretic mobility shift assays with radioactively labeled poly (A_{25}) and a 20-mer oligonucleotide containing the RPS6 TOP motif (Figures 3.4A and 3.4B), as is standard in the field [5, 6, 28]. We observed a concentration-dependent increase in binding of both the WT and T449A to RPS6 TOP motif and Poly (A_{25}). We observed that both the WT and T449A mutant had a higher affinity for poly (A_{25}) compared with RPS6 TOP. Dissociation constant (K_d) is used to describe the affinity of a ligand (RNA) to a protein (La-module). The apparent affinity of the interaction (K_{dapp}) for WT La-Module to RPS6 was 3.116 µM, while the K_{dapp} of WT La-Module for poly (A_{25}) was 0.3679 µM (Figures 3.4A and 3.4B). Similarly, in the T449A mutant, we observed a K_{dapp} of 1.556 µM and 0.3737 µM for RPS6 TOP and poly (A_{25}) respectively (Figures 3.4A and 3.4B). Due to the conformational flexibility of the La-Module, we were unable to determine the RNA-binding activities of the constructs; we are therefore unable to directly compare the differences in RNA-binding affinities between the WT and T449A mutant. It is reasonable, however, to compare the ability of each protein construct to bind different RNAs. We observed that the $K_{d}{}_{app}$ ratio between poly (A_{25}) and RPS6 TOP of the T449A mutant was lower than that for the WT La-Module (1:4.16 vs. 1:8.46) (Figures 3.4A and 3.4B). These K_d ratios suggest that the T449A mutant more readily associates with RNA compared with the WT La-Module.

Thus, we propose that upon MNK1 inhibition, LARP1 would not be phosphorylated on T449, and would likely result in a higher affinity for RNA compared with WT LARP1.

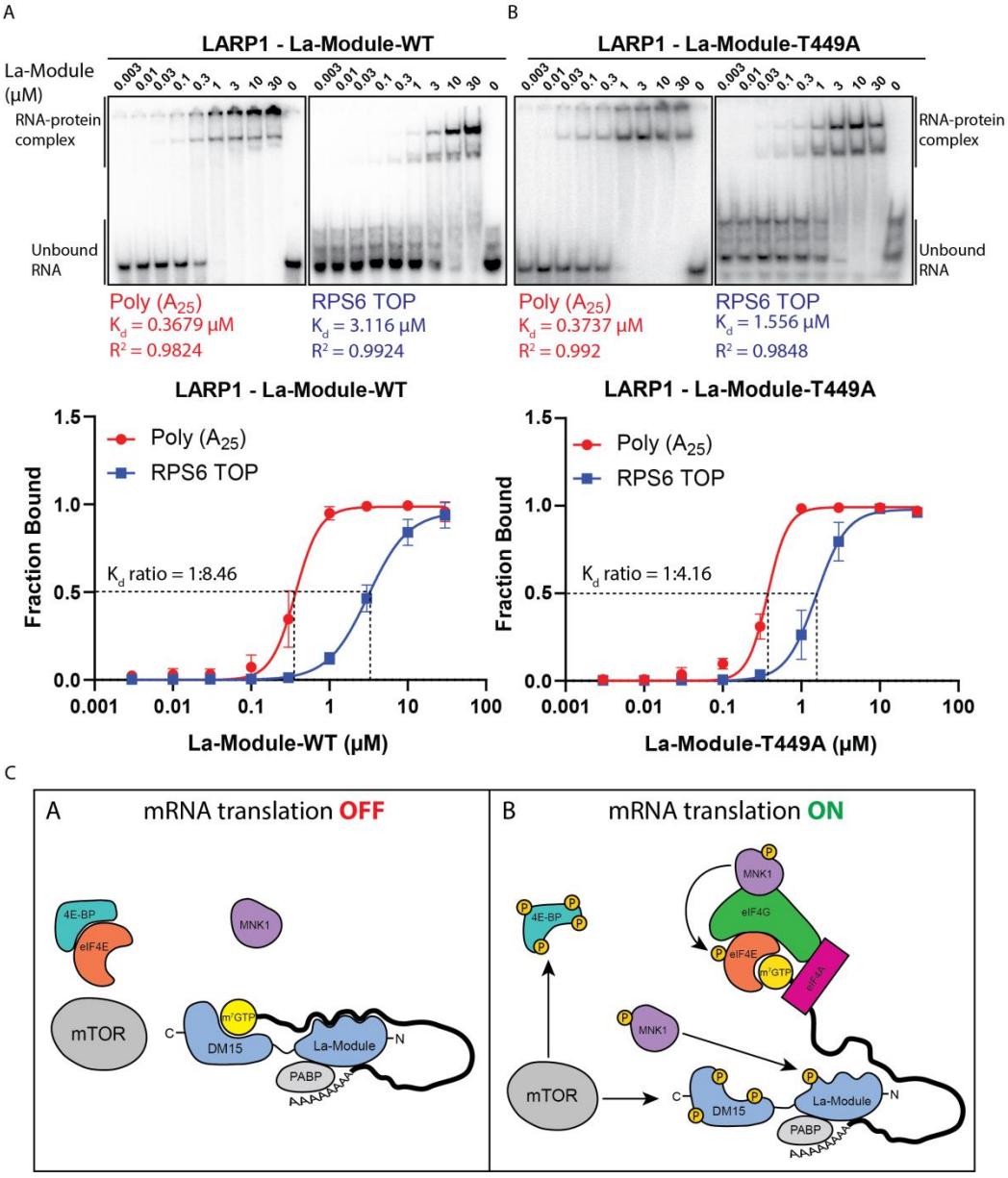

Figure 3.4: Phosphodeficient T449A mutant of the La-Module has a higher affinity for RNA compared to WT.
A: Electrophoretic mobility shift assay demonstrating the binding of WT La-Module to Poly (A_{25}) and RPS6 TOP motif. Graphs are represented as the average of 3 biological replicates. **B:** Electrophoretic mobility shift assay demonstrating the binding of phosphodeficient T449A La-Module to Poly (A_{25}) and RPS6 TOP motif. Graphs are represented as the average of at least 3 biological replicates. **C:** Proposed model depicting the proposed role of MNK1 kinase activity on mRNA translation. On the left panel (A), in translation repressive conditions, mTOR is inactive and as a result, LARP1 binds TOP mRNA and 4E-BP

sequesters and inhibits eIF4E. On the right panel (B), activated mTOR, phosphorylates 4E-BP to release eIF4E. Simultaneously, mTOR phosphorylates LARP1 on the DM15, resulting in the release of 5'cap. Meanwhile, MNK1 phosphorylates LARP1 on the La-module at T449, promoting the release of the TOP-motif. Finally, MNK1 phosphorylates eIF4E on serine 209, thereby promoting the translation of the mRNA.

3.5 Discussion

In this study we have identified LARP1 as a novel interacting protein of MNK1 and, we posit that one functional outcome of this interaction is the phosphorylation of LARP1 on T449. Furthermore, LARP1's ability to bind RNA may be regulated by MNK1 kinase activity on T449. These data add to the overall consensus of LARP1 acting as a translation repressor in cells and, additionally, provides new insight into how its RNA-binding activity may be regulated by kinases.

Our data demonstrate that endogenous LARP1 co-immunoprecipitates with both exogenous and endogenous MNK1 (Figures 3.1C to 3.1F, 3.2C, and Supplemental Figure 3.1B to 3.1D). This is not entirely surprising given the well-characterized role MNK1 plays in binding and regulating mRNA translation through interaction with the scaffold protein eIF4G and the phosphorylation of eIF4E at serine 209 [19 – 21]. Given that MNK1 and MNK2 are able to augment mRNA translation by phosphorylating eIF4E, a logical next step was to determine whether MNK2 interacts with LARP1. As there are no reliable antibodies against MNK2, we transiently transfected GST-MNK2 into HEK293T cells. Immunoprecipitation of GST-MNK2 resulted in no LARP1 being co-immunoprecipitated. However, GST-MNK1 was able to co-immunoprecipitate LARP1 (Figure 3.1D). This is not unexpected, as it has been demonstrated that MNK1 and MNK2 possess differences in substrate specificity [29]. Next, we performed endogenous immunoprecipitation of MNK1 in cell lysates treated with RNAse A. Indeed, we were

able to successfully co-immunoprecipitate endogenous LARP1 with endogenous MNK1 in RNAse A treated samples. Moreover, we observed that the depletion of endogenous RNA from the cell lysates enhanced the binding of MNK1 and LARP1 in A375 and HEK293T cells (Figure 3.1F and Supplemental Figure 3.1E). It has been demonstrated that RNA may mediate the binding between two proteins, and degradation of the RNA may result in the loss of the interaction [23, 24]. In our data, the increased binding of MNK1 to LARP1 in the absence of RNA suggests a direct interaction between the two proteins. Moreover, the ability of MNK1 to interact with LARP1 in conditions in the presence of RNA may suggest a role for MNK1 in regulating LARP1's affinity to specific RNA molecules.

We and others have demonstrated that LARP1 interacts with PABPC1 through the La-Module (Supplemental Figure 3.2A) [7]. Importantly, we have observed that MNK1 interacts with LARP1 specifically through the La-Module, but not through other regions on LARP1 (Figure 3.2A and 3.2B). As the La-Module of LARP1 does not interact with the 5'cap, but instead with the TOP motif and the poly (A) tails of RNA, this provides us insight into how MNK1 may be able to regulate LARP1 activity [28]. Similarly, we also wanted to map what region on MNK1 is critical for its interaction with LARP1. Using a mutant of MNK1 that prevents its interaction with eIF4G, we tested whether mutations in the polybasic NLS sequence at the N-terminal would also thwart this interaction. Surprisingly, we observed that the MNK1 26-28 R-A mutant was unable to co-immunoprecipitate LARP1 or PABPC1 (Figure 3.2C). Meanwhile, WT MNK1 or the MNK1 L390S mutant was able to successfully co-immunoprecipitate LARP1, eIF4G

and PABPC1 (Figure 3.2C). These data also suggest that the interaction between MNK1 and LARP1 may be mediated by eIF4G and warrants further investigation. The mapping of the domains required for MNK1 binding to LARP1 is important, as it may allow us to specifically target this interface and inhibit the interaction.

LARP1 is a potential substrate of several kinases including mTOR, CDK1, CDK2, and AKT [7, 30 – 32]. After establishing the interaction between MNK1 and LARP1, we next hypothesized that MNK1 may be able to phosphorylate LARP1. Using phosphoproteomics and *in vitro* kinase assays, we discovered that MNK1 phosphorylates LARP1 at threonine 449 (Figure 3.3A to 3.3F). Moreover, as MNK1 was unable to bind the DM15 region, MNK1 was also unable to phosphorylate the DM15 region of LARP1, as expected (Figure 3.3F). It is important to consider that MNK1 may be able to phosphorylate the La-Module at a serine or threonine other than T449, as we observed that the T449A mutant was phosphorylated by MNK1, albeit to a lesser extent compared to the WT La-Module (Figure 3.3F). CDK2 has recently been demonstrated to phosphorylate LARP1 on T449 and thereby potentially regulate the translation of RPS3 and RPL15 [31]. It is entirely possible that T449 on LARP1 may be a substrate for multiple kinases, as it has been demonstrated that cyclin-dependent kinases can phosphorylate the translation machinery to regulate mRNA translation with the cell cycle [30, 33]. Hence, LARP1 may be phosphorylated by CDK2 to potentially regulate translation of mRNAs as cells progress through the cell cycle [31].

Finally, we wanted to assess the possible functional consequences of the phosphorylation of LARP1 at T449 by MNK1. Using electrophoretic mobility shift

assays, we demonstrate that a phosphodeficient T449A La-Module binds to RNA with a higher affinity compared with WT La-Module (Figure 3.4A and 3.4B). Due to the experimental conditions used, we were unable to correct the T449A and WT La-Module protein concentrations for activity, and so instead we calculated and compared their actual dissociation constants for the RNA. We were able to compare the ratio of affinities of the individual proteins (LARP1 La-Module WT and T449A) to RPS6 TOP and poly (A_{25}) RNA. We observed that the apparent K_d ratio between poly (A_{25}) and RPS6 TOP in the T449A mutant was lower than the WT La-Module (Figures 3.4A and 3.4B) suggesting that the T449A mutant likely has a higher affinity for the RNA compared with the WT La-Module. While it has been demonstrated that the La-Module binds poly (A_{25}) and the RPS6 TOP with similar affinities [28], we observe that both the WT and T449A La-Modules consistently have a higher affinity for poly (A_{25}) compared with RPS6 TOP (Figure 3.4A and 3.4B). This could be due to the conformational flexibility of the La-Module. While it hasn't been thoroughly investigated, it has been shown that LARP family of proteins contain intrinsically disordered regions [34 – 36], which can allow proteins to fold into conformations that permit certain interactions with a ligand while inhibiting others [37 – 40].

In conclusion, our data demonstrate that MNK1 interacts with LARP1 on the La-Module. Importantly, MNK1 can phosphorylate LARP1 and could potentially regulate the affinity of LARP1 to RNA and possibly impact mRNA translation. We would thus hypothesize that, in growth permissive conditions, MNK1 could phosphorylate LARP1 to promote the latter from dissociating with TOP mRNAs. This would allow eIF4E to bind to

the mRNA, upon which MNK1/2 could phosphorylate eIF4E to enhance the translation of the mRNA (Figure 3.4C). Importantly, it has been shown that LARP1 can regulate the translation of oncogenic mRNAs previously reported to be sensitive to phosphorylation of eIF4E [41]. While the phosphorylated eIF4E has been shown to augment the translation of oncogenic mRNAs [41], the exact mechanism has eluded researchers. These data could provide an exciting new link to allow us to better understand the intricacies of mRNA translation. Furthermore, given that the T449A LARP1-mutant can possibly regulate the translation of RPS3 and RPL15 [31], we would postulate that this process can also be regulated by the MNK1-LARP1-eIF4E axis.

3.6 Methods and Materials

Cell lines and Reagents

D4M.3a murine melanoma cells were kindly provided by Dr. Constance Brinckerhoff (Geisel School of Medicine, Dartmouth College, Hanover, NH, USA). A375 human melanoma cells were purchased from Plexxikon Inc. BLM cells were a generous gift from Dr. Ghanem Ghanem (Institut Jules Bordet, Bruxelles). HEK293T cells were a generous gift from Dr. Sidong Huang. MCF7 breast cancer cells were a generous gift from Dr. Ivan Topisirovic. HEK293 cells were a generous gift from Dr. Philippe Roux (University of Montreal). A375, HEK293, HEK293T, and BLM cells were cultured in DMEM media supplemented with 10% FBS and 100 I.U/mL penicillin and 100 I.U/mL streptomycin at 37°C and 5% CO_2. D4M.3a cells were cultured in Advanced DMEM media containing 5% FBS, 5 ml Glutamax (×100), and antibiotics. MCF7 cells were cultured in RPMI supplemented with 10% FBS and antibiotics. All experiments were

initiated within 5 passages of thawing a master stock of cells. Cell lines were routinely tested for Mycoplasma using the e-Myco™ VALID Mycoplasma PCR Detection Kit. Identity of cell lines was verified by short tandem repeat (STR) profiling. SEL201 was provided by RYVU therapeutics and prepared as a stock of 10 mM in DMSO. FLAG-LARP1 and the fragments were a generous gift from Dr. Bruno Fonesca (Primergen). GST-MNK1 and GST-MNK2 plasmids were a generous gift from Dr. Christopher Proud (South Australian Health and Medical Research Institute). MNK1 (pLX-317) mutants (26-28 R-A, and L390S) were generated by Mutagenex (The Ohio State University Wexner Medical Center).

Transfection

HEK293T ($1.2x10^6$) cells were seeded in 10 cm dishes and allowed to adhere overnight. The next day, the cells were transfected with 4 µg of plasmid using 30 µL of Lipofectamine 2000. 16 to 18 hours later, the media was changed to fresh DMEM supplemented with 10% FBS. The next day, prior to harvest, the media was changed and refreshed for 3 hours and at this point inhibitors were added if necessary (unless specified otherwise)

Immunoblotting

Protein concentration was measured by Bradford assay. 20 to 50 µg of protein lysate were PAGE-separated (40% Acrylamide/Bis Solution, 37.5:1 Bio-Rad #1610148) and transferred onto PVDF membranes (Roche #0301004001), blocked for one hour in 5% non-fat milk, and incubated with primary antibody overnight at 4°C. The following day, the membranes were washed and incubated with secondary antibody for 1 hour. The membranes were developed using Amersham ECL Western Blotting Reagent

(#RPN2106) or Immobilon Western Chemiluminescent HRP Substrate (#WBKLS0500). Antibody details can be found in Supplemental Table 1.

Immunoprecipitation

Cells were seeded in 15 cm dishes and allowed to adhere overnight and allowed to proliferate for an additional 24 hours. Two to Four 15cm dishes of cells were used per immunoprecipitation condition. Three hours prior to harvest, the media was changed to fresh media supplemented with 10% FBS. At harvest, the cells were washed twice with ice-cold PBS and scraped into a falcon tube. Subsequently, cells were lysed in HEPES-Acetate-CHAPS immunoprecipitation buffer containing 25 mM HEPES, 115 mM Potassium Acetate, 1 mM EDTA, and 0.3% CHAPS detergent supplemented with protease (Roche #11697498001) and phosphatase (Roche #4906845001) inhibitors. Approximately, 750 µL of complete lysis buffer was used per 15 cm dish of cells. For immunoprecipitation in the presence of RNAse A, the enzyme was added to the lysis buffer at this point. The cells were allowed to lyse on a nutator at 4°C for 1 hour. The debris in the lysates was then cleared by centrifugation at max speed for 15 minutes at 4°C. The lysates were then pre-cleared on a nutator for 20 to 30 minutes at 4°C with Sephadex-G25 (Sigma-Aldrich # G25150) beads that had been hydrated, washed three times with ice-cold HEPES-Acetate-CHAPS buffer, and re-suspended in 50% slurry with the lysis buffer. The beads were then separated from the lysate by centrifugation at 1000xg for 5 minutes at 4°C. Protein concentration in lysates was measured by Bradford assay and input samples collected. Endogenous MNK1 was immunoprecipitated from 2 to 4 mg of lysates at an antibody concentration of 1ug/mg of lysate on a nutator for 1.5 hours at 4°C. IgG concentration was used at one-fifth of the

concentration of the MNK1 antibody according to manufacturer's instructions. After 1.5 hours, 20 to 40 µL of pre-washed protein-G magnetic beads (Sigma-Aldrich # 10003D) were added to the antibody-lysate samples and incubated on a nutator for 1 hour at 4°C. The beads are then briefly collected to the bottom by centrifugation at 1000xg for 2 minutes and washed 5 times with 1 mL ice-cold HEPES-Acetate-CHAPS buffer (without inhibitors) using a magnetic stand. Finally, the beads are boiled in 30 to 50 µL of 1x Laemmli's SDS buffer supplemented with B-mercaptoethanol and boiled for 10 minutes at 95°C. For immunoprecipitation from samples harvested from cells transiently or stably overexpressing MNK1, the same steps are followed. However, for more stringency, the lysis buffer substituted 0.3% CHAPS for 1% NP40. For immunoprecipitation experiments involving the use of DTSSP as a crosslinker, a final concentration of 5 µM DTSSP was achieved during lysis for 5 minutes only. After 5 minutes, excess DTSSP was quenched by adding Tris-HCl (pH 7.4) to a final concentration of 40mM and 15 minute incubation on ice.

Lentivirus production and transduction

Lentiviral plasmids were co-transfected with the packaging plasmids Pax2 and MD2G into HEK293T cells using calcium phosphate precipitation. Viral supernatant was harvested 72 hours post transfection, spun down at 500xg for 5 minutes, and filtered through a 0.45 µm filter. 500 µL of viral supernatant were used to transduce 100,000 cells in the presence of 8 µg/mL polybrene for 24 hours. The following day, media was changed, and transduced cells were selected using 2 µg/mL of puromycin.

Mass spectrometry to identify the MNK1 interactome

D4M.3a ($1.25x10^6$) and A375 ($2x10^6$) cells were seeded in 15 cm dishes and allowed to adhere overnight. Approximately 18 hours before harvesting the cells, the media was aspirated and refreshed. Cells were harvested and immunoprecipitation was performed as described above in the presence of 50 μM DTSSP. Immunoprecipitated antigen-antibody complex was collected using protein-G sepharose beads for 1 hour. The beads were washed 3 times in ice-cold HEPES-Acetate lysis buffer (without NP40 detergent and inhibitors). Beads were eluted using 50:50 NH_4OH:H_20 for 5 minutes at room temperature. Samples were then vacuum dried for 1 hour and 25 minutes on medium heat setting. Samples were resolubilized and digested in 5 μL proteomics-grade Trypsin (Promega) at a concentration of 12 ng Trypsin per μL, overnight. Samples were then dried again in a Speedvac and resolubilized in 20 μL of water with 0.1% formic acid. High performance liquid chromatography was conducted using a 2 cm pre-column (Acclaim PepMap 50 mm × 100 μm inner diameter (ID)), and 25 cm analytical column (Acclaim PepMap, 500 mm × 75 μm diameter; C18; 2 μm; 100 Å, Thermo Fisher Scientific), running a 120 min reversed-phase buffer gradient at 350 nl/min on a Thermo EASY-nLC 1000 pump in-line with a Thermo Q-Exactive HF quadrupole-Orbitrap mass spectrometer. A parent ion scan was performed using a resolving power of 120,000, then up to the 25 most intense peaks were selected for MS/MS (minimum ion count of 1000 for activation) using higher energy collision induced dissociation (HCD) fragmentation. Dynamic exclusion was activated such that MS/MS of the same m/z (within a range of 10 ppm; exclusion list size = 500) were excluded from analysis by above duty cycle for 3.5 seconds. For protein identification, raw files were converted to mgf format using Mascot Distiller (v3.0.10800), then searched using the

Mascot Search engine (Matric Science Ltd) against the Human Uniprot database. Search parameters specified as: parent MS tolerance at 6 ppm and MS/MS fragment ion tolerance at 50 mmu, and with 1 missed cleavage allowed for trypsin. No fixed modifications, but oxidation of methionine was allowed as a variable modification. Data were re-searched using X!Tandem, additionally allowing deamidations of glutamine and asparagine as variable modifications. The combined search data were validated using standard validation software of the Scaffold proteome software platform (Proteome Software). Proteins identified with an FDR of 1% on the peptide level and protein level were considered and quantified, relative to the other samples, by total spectral counts.

Mass spectrometry – Shotgun Phosphoproteomics of MNK1/2

HEK293 cells were serum starved overnight. The next day, the cells were pre-treated with DMSO or SEL201 for 1 hour. The cells were then stimulated with PMA for 30 minutes (in the presence of DMSO or SEL201). The cells were then harvested. Proteins from cell pellets were extracted in lysis buffer containing 5% sodium dodecyl sulfate (SDS), 100 mM TRIS pH 7.8 supplemented with PhosStop phosphatase inhibitor cocktail (Roche). Samples were subsequently heated to 99°C for 10 minutes and subjected to probe-based sonication using a Thermo Sonic Dismembrator at 25 % amplitude for 3 cycles x 5 seconds. Remaining debris was pelleted by centrifugation at 20,000 x g for 5 minutes. An aliquot of the supernatant was diluted to <1% SDS and used for estimation of protein concentration by bicinchoninic acid assay (BCA) (Pierce/Thermo). Lysates were clarified by centrifugation at 14,000 x g for 5 minutes, and transferred into a new reaction tube and disulfide bonds were reduced by the addition of tris(2-carboxyethyl)phosphine (TCEP) to a final concentration of 20 mM and

incubated at 60°C for 30 minutes. Free cysteines were alkylated using iodoacetamide at a final concentration of 30 mM and subsequent incubation at 37°C for 30 minutes in the dark. An equivalent of 250 µg of total protein was used for proteolytic digestion using suspension trapping (STRAP). In brief, proteins were acidified through the addition of phosphoric acid to a final concentration of 1.3% v/v. The sample was subsequently diluted 6-fold in STRAP loading buffer (9:1 methanol:water in 100 mM TRIS, pH 7.8) and loaded onto an S-TRAP Mini cartridge (Protifi LLC, Huntington, NY) and spun at 4000 x g for 2 minutes. Samples were washed three times using 200 µL of STRAP loading buffer. Proteins were then proteolytically digested using trypsin (Sigma) at a 1:10 enzyme to substrate ratio for 16 hours at 37°C. Peptides were sequentially eluted in 50 mM ammonium bicarbonate, 0.1% formic acid in water, and 50% acetonitrile. Peptide containing samples were then vacuum concentrated, and desalted using Oasis HLB SPE cartridges (30 mg, 1 CC, Waters).

Desalted peptides were vacuum concentrated and reconstituted in 100 mM triethylammonium carbonate (TEAB) and combined 1:1 (w/w) with their respective TMT 10-plex (Thermo) label which was reconstituted in 100% acetonitrile. Peptides were labelled for 60 minutes at room temperature, followed by quenching with 5% hydroxylamine (to a final concentration of 0.4%). Labelled peptides were then pooled, vacuum concentrated, and desalted by SPE using Waters tC18 cartridges (500 mg). TMT labelled peptides were then reconstituted in 20 uL of 5 mM ammonium acetate pH 10, fractionated by basic reversed phase chromatography using a Waters XBridge BEH C18 column (4.6 x 150 mM, 5 uM), and pooled into 24 fractions. 10% of each sample was reserved for measurement of the total proteome and the remainder was combined

into a total of 8 fractions which were used for phosphopeptide enrichment by immobilized metal affinity chromatography (IMAC) using AssayMap Fe-NTA (III) cartridges (Agilent) and an Agilent Bravo liquid handling system.

Samples for both total proteome and phosphoproteome analysis were analyzed by data dependent acquisition (DDA) using an Easy-nLC 1200 online coupled to a Q Exactive Plus (both Thermo Fisher Scientific). Samples were loaded onto the precolumn (Acclaim PepMap 100 C18, 3 µm particle size, 75 µm inner diameter x 2 cm length) in 0.1% formic acid (buffer A). Peptides were separated using a 50-min binary gradient ranging from 3-40% of buffer B (84% acetonitrile, 0.1% formic acid) on the main column (Acclaim PepMap 100 C18, 2 µm particle size, 75 µm inner diameter x 25 cm length) at a flow rate of 300 nL/min. Full MS scans were acquired from m/z 375-1,400 at a resolution of 70,000, with an automatic gain control (AGC) target of 3 x 106 ions and a maximum injection time of 50 ms. The 15 most intense ions (charge states +2 to +4) were isolated with a window of m/z 0.7, an AGC target of 1 x 105 and a maximum injection time of 120 ms and fragmented using a normalized higher-energy collisional dissociation (HCD) energy of 33. MS/MS were acquired at a resolution of 35,000 and the dynamic exclusion was set to 30 s. DDA MS raw data was processed with Proteome Discoverer 2.4 (Thermo Scientific) and searched using Sequest HT against a human UniProt FASTA database. The enzyme specificity was set to trypsin, with a maximum of 2 missed cleavages. TMT 10plex labelling (229.163 Da) of peptide N-termini and lysine residues and carbamidomethylation of cysteines were set as fixed modifications and oxidation of methionine as variable modification. The precursor ion mass tolerance was set to 10 ppm, and the product ion mass tolerance was set to 0.02 Da. Percolator was

used to assess posterior error probabilities and the data was filtered using a false discovery rate (FDR) <1% on peptide and protein level. Reporter ion quantification was performed using the appropriate nodes in Proteome Discoverer 2.5.

Proteins and phosphopeptides TMT abundances were filtered such that only proteins or peptides were retained if quantified in >50% of at least one sample group. Missing values were imputed by sampling randomly generated values between the minimum and lowest 5% of LFQ abundances. Protein abundances were scaled (normalized) based on the total peptide amount per sample. Proteins quantified by a single peptide were retained in the data summary but labelled in red. Differences in protein expression were calculated by taking the ratio of grouped median protein or phosphopeptide abundances. Statistical significance was determined by background based t-tests which were calculated for each specified group abundance ratio, and adjusted for false discovery rate (FDR) using Benjamini-Hochberg method within Proteome Discoverer 2.5. Regulation was defined on the basis of having an adjusted p-value of less than 0.05, and a fold change corresponding to 2-sigma of the distribution of all calculated fold-changes. Dimensional reduction by principal component analysis and hierarchical clustering were conducted using the normalized protein and phosphopeptide LFQ abundances as inputs for Instant Clue (http://www.instantclue.uni-koeln.de/).

Mass spectrometry – Targeted Phosphoproteomics of FLAG-LARP1

HEK293T ($1.2x10^6$) cells were seeded in 10 cm dishes and allowed to adhere overnight. One 10 cm dish was used per immunoprecipitation sample. The next day, the cells were transfected with 4 µg of FLAG-LARP1/ or FLAG-205 to 509 LARP1 fragment

plasmid using 30 µL of Lipofectamine 2000. 16 to 18 hours later, the media was changed to fresh DMEM supplemented with 10% FBS. The next day, prior to harvest, the media was changed and refreshed for 3 hours and at this point DMSO or SEL201 was added to a final concentration of 2.5 µM to half the dishes. FLAG-LARP1 was immunoprecipitated from these samples and after 3 washes were boiled in 1xLaemmli buffer containing SDS. 5% of the sample was used for determination of protein concentration by bicinchoninic acid assay (BCA) (Thermo/Pierce) which was used to normalize the total amount of material digested per sample. Proteins were reduced in 20 mM TCEP at 60°C for 30 minutes, and alkylated with 25 mM iodoacetamide at room temperature in the dark for 30 minutes. Samples were then acidified with phosphoric acid (1.3% volume / volume) prior to dilution with S-TRAP binding buffer (90% methanol, 100 mM TRIS pH 8.5) and sample cleanup and proteolytic cleavage using S-TRAP micro cartridges according to the vendor provided protocol (Protifi LLC). 1 ug of trypsin (Promega) in 50 mM ammonium bicarbonate was used for digestion overnight at 37°C. Peptides were extracted from S-TRAP cartridges using 3 sequential washes with ABC, 0.1% formic acid, and 50% acetonitrile prior to vacuum concentration. Samples were rehydrated in a final volume of 100 µL (80% acetonitrile, 0.1% TFA final concentration) and used for automated phosphopeptide enrichment using Fe(III)-NTA immobilized metal affinity chromatography (IMAC) tips (Agilent, part # G5496-60085) and an Agilent Bravo liquid handling system equipped with an AssayMap head. Flowthrough was retained for the analysis of non-modified peptides, and both the phosphopeptide containing eluate and flowthrough were evaporated to dryness and rehydrated in 0.1% TFA prior to analysis by LC-MS/MS. Both the phosphopeptide

containing eluate and flowthrough were analyzed by data dependent acquisition (DDA) using an Easy-nanoLC 1200 and Q Exactive Plus (Thermo Fisher Scientific). Peptides were first loaded onto a precolumn (Acclaim PepMap 100 C18, 3 µm particle, 75 µm x 2 cm) in 0.1% formic acid (mobile phase A), and separated using a 60 minute gradient from 3-40% acetonitrile (mobile phase B) using an Acclaim PepMap C18 column (250 mm x 75 µm inner diameter, 2 µm particle) at a flow rate of 300 nL/min. Survey scans were collected between 350-1,500 m/z at 70,000 resolution, automatic gain control (AGC) was set to 1 x $10E^6$ and the maximum injection time was set to 50 ms. The 15 most abundant precursor ions with a charge of +2 to +4 were selected for MS/MS. Isolation width was set to 1.2 Th, AGC target was 2 x $10E^4$ and a maximum injection time of 64 ms. Normalized collision energy (NCE) was set to 28. The resolution for MS/MS scans was set to 17,500 and the dynamic exclusion was set to 30s. Raw MS data was processed with Proteome Discoverer 2.5 (Thermo Scientific) using the Sequest HT node for database searching against a human reference proteome FASTA database from Uniprot (downloaded August 25th 2021). The enzyme specificity was set to trypsin, with a maximum of 2 missed cleavages. Carbamidomethylation of cysteine was set as a fixed modification and oxidation of methionine, and serine, threonine, and tyrosine phosphorylation as variable modifications. The ptmRS node was used in phosphoRS mode to assess the probability of phosphosite localization. Precursor and product ion mass error tolerance was set to 10 ppm, and the product ion mass tolerance was set to 0.02 Da. Percolator was used to assess posterior error probabilities and the data was filtered using a false discovery rate (FDR) <1% on peptide and protein level. The Minora node of Proteome Discoverer was used for label free quantitation. Protein

and phosphopeptides abundances were scaled based on total peptide amounts per sample, and only proteins or phoshopeptides quantified in at least 50% of an experimental group were retained. Missing values were imputed using the low abundance resampling method in the precursor ions quantifier node.

La-Module (310 - 540) expression and purification

The La-Module (amino acids 310-540) of LARP1 was cloned by PCR into a modified pET28a SMT3 vector (Mossessova and Lima, 2000; Al-Ashtal et al. 2019). This construct expressed La-Module with a His_{10}-SMT fusion tag. The resulting constructs were used to transform BL21 (BE3) bacteria and were grown overnight on LB plates supplemented with 30 µg of kanamycin. The His10-SMT-LaModule fusion protein was expressed by autoinduction for 2.5 hours at 37°C followed by overnight incubation (18-20 hours) at 18°C. The bacteria were subsequently centrifuged down, frozen in liquid nitrogen, and stored at -80°C.

Approximately 6 grams of bacteria were resuspended in 50 mL lysis buffer (50 mM Tris-HCl, pH 8.0, 400 mM NaCl, 10 mM imidazole, and 10% glycerol) supplemented with Pierce Protease Inhibitor Mini Tablets (#A32953) in on a magnetic stirrer at 4°C for 30 minutes. The bacteria were then flash frozen and thawed 4 times in liquid nitrogen to promote efficient. Subsequently, the bacteria were sonicated (output power 2) in 45 second ON, 45 second-OFF intervals six times in an ethanol-ice bath. The sonicated lysate was cleared by centrifugation at 9700 x g for 20 min at 4°C. The clarified bacterial lysate were incubated with 8 mL of Ni-NTA Resin (ThermoFisher) on a nutator for 1 hour at 4°C. The nickel beads were then washed once with 20 mL lysis buffer (without inhibitors) and twice with wash buffer (50 mM Tris-HCl, pH 8.0, 400 mM

NaCl, 35 mM imidazole, and 10% glycerol). The beads were eluted twice with 20 mL elution buffer (50 mM Tris-HCl, pH 8.0, 400 mM NaCl, 250 mM imidazole, and 10% glycerol) on a nutator at 4°C for 30 minutes each. 1 mg of in-house made ULP1 was added to the eluted proteins which were then altogether dialyzed against 2 liters of dialysis buffer (50 mM Tris-HCl, pH 8.0, 150 mM NaCl, 0.5mM EDTA, 0.5mM DTT, 0.5mM TCEP, and 10% glycerol) for 3 hours at 4°C on a magnetic stirrer with gentle mixing. The lysate was then cleared by centrifugation at 9700 x g for 15 min at 4°C. Nucleic acid and protein contaminants were removed using HiTrap Heparin followed by tandem HiTrap S and HiTrap QP (GE Healthcare Lifesciences) chromatography with an NaCl gradient (150 mM-1M), with La-Module flowing through the Heparin column and subsequently eluting from the Q columns. Fractions containing the La-Module were collected, dialyzed into storage buffer (50 mM Tris-HCl, pH 7.5, 250 mM NaCl, 25% glycerol, and 4 mM TCEP), concentrated, frozen in liquid nitrogen and stored at -80°C. T449A mutations were performed using QuikChange Site-Directed Mutagenesis and expressed and purified as described above.

***In vitro* kinase assay**

Human recombinant GST-tagged active MNK1 was purchased from Abcam (#ab125635). Human recombinant GST-eIF4E was purchased from SignalChem (#E34-30G-50). Kinase reactions between MNK1 and LARP1 were performed in a buffer containing 20 mM HEPES-KOH, 10 mM MgCl2, 1 mM DTT, 25 µM ATP, 1x phosphatase inhibitor (Roche #4906845001) and 2.5 µCi of ATP (γ-32P) (Perkin Elmer) using 150 ng (1.95 pmol) of MNK1 per 500 ng (18.61 pmol) of La-Module (310 to 540) or 346 ng (18.51 pmol) of DM15 (796-946). Kinase reactions were incubated at 30°C for

1 hour in a thermocycler without heated lid. The kinase reaction was stopped by adding Laemmli's loading dye and subsequent boiling for 5 minutes at 95°C. The samples were then PAGE-separated and the gel was dried for 45 minutes at 80°C. Phosphor screens (GE Healthcare Lifesciences) were exposed for 20 to 30 minutes and were imaged on a Typhoon FLA reader (GE Healthcare Lifesciences). Kinase assay reaction between GST-MNK1 (0.65 pmol) and GST-eIF4E (3.94 pmol) were performed in the same conditions as above, with 200 μM ATP, and without radioactive ATP (γ-32P). Phosphorylation of eIF4E was detected by immunoblotting using a phosphorylated eIF4E (S209) antibody

La-Module Electrophoretic Mobility Shift Assays (EMSA)

RPS6 TOP motif (20-mer) or Poly (A_{25}) RNA oligonucleotides were 5'-end labeled with [γ32P]-ATP (Perkin Elmer) using T4- polynucleotide kinase (New England Biolabs) and purified with MicroSpin™ G-25 Columns (Cytiva Life Sciences). 5X stocks of La-Module (WT and T449A) were prepared in dilution buffer (50 mM Tris-HCl pH, 7.5, 250 mM NaCl, 25% glycerol, 4 mM TCEP). Reactions were performed in 10 μL reactions in above dilution buffer (treated as 5x reaction buffer) containing 1 μL of (10 U/mL) poly(dI-dC) (Sigma-Aldrich), 1 μM BSA, 0.61 nM radiolabeled Poly (A) or RPS6 (20-mer) RNA and respective concentrations of La-Module. The reactions were incubated on ice for 45 minutes and subsequently run on a 7% polyacrylamide (29:1) native 0.5X TBE gel. The gel was then dried and then exposed to phosphor screens (GE Healthcare Lifesciences) overnight, which were then imaged on a Typhoon FLA reader (GE Healthcare Lifesciences) and quantitated using Imagequant TL (GE Healthcare Lifesciences). Dissociation constants were determined by plotting

(KaleidaGraph) the fraction of shifted RNA versus the concentration of protein after band intensities were corrected for background (ImageQuant) TL

Metascape Pathway Analysis

The list of proteins that were commonly co-immunoprecipitated by MNK1 in A375 D4M.3a cells were input and analyzed for pathway enrichment into Metascape using default settings. The top five pathways were maintained and illustrated in Figure 3.1C.

Data Availability

All raw proteomics and phosphoproteomics data are available upon request from the corresponding authors.

3.7 References

1. Jackson RJ, Hellen CUT, Pestova TV. The mechanism of eukaryotic translation initiation and principles of its regulation. Nat Rev Mol Cell Biol. 2010;11(2):113-127.
2. Batool A, Aashaq S, Andrabi KI. Eukaryotic initiation factor 4E (Eif4e): A recap of the cap-binding protein. J Cell Biochem. 2019;120(9):14201-14212.
3. Prabhu SA, Moussa O, Miller WH, Del Rincón SV. The MNK1/2-eIF4E axis as a potential therapeutic target in melanoma. Int J Mol Sci. 2020;21(11):4055.
4. Roux PP, Topisirovic I. Signaling pathways involved in the regulation of mrna translation. Mol Cell Biol. 2018;38(12):e00070-18.
5. Lahr RM, Mack SM, Héroux A, et al. The La-related protein 1-specific domain repurposes HEAT-like repeats to directly bind a 5'TOP sequence. Nucleic Acids Res. 2015;43(16):8077-8088.
6. Lahr RM, Fonseca BD, Ciotti GE, et al. La-related protein 1 (Larp1) binds the mRNA cap, blocking eIF4F assembly on TOP mRNAs. Elife. 2017;6:e24146.
7. Jia JJ, Lahr RM, Solgaard MT, et al. Mtorc1 promotes top mrna translation through site-specific phosphorylation of larp1. Nucleic Acids Res. 2021;49(6):3461-3489.
8. Fonseca BD, Zakaria C, Jia JJ, et al. La-related protein 1 (Larp1) represses terminal oligopyrimidine (Top) mrna translation downstream of mtor complex 1(Mtorc1). J Biol Chem. 2015;290(26):15996-16020.
9. Berman, A.J., C.C. Thoreen, Z. Dedeic, J. Chettle, P.P. Roux, et al., Controversies around the function of LARP1. RNA biology, 2020: p. 1-11.
10. Huang F, Gonçalves C, Bartish M, Rémy-Sarrazin J, Issa ME, Cordeiro B, et al. Inhibiting the MNK1/2-eIF4E axis impairs melanoma phenotype switching and potentiates antitumor immune responses. The Journal of clinical investigation 2021;131
11. Geter PA, Ernlund AW, Bakogianni S, Alard A, Arju R, Giashuddin S, et al. Hyperactive mTOR and MNK1 phosphorylation of eIF4E confer tamoxifen resistance and estrogen independence through selective mRNA translation reprogramming. Genes & development 2017;31:2235-49
12. Zhan Y, Guo J, Yang W, Goncalves C, Rzymski T, Dreas A, et al. MNK1/2 inhibition limits oncogenicity and metastasis of KIT-mutant melanoma. The Journal of clinical investigation 2017;127:4179-92
13. Robichaud N, del Rincon SV, Huor B, Alain T, Petruccelli LA, Hearnden J, et al. Phosphorylation of eIF4E promotes EMT and metastasis via translational control of SNAIL and MMP-3. Oncogene 2015;34:2032-42
14. Yang W, Khoury E, Guo Q, et al. MNK1 signaling induces an ANGPTL4-mediated gene signature to drive melanoma progression. Oncogene. 2020;39(18):3650-3665.
15. Irie F, Tobisawa Y, Murao A, Yamamoto H, Ohyama C, Yamaguchi Y. The cell surface hyaluronidase TMEM2 regulates cell adhesion and migration via degradation of hyaluronan at focal adhesion sites. J Biol Chem. 2021;296:100481.
16. Lee JY, Dominguez AA, Nam S, Stowers RS, Qi LS, Chaudhuri O. Identification of cell context-dependent YAP-associated proteins reveals β1 and β4 integrin mediate YAP translocation independently of cell spreading. Sci Rep. 2019;9(1):17188.
17. Koo BH, Apte SS. Cell-surface processing of the metalloprotease pro-ADAMTS9 is influenced by the chaperone GRP94/gp96. J Biol Chem. 2010;285(1):197-205.
18. Wang H, He M, Willard B, Wu Q. Cross-linking, immunoprecipitation and proteomic analysis to identify interacting proteins in cultured cells. Bio Protoc. 2019;9(11):e3258.
19. Pyronnet S, Imataka H, Gingras AC, Fukunaga R, Hunter T, Sonenberg N. Human eukaryotic translation initiation factor 4G (Eif4g) recruits mnk1 to phosphorylate eIF4E. EMBO J. 1999;18(1):270-279.
20. Waskiewicz AJ, Johnson JC, Penn B, Mahalingam M, Kimball SR, Cooper JA. Phosphorylation of the cap-binding protein eukaryotic translation initiation factor 4E by protein kinase Mnk1 in vivo. Mol Cell Biol. 1999;19(3):1871-1880.

21. Bellsolell L, Cho-Park PF, Poulin F, Sonenberg N, Burley SK. Two structurally atypical HEAT domains in the C-terminal portion of human eIF4G support binding to eIF4A and Mnk1. Structure. 2006;14(5):913-923.
22. Chettle J, Dedeic Z, Fischer R, et al. LARP1 Regulates Metabolism and MTORC1 Activity in Cancer. Cancer Biology; 2022.
23. Caillet J, Baron B, Boni IV, Caillet-Saguy C, Hajnsdorf E. Identification of protein-protein and ribonucleoprotein complexes containing Hfq. Sci Rep. 2019;9(1):14054.
24. Graindorge A, Pinheiro I, Nawrocka A, et al. In-cell identification and measurement of RNA-protein interactions. Nat Commun. 2019;10(1):5317.
25. Shveygert M, Kaiser C, Bradrick SS, Gromeier M. Regulation of eukaryotic initiation factor 4E (Eif4e) phosphorylation by mitogen-activated protein kinase occurs through modulation of Mnk1-eIF4G interaction. Mol Cell Biol. 2010;30(21):5160-5167.
26. Parra-Palau JL, Scheper GC, Wilson ML, Proud CG. Features in the N and C termini of the MAPK-interacting kinase Mnk1 mediate its nucleocytoplasmic shuttling. J Biol Chem. 2003;278(45):44197-44204.
27. Cuesta R, Xi Q, Schneider RJ. Structural basis for competitive inhibition of eIF4G-Mnk1 interaction by the adenovirus 100-kilodalton protein. J Virol. 2004;78(14):7707-7716.
28. Al-Ashtal HA, Rubottom CM, Leeper TC, Berman AJ. The LARP1 La-Module recognizes both ends of TOP mRNAs. RNA Biol. 2021;18(2):248-258.
29. Buxade M., Morrice N., Krebs D.L., Proud C.G. The PSF {middle dot} p54nrb Complex Is a Novel Mnk Substrate That Binds the mRNA for Tumor Necrosis Factor. J. Boil. Chem. 2007;283:57–65. doi: 10.1074/jbc.M705286200
30. Haneke K, Schott J, Lindner D, et al. CDK1 couples proliferation with protein synthesis. J Cell Biol. 2020;219(3):e201906147.
31. Ramani K, Robinson AE, Berlind J, et al. S-adenosylmethionine inhibits la ribonucleoprotein domain family member 1 in murine liver and human liver cancer cells. Hepatology. 2022;75(2):280-296.
32. Hong S, Freeberg MA, Han T, et al. LARP1 functions as a molecular switch for mTORC1-mediated translation of an essential class of mRNAs. Elife. 2017;6:e25237.
33. Mitchell DC, Menon A, Garner AL . Cyclin-dependent kinase 4 inhibits the translational repressor 4E-BP1 to promote cap-dependent translation during mitosis-G1 transition. FEBS Lett 2020;594:1307–18.
34. Bousquet-Antonelli, C. & Deragon, J.M. A comprehensive analysis of the La-motif protein superfamily. RNA 15, 750-64 (2009).
35. Maraia, R.J., Mattijssen, S., Cruz-Gallardo, I. & Conte, M.R. The La and related RNAbinding proteins (LARPs): structures, functions, and evolving perspectives. WIREs RNA 8, e1430 (2017).
36. Marella, S.A. et al. An interdomain bridge influences RNA binding of the human La protein. Journal of Biological Chemistry 294, 1529-1540 (2018).
37. Dunker AK, Lawson JD, Brown CJ, et al. Intrinsically disordered protein. J Mol Graph Model. 2001;19(1):26-59.
38. Maiti S, Acharya B, Boorla VS, Manna B, Ghosh A, De S. Dynamic studies on intrinsically disordered regions of two paralogous transcription factors reveal rigid segments with important biological functions. J Mol Biol. 2019;431(7):1353-1369.
39. van der Lee R, Buljan M, Lang B, et al. Classification of intrinsically disordered regions and proteins. Chem Rev. 2014;114(13):6589-6631.
40. Bu Z, Callaway DJE. Proteins move! Protein dynamics and long-range allostery in cell signaling. Adv Protein Chem Struct Biol. 2011;83:163-221.
41. Robichaud N, Hsu BE, Istomine R, et al. Translational control in the tumor microenvironment promotes lung metastasis: Phosphorylation of eIF4E in neutrophils. Proc Natl Acad Sci U S A. 2018;115(10):E2202-E2209.

3.8 Supplemental Data

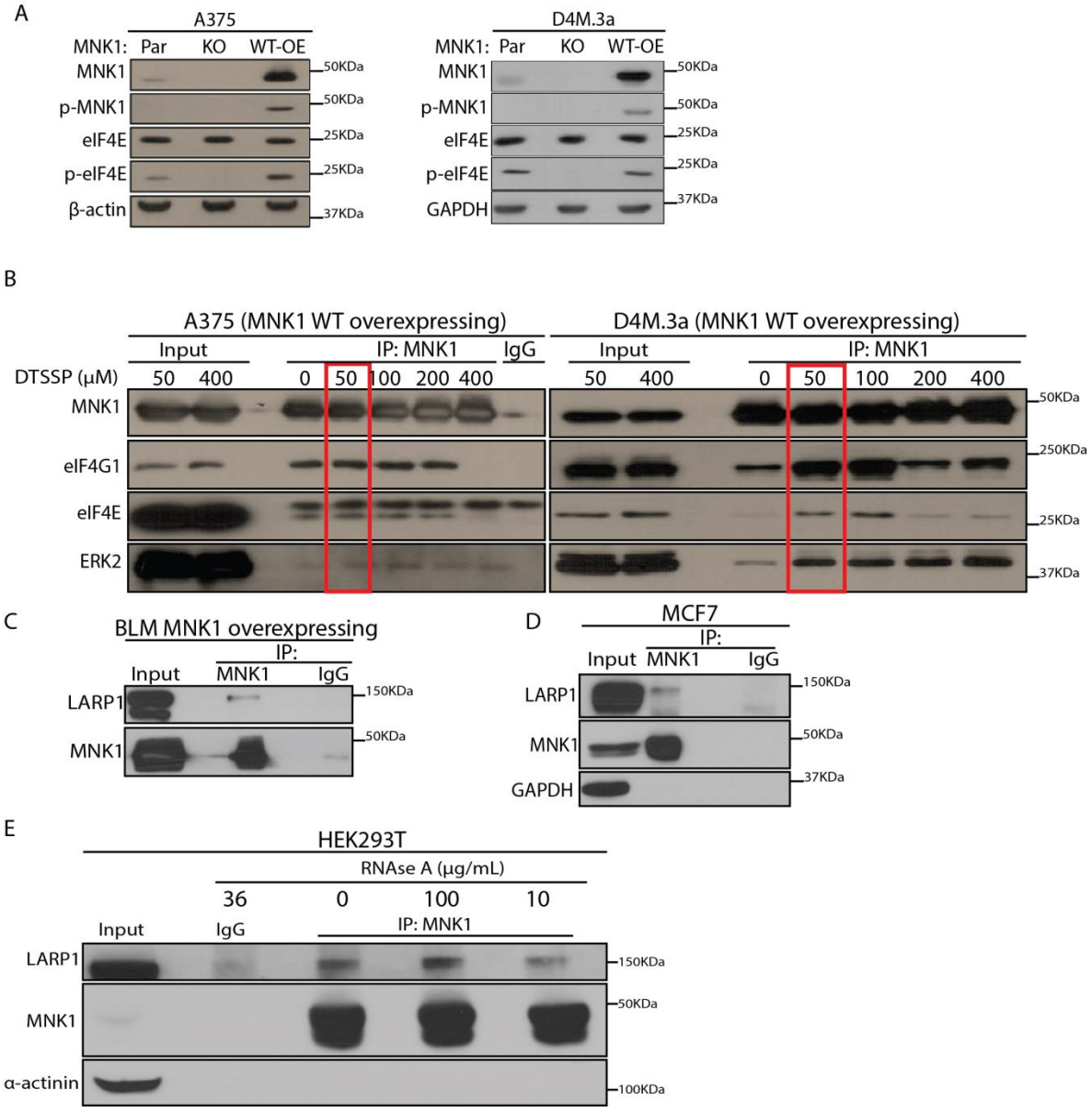

Supplemental Figure 3.1: DTSSP-based immunoprecipitation optimization and MNK1:LARP1 immunoprecipitation experiments related to Figure 3.1

A: Immunoblot demonstrating MNK1 expression in A375 and D4M.3a cells across the parental, knockout and knockout cells overexpressing WT-MNK1. **B:** Immunoprecipitation experiment to optimize DTSSP concentration to be used for the mass spectrometry experiment in A375 and D4M.3a cells (related to Figure 3.1A). **C:** Immunoblot demonstrating that endogenous LARP1 co-immunoprecipitates with MNK1 in BLM melanoma cells overexpressing MNK1. **D:** Immunoblot demonstrating that endogenous LARP1 co-immunoprecipitates with endogenous MNK1 in MCF7 cells. **E:** Immunoblot demonstrating that endogenous LARP1 co-immunoprecipitates with endogenous MNK1 in HEK293T cells in an RNA-independent manner.

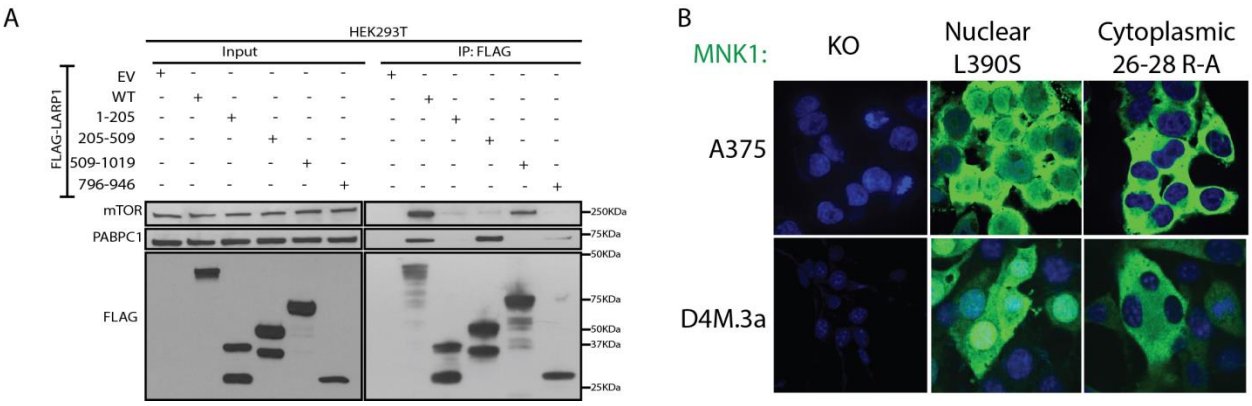

Supplemental Figure 3.2: Interactions between FLAG-LARP1 and PABPC1 or mTOR

A: Immunoblot demonstrating that endogenous PABPC1 co-immunoprecipitates with FLAG-tagged LARP1 WT and fragment 205-509 in HEK293T cells. Additionally, endogenous mTOR co-immunoprecipitates with FLAG-tagged LARP1 WT and fragment 509-1019 in HEK293T cells. **B:** Immunofluorescence of A375 and D4M.3a cells demonstrating the expression and localization of MNK1 (L390S) and MNK1 (26-28 R-A); MNK1 is depicted in green and DAPI in blue.

A

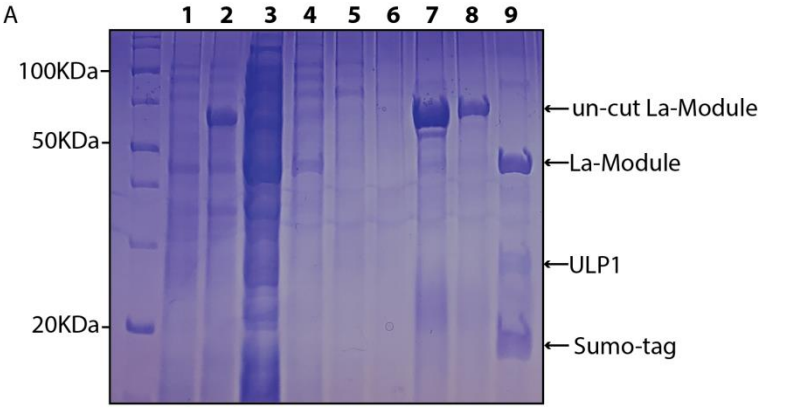

1. Pre-induction
2. Post-induction
3. Unbound fraction/ Flow through
4. Wash 1
5. Wash 2
6. Wash 3
7. Elution 1
8. Elution 2
9. Elutions; post dialysis and ULP1 cleavage

B

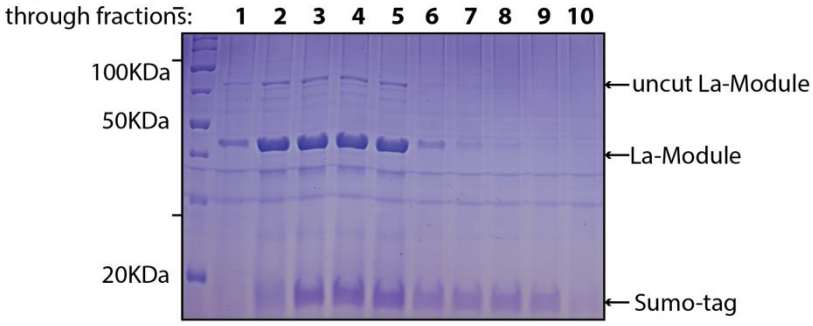

C

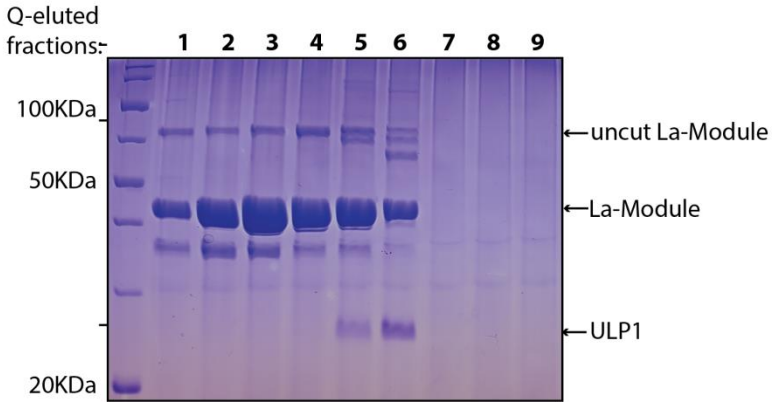

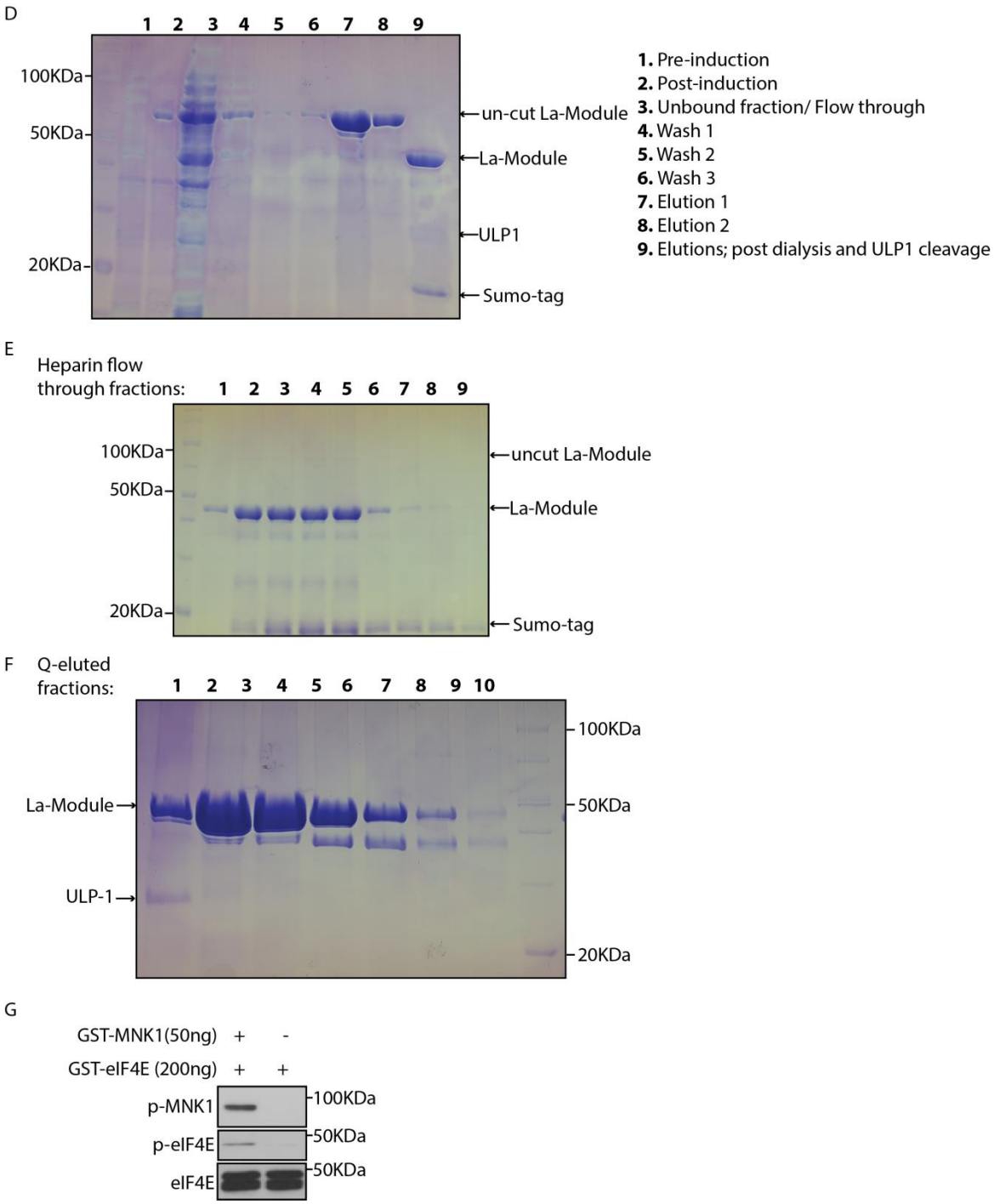

Supplemental Figure 3.3: Expression and purification of WT and T449A La-Module; *in vitro* kinase assay of eIF4E

A: Coomassie-stained SDS-PAGE gel showing the BL21 (BE3) induction, nickel-bead batch binding, elution, and tag cleavage of the WT La-Module (310 to 540)**. B:** Coomassie-stained SDS-PAGE gel demonstrating the heparin flow through fractions containing the WT La-Module (310 to 540). **C:** Coomassie-stained SDS-PAGE gel demonstrating the Q-column eluted fractions containing the purified

WT La-Module (310 to 540). **D:** Coomassie-stained SDS-PAGE gel showing the BL21 (BE3) induction, nickel-bead batch binding, elution, and tag cleavage of the T449A La-Module (310 to 540). **E:** Coomassie-stained SDS-PAGE gel demonstrating the heparin flow through fractions containing the T449A La-Module (310 to 540). **F:** Coomassie-stained SDS-PAGE gel demonstrating the Q-column eluted fractions containing the purified T449A La-Module (310 to 540). **G:** Immunoblot demonstrating GST-MNK1 phosphorylation of GST-eIF4E at serine 209 by non-radioactive *in vitro* kinase assay.

Chapter 4: Discussion and future directions

4.1 Comprehensive scholarly discussion of all findings

This body of work encompasses many interesting facets of MNK1/2 biology and their therapeutic implications. Despite their discovery over two decades ago, our knowledge about these kinases and the roles they play in cells is limited.

In chapter 2 of this thesis, we focused our efforts to better understand how the inhibition of the MNK1/2-eIF4E axis could improve current therapies in the management of neoplasms. Numerous inhibitors of MNK1/2 are either in development or being clinically tested. The importance of targeting MNK1/2 stems from the basic fact that the kinases and their most well characterized function of phosphorylating eIF4E is not a prerequisite for normal development (21, 55). Moreover, multiple studies have demonstrated that activated MNK1/2 and phosphorylation of eIF4E is critical to the oncogenic potential of this axis in a myriad of cancers (51-64). However, single-agent efficacy of MNK1/2 inhibitors has proven to be limited, and, therefore, focusing our efforts in determining cellular conditions that results in a dependence on this axis could, in theory, present as a vulnerability in cancer that we may be able to exploit.

It is well characterized that in response to many targeted inhibitors and chemotherapeutic agents, therapy naïve cells express higher levels of phosphorylated of eIF4E (8, 90). Simultaneously, it has been demonstrated that phosphorylated eIF4E selectively enhances the translation of mRNAs with pro-tumorigenic functions (53, 65-69). The reliance of cancer cells on this single phosphorylation event can have a

significant impact on cell survival. In our data we have shown that treatment of melanoma and breast cancer cells with the CDK4/6 inhibitor, palbociclib results in an increase in phosphorylated eIF4E (91). We further demonstrate that by genetically or pharmacologically inhibiting the MNK1/2 kinases, we further sensitize these cells to palbociclib (91). This effect is recapitulated in our therapy naïve murine models of melanoma where the combined inhibition of MNK1/2 and CDK4/6 results in significant delay in tumor outgrowth and overall survival (91).

However, the impact of inhibiting the MNK1/2-eIF4E axis is not limited to therapy naïve cells as many studies have demonstrated that phosphorylated eIF4E mediates resistance to cellular stresses and therapeutic agents (39, 65). Researchers have shown that cells that express the eIF4E phosphomimetic (S209D), are more resistant cellular stresses such as starvation, oxidative stress and even the effects DNA damaging agents compared with the phosphodeficient mutant of eIF4E (S209A) (39). This was recapitulated when murine embryonic fibroblast cells knocked out for MNK1/2 were discovered to be more sensitive than their WT equivalent to stress and DNA damaging agents (39). In breast cancer patients, it has been demonstrated that resistance to tamoxifen is partly mediated by an increase in phosphorylated eIF4E (65). Furthermore, in tamoxifen resistant cells, the pharmacologic inhibition of MNK1/2 or the ectopic expression of the eIF4E phosphodeficient mutant (S209A) - coupled with the knockdown of endogenous eIF4E - results in increased sensitivity to tamoxifen (65). Similarly to these studies, we and others have observed that increased expression of *MKNK2* and phosphorylated eIF4E in part mediates the process by which breast cancer

cells acquire resistance to palbociclib (91, 213). We observed that MCF7 and T47D palbociclib resistant cells express higher levels of phosphorylated eIF4E compared with their parental counterparts (91). This increase in phosphorylated eIF4E is mediated by a significant increase in *MKNK2* expression in the palbociclib resistant cells. Importantly, we further demonstrate that pharmacologically inhibiting MNK1/2 results in resensitization of these therapy resistant cells to palbociclib (91). Overall, these data and our own demonstrate that the MNK1/2-eIF4E axis is an exploitable therapeutic vulnerability in therapy naïve and therapy resistant cancer cells and warrants further interrogation. It is possible that palbociclib-resistant cancer cells have an increased dependence on proteins whose synthesis is augmented by phosphorylated eIF4E. It would be critical to compare the transcriptomes and proteomes between therapy naïve and palbociclib-resistant tumor cells.

Having been discovered and studied for over two decades, our basic knowledge of the MNK1/2 kinases are lacking. While numerous other substrates of MNK1 and MNK2 have been identified, the *in vivo* impact of the interaction has been challenging to verify and, hence, researchers commonly attribute the impact of MNK1 and MNK2 solely to their ability to phosphorylate eIF4E. This is perhaps naïve as the literature indicates that MNK1 and MNK2 play critical roles in senescence (214), cell cycle (215), and additionally, possess nuclear localization and export signal domains, and have been shown to localize to the nucleus (11-13). While studies have shown that eIF4E and activated MNK1/2 can be present in the nucleus (51, 216), it is exciting to predict that MNK1/2 have additional roles other than phosphorylating eIF4E. Uncoupling the

predominantly studied function of phosphorylating eIF4E, and evaluating other interactors and substrates of MNK1/2 will provide us with a deeper understanding of the oncogenic functions of these kinases and perhaps allow us to better target them.

In chapter 3 of this thesis, we used a proteomics based approach to determine whether MNK1 has substrates other than eIF4E. Remarkably, we discovered that MNK1, but not MNK2, interacts with another 5'cap binding protein, LARP1. This study provides us with insight into how MNK1 activity may regulate the translation of TOP mRNAs. While LARP1 also interacts with the m^7GTP cap of TOP mRNAs, its role in protein synthesis has been shown to be repressive (101-105). In cellular conditions that are growth restrictive, wherein mTOR is inactive, eIF4E remains bound to 4E-BP1/2 and, simultaneously, LARP1 binds and represses the translation of TOP mRNA transcripts (103, 105, 106, 111). However, when nutrients become available, activated mTOR phosphorylates 4E-BP1/2 and LARP1, allowing the release of eIF4E and the mRNA respectively (103, 105, 106, 111). Finally, this allows eIF4E to bind the mRNA and begin the process of translation initiation (103, 105, 106, 111). It has been shown that MNK2 phosphorylates eIF4E basally while MNK1 activity is inducible by extracellular signals (4, 13). Hence, the specificity of the interaction between MNK1 and LARP1 may be regulated by specific upstream signaling mediators such as ERK1/2 or p38. MNK1 specifically interacts with the La-module on LARP1, possibly through its N-terminal region. Moreover, we demonstrate that the interaction between the two proteins is likely not mediated by RNA. This is interesting for two reasons: (1) Similar to LARP1, MNK1 also interacts with the scaffold protein eIF4G via the polybasic sequence in its N-

terminal region (13). Substitution mutations in this polybasic region abrogates the interaction between MNK1 and both eIF4G and LARP1. (2) LARP1 also binds PABP through the La-module. These raise some thought-provoking questions, with potentially exciting answers. Does the interaction between MNK1 and LARP1 depend on eIF4G or PABP? Are there pools of LARP1-bound mRNA in cells whose translation may be sensitive to MNK1 activity? To add on to our curiosity, we have demonstrated that MNK1 can phosphorylate the La-module on threonine 449. While the DM15 region on LARP1 interacts with the m^7GTP cap, the La-module interacts with the TOP motif and the poly (A) tails of RNA. In the context of MNK1, this is particularly interesting as MNK1 does not appear to bind or phosphorylate the cap-binding domain of LARP1, as it does with eIF4E. Importantly, we demonstrate, using electrophoretic mobility shift assays, that a phosphodeficient T449A La-module (mimicking a cellular condition wherein MNK1 would be inhibited) has a higher affinity for RNA compared with its WT LARP1 equivalent. Overall, these data suggest that, when nutrients are available, MNK1 phosphorylates LARP1to facilitate the latter from dissociating from TOP mRNA, allowing free eIF4E to associate with and promote mRNA translation. Additionally, these data provides us with a broader view of how MNK1 and mTOR kinases may work in conjunction to orchestrate the process of ribosome biogenesis.

4.2 Research limitations and future directions

While this body of work has provided us with novel insights into MNK1/2 biology, a lot of questions related to the work presented in both chapters remain and allow for further avenues of investigation.

4.2.1 Investigating the combination of CDK4/6 and MNK1/2 inhibition in models of cancer metastasis

While our study primarily focused on the impact of the combination on proliferation and cell cycle arrest, there is an abundance of literature indicating the critical roles CDK4/6 and MNK1/2 play in metastasis. The MNK1/2-eIF4E axis promotes the synthesis of proteins associated with invasion and metastasis such as Snail, MMP3, MMP9 (68, 217). It has also been demonstrated that increased expression of phosphorylated eIF4E is associated with poor prognosis in metastatic breast cancer (218, 219). Additionally, MNK2 expression is correlated with increased metastasis and acts as an independent prognostic factor in patients with non-small cell lung cancer (220). Furthermore, data generated from our lab has demonstrated that the MNK1/2-eIF4E axis promotes invasion and metastasis of melanoma and breast cancer (53, 54, 64, 68, 78, 99). Similarly, CDK4/6 activity has been associated with increased cancer metastasis in triple-negative breast cancer through stabilization of SNAIL1, while inhibition of CDK4/6 has been demonstrated to repress tumor metastasis. (221, 222) Given the established role of phosphorylated eIF4E in driving breast cancer metastasis, it would be prudent to investigate the combination of CDK4/6 and MNK1/2 inhibitors in the context of metastatic models of cancer.

4.2.2 Determining the impact of the CDK4/6 and MNK1/2 combination on the tumor microenvironment

We and others have demonstrated the importance of the MNK1/2-eIF4E axis in regulating the tumor microenvironment. Our lab has demonstrated that whole body

phospho-eIF4E deficient mice are more protected from tumor outgrowth and metastasis (96). Moreover, it has been demonstrated that the MNK1/2-eIF4E axis has a profound impact on tumor-associated cells within the tumor microenvironment (54, 94, 99). We have demonstrated that the MNK1/2-eIF4E axis controls the expression of PD-L1 on dendritic cells (DCs), which is significant since PD-L1 expressed by DCs promotes immune evasion against tumors (54). Furthermore, in co-culture studies, eIF4E phosphodeficient DCs increased the number of $CD8^+$ T cells that release IFN-γ, a potent mediator of the cytotoxic T cell response (54). Studies in murine models of hepatocellular carcinoma have demonstrated that inhibition of the MNK1/2-eIF4E axis resulted in increased PD-L1 expression (98). Importantly, MNK1/2 inhibitors are currently being tested in combination with anti-PD-1/PD-L1 immunotherapy in solid tumors (NCT03616834).

There is increasing evidence that CDK4/6 inhibitors boost anti-tumor immunity by promoting T-cell activation and tumor infiltration (223-225). Furthermore, it has been demonstrated that exposure of murine melanoma and colorectal cells to CDK4/6 inhibitors can increase the surface expression of PD-L1 (226). Additionally, it has been shown that CDK4/6 inhibition augments the therapeutic efficacy of anti-PD-L1 therapy in murine models of oral squamous cell carcinoma (227). In HR+ breast cancer patients, it has been demonstrated that CDK4/6 inhibition reduces the circulating levels of immunosuppressive regulatory T cells (Tregs) and myeloid-derived suppressor cells (MDSCs), two well-known mechanisms serving to override the anti-tumor immune response (228). Importantly, the combination of palbociclib, pembrolizumab and

letrozole in HR+ breast cancer are well tolerated and patients achieved a 31% complete response (229). Overall, these data highlight the importance for investigating the impact of the combined inhibition of MNK1/2 and CDK4/6 in the tumor microenvironment and immune landscape.

4.2.3 Investigate the mechanism by which phosphorylated eIF4E mediates resistance to CDK4/6 inhibition

Feedback from the translation machinery has been reported to mediate resistance to CDK4/6 inhibitors (207-212) and it has been demonstrated that the addition of inhibitors of mRNA translation can result in potent repression of these therapy-resistant cells. In chapter 2 we show that breast cells resistant to palbociclib have increased expression of *MKNK2* and phosphorylated eIF4E compared to their parental counterparts. Moreover, we further demonstrate that blocking this increase in phosphorylated eIF4E results in resensitization of the cells to palbociclib *in vitro*. In subsequent studies, it would be important to investigate the mechanism by which these CDK4/6 therapy-resistant cells depend on phosphorylated eIF4E as it may provide us with other exploitable vulnerabilities in these cells. Furthermore, it would be important to assess whether palbociclib-resistant cells are specifically dependent on MNK2 or whether MNK1 may promote therapy resistance to palbociclib.

4.2.4 Characterizing the impact of eIF4G and PABP on the interaction between MNK1 and LARP1

Our work in chapter 3 has introduced LARP1 as a novel substrate of MNK1. However, many questions regarding the interaction remain. Since we have demonstrated that MNK1 binds LARP1 via the La-module, it is possible that this interaction is mediated by PABPC1, as PABPC1 and LARP1 have been shown to endogenously interact with each other (111, 230). Similarly, we have shown that the polybasic region within the N-terminal of MNK1 is required for its interaction with both LARP1 and eIF4G, thus it would be important to determine whether eIF4G mediates the interaction with LARP1. eIF4G is the scaffold protein of the eIF4F complex, and can endogenously interact with PABPC1 as well. Hence, it is possible that MNK1 can be in complex with these proteins, which may mediate its interaction with LARP1. Deciphering the underpinnings of the interaction may provide us with a better understanding of the dynamics of the mRNA translation process. Ultimately, we do demonstrate that MNK1 can interact with LARP1 in an RNA-independent manner, suggesting that the proteins may directly bind each other. We also demonstrate, using mass spectrometry and *in vitro* kinase assays, that MNK1 can phosphorylate LARP1 at T449.

4.2.5 Investigating other MNK1-dependent phosphorylation sites on LARP1

We have demonstrated using mass spectrometry and *in vitro* kinases assays that MNK1 can indeed phosphorylate LARP1 on the La-module and not the DM15. However, it remains unclear whether MNK1 is able to phosphorylate other serines or threonines on the La-module. While our mass spectrometry data revealed the threonine 449 site as being the only significant MNK1 phosphosite on LARP1, we observed that

MNK1 still can phosphorylate the phosphodeficient T449A La-module in our *in vitro* kinase assays, albeit to a lesser extent that the unmutated La-module. Therefore, it is entirely possible that MNK1 can phosphorylate LARP1 at multiple sites. Discovery and investigation of other MNK1-dependent phosphosites would provide invaluable information about the impact of MNK1 kinase activity on LARP1.

4.2.6 Impact of the MNK1 and LARP1 interaction on mRNA translation and cancer

While our *in vitro* data has demonstrated that the MNK1-dependent phosphorylation of LARP1 likely impacts the ability of LARP1 to associate with RNA, we have yet to investigate the importance of the interaction in living cells. There is emerging data demonstrating the importance of the expression and function of LARP1 in cancer development and progression. LARP1 is overexpressed in multiple malignancies and is associated with poor prognosis (113, 115-117). However, the data investigating the function of LARP1 in cancer is still emerging. While knockout of LARP1 is not lethal, cells deficient in LARP1 exhibit decreased cell proliferation, invasion, and increased apoptosis (113, 114, 231). Furthermore, it has been shown that LARP1 can positively regulate the expression of oncogenic mRNAs like *mTOR*, *BCL2*, *AKT3*, and *ERBB3*, and negatively regulate anti-tumorigenic transcripts like *BIK* and *TNF* (113, 114). It has been demonstrated that the MNK1/2-eIF4E axis can promote the expression of oncogenic mRNAs such as *BCL2* and *TNFα* (5, 28, 96). Therefore, we would hypothesize that the activity of MNK1 on LARP1 may potentially play a role in the process by which these mRNAs are translated. Overall, these data highlight the importance of investigating the role of LARP1 in cancer. Pertinent to our data, it would

be critical to study the *in vivo* phenotype of the phosphodeficient T449A mutant compared with WT and the phosphomimetic T449D mutant. Additionally, it would be important to understand the relationship between the various phosphorylation events of LARP1 in the context of eIF4E phosphorylation. Another important aspect that remains uninvestigated is the role of LARP1 in immune cell function.

4.2.7 Investigate the function of exon 1 in LARP1 isoforms

LARP1 is expressed as two distinct isoforms i.e. the long isoform consisting 1096 amino acids and the shorter, 1019 amino acid isoform. It has been demonstrated that the longer isoform is dominantly expressed in human cancer cell lines (232). Apart from the first exon, both isoforms are entirely homologous. While we have not thoroughly studied the relevance of the individual isoforms, we have demonstrated that MNK1 interacts with the La-Module, a region that is homologous between both isoforms. Additionally, the threonine on LARP1 that we propose is phosphorylated by MNK1, namely T526 within the longer isoform and T449 within the shorter isoform – is also conserved between the two isoforms. However, it would be prudent to investigate the importance of the amino acids encoded by the first exon in both isoforms, as it may possess additional and potentially different functions in regulating mRNA translation.

4.3 Final conclusion and summary

In conclusion, this thesis presents novel mechanisms by which the MNK1/2 kinases can regulate the efficacy of therapeutic agents. Furthermore, we present the discovery and potential impact of a novel substrate of MNK1 kinase.

The objectives of our studies were as follows:

1. To determine the impact of combining the FDA-approved CDK4/6 inhibitor, palbociclib with preclinical and clinically available MNK1/2 inhibitors.
2. To identify the mechanism of response to the therapeutic combination.
3. To assess whether therapeutic resistance to palbociclib occurs through mechanisms involving the MNK1/2-eIF4E axis.
4. To determine the *in vivo* efficacy of the therapeutic combination in melanoma models.
5. To identify novel interactors and substrates of MNK1.
6. To characterize the binding dynamics of any identified protein:protein interactions.
7. To determine whether MNK1/2 can phosphorylate identified interacting proteins.
8. To determine the functional impact of the MNK1-dependent phosphorylation of the substrate.

The objectives of our studies were accomplished as follows:

In chapter 2 of this thesis, we assessed the *in vitro* efficacy of the combined pharmacologic CDK4/6 and MNK1/2 (pharmacologic or genetic) inhibition using colony forming assays and demonstrated that melanoma and breast cancer exposed to the combination had significantly repressed clonogenic outgrowth compared to either single agent alone. Using quantitative proteomics, we discovered that melanoma cells treated with the combination had repressed expression of proteins critical for mitosis. Cell cycle analysis using propidium iodide staining demonstrated that the combination increased

G1 cell cycle arrest in melanoma and breast cancer cells. The effect of the combination on G1 cell cycle arrest in melanoma cells were verified using the FUCCI cell cycle system. We further demonstrate that the combination of CDK4/6 and MNK1/2 inhibition significantly increased β-gal associated senescence compared with either single agent. Next, using colony forming assays we show that CDK4/6 therapy-resistant melanoma and breast cancer cells can be resensitized to palbociclib upon treatment with a MNK1/2 inhibitor. We further demonstrate using qPCR and immunoblotting that palbociclib-resistant breast cancer cells express higher levels of *MKNK2* and phosphorylated eIF4E respectively compared with their parental counterparts. Finally, using *in vivo* models of therapy-naïve melanoma, we show that the combined inhibition of CDK4/6 and MNK1/2 significantly delays tumor outgrowth, and increases overall survival compared with single agents. Additionally, immunoblotting of the tumors harvested from mice treated with the combination showed repressed expression of proteins discovered to be downregulated in our *in vitro* proteomics experiment.

In chapter 3 of this thesis, we use a crosslinking proteomics approach to identify novel interactors of MNK1. In our proteomics, we identified LARP1 as a novel binding partner of MNK1. Using immunoprecipitation assays we discovered that MNK1, but not MNK2, can interact with LARP1. We further demonstrate that LARP1 interacts with MNK1 in an RNA-independent manner. Additionally, we map the domains on LARP and MNK1 that are necessary for the interaction. We next determined that MNK1 can phosphorylate LARP1 using a combination of quantitative phosphoproteomics and radioactivity based *in vitro* kinase assays. Finally, we purified recombinant La-module (WT and T449A) and

by electrophoretic mobility shift assays, we demonstrate that the phosphodeficient T449A mutant has a higher affinity for RNA compared with its WT equivalent. With the support of McGill University's annual Graduate Mobility Award (2021 – 2022), I performed the La-Module protein purifications, *in vitro* kinase assays, and the electrophoretic mobility shift assays in the laboratory of Dr. Andrea Berman at the University of Pittsburgh.

Chapter 5: Bibliography (Chapters 1 and 4)

1. Fukunaga R, Hunter T. MNK1, a new MAP kinase-activated protein kinase, isolated by a novel expression screening method for identifying protein kinase substrates. Embo j. 1997;16(8):1921-33.
2. Waskiewicz AJ, Flynn A, Proud CG, Cooper JA. Mitogen-activated protein kinases activate the serine/threonine kinases Mnk1 and Mnk2. Embo j. 1997;16(8):1909-20.
3. Slentz-Kesler K, Moore JT, Lombard M, Zhang J, Hollingsworth R, Weiner MP. Identification of the human Mnk2 gene (MKNK2) through protein interaction with estrogen receptor beta. Genomics. 2000;69(1):63-71.
4. O'Loghlen A, González VM, Piñeiro D, Pérez-Morgado MI, Salinas M, Martín ME. Identification and molecular characterization of Mnk1b, a splice variant of human MAP kinase-interacting kinase Mnk1. Exp Cell Res. 2004;299(2):343-55.
5. Buxadé M, Parra JL, Rousseau S, Shpiro N, Marquez R, Morrice N, et al. The Mnks are novel components in the control of TNF alpha biosynthesis and phosphorylate and regulate hnRNP A1. Immunity. 2005;23(2):177-89.
6. Liu H, Gong Z, Li K, Zhang Q, Xu Z, Xu Y. SRPK1/2 and PP1α exert opposite functions by modulating SRSF1-guided MKNK2 alternative splicing in colon adenocarcinoma. J Exp Clin Cancer Res. 2021;40(1):75.
7. Maimon A, Mogilevsky M, Shilo A, Golan-Gerstl R, Obiedat A, Ben-Hur V, et al. Mnk2 alternative splicing modulates the p38-MAPK pathway and impacts Ras-induced transformation. Cell Rep. 2014;7(2):501-13.
8. Adesso L, Calabretta S, Barbagallo F, Capurso G, Pilozzi E, Geremia R, et al. Gemcitabine triggers a pro-survival response in pancreatic cancer cells through activation of the MNK2/eIF4E pathway. Oncogene. 2013;32(23):2848-57.
9. García-Recio EM, Pinto-Díez C, Pérez-Morgado MI, García-Hernández M, Fernández G, Martín ME, et al. Characterization of MNK1b DNA Aptamers That Inhibit Proliferation in MDA-MB231 Breast Cancer Cells. Mol Ther Nucleic Acids. 2016;5(1):e275.
10. Goto S, Yao Z, Proud CG. The C-terminal domain of Mnk1a plays a dual role in tightly regulating its activity. Biochem J. 2009;423(2):279-90.
11. Parra-Palau JL, Scheper GC, Wilson ML, Proud CG. Features in the N and C termini of the MAPK-interacting kinase Mnk1 mediate its nucleocytoplasmic shuttling. J Biol Chem. 2003;278(45):44197-204.
12. Waskiewicz AJ, Johnson JC, Penn B, Mahalingam M, Kimball SR, Cooper JA. Phosphorylation of the cap-binding protein eukaryotic translation initiation factor 4E by protein kinase Mnk1 in vivo. Mol Cell Biol. 1999;19(3):1871-80.
13. Scheper GC, Parra JL, Wilson M, Van Kollenburg B, Vertegaal AC, Han ZG, et al. The N and C termini of the splice variants of the human mitogen-activated protein kinase-interacting kinase Mnk2 determine activity and localization. Mol Cell Biol. 2003;23(16):5692-705.
14. Pyronnet S, Imataka H, Gingras AC, Fukunaga R, Hunter T, Sonenberg N. Human eukaryotic translation initiation factor 4G (eIF4G) recruits mnk1 to phosphorylate eIF4E. Embo j. 1999;18(1):270-9.
15. McKendrick L, Thompson E, Ferreira J, Morley SJ, Lewis JD. Interaction of eukaryotic translation initiation factor 4G with the nuclear cap-binding complex provides a link between nuclear and cytoplasmic functions of the m(7) guanosine cap. Mol Cell Biol. 2001;21(11):3632-41.
16. Parra JL, Buxadé M, Proud CG. Features of the catalytic domains and C termini of the MAPK signal-integrating kinases Mnk1 and Mnk2 determine their differing activities and regulatory properties. J Biol Chem. 2005;280(45):37623-33.

17. Jauch R, Cho MK, Jäkel S, Netter C, Schreiter K, Aicher B, et al. Mitogen-activated protein kinases interacting kinases are autoinhibited by a reprogrammed activation segment. Embo j. 2006;25(17):4020-32.
18. Treiber DK, Shah NP. Ins and outs of kinase DFG motifs. Chem Biol. 2013;20(6):745-6.
19. Kannan S, Pradhan MR, Cherian J, Joseph TL, Poh ZY, Hai Yan Y, et al. Small Molecules Targeting the Inactive Form of the Mnk1/2 Kinases. ACS Omega. 2017;2(11):7881-91.
20. Flynn A, Proud CG. Serine 209, not serine 53, is the major site of phosphorylation in initiation factor eIF-4E in serum-treated Chinese hamster ovary cells. J Biol Chem. 1995;270(37):21684-8.
21. Ueda T, Watanabe-Fukunaga R, Fukuyama H, Nagata S, Fukunaga R. Mnk2 and Mnk1 are essential for constitutive and inducible phosphorylation of eukaryotic initiation factor 4E but not for cell growth or development. Mol Cell Biol. 2004;24(15):6539-49.
22. Frank MJ, Dawson DW, Bensinger SJ, Hong JS, Knosp WM, Xu L, et al. Expression of sprouty2 inhibits B-cell proliferation and is epigenetically silenced in mouse and human B-cell lymphomas. Blood. 2009;113(11):2478-87.
23. Lee CC, Putnam AJ, Miranti CK, Gustafson M, Wang LM, Vande Woude GF, et al. Overexpression of sprouty 2 inhibits HGF/SF-mediated cell growth, invasion, migration, and cytokinesis. Oncogene. 2004;23(30):5193-202.
24. Sánchez A, Setién F, Martinez N, Oliva JL, Herranz M, Fraga MF, et al. Epigenetic inactivation of the ERK inhibitor Spry2 in B-cell diffuse lymphomas. Oncogene. 2008;27(36):4969-72.
25. DaSilva J, Xu L, Kim HJ, Miller WT, Bar-Sagi D. Regulation of sprouty stability by Mnk1-dependent phosphorylation. Mol Cell Biol. 2006;26(5):1898-907.
26. Roy R, Huang Y, Seckl MJ, Pardo OE. Emerging roles of hnRNPA1 in modulating malignant transformation. Wiley Interdiscip Rev RNA. 2017;8(6).
27. Chen Y, Liu J, Wang W, Xiang L, Wang J, Liu S, et al. High expression of hnRNPA1 promotes cell invasion by inducing EMT in gastric cancer. Oncol Rep. 2018;39(4):1693-701.
28. Buxadé M, Morrice N, Krebs DL, Proud CG. The PSF.p54nrb complex is a novel Mnk substrate that binds the mRNA for tumor necrosis factor alpha. J Biol Chem. 2008;283(1):57-65.
29. Mitobe Y, Iino K, Takayama KI, Ikeda K, Suzuki T, Aogi K, et al. PSF Promotes ER-Positive Breast Cancer Progression via Posttranscriptional Regulation of ESR1 and SCFD2. Cancer Res. 2020;80(11):2230-42.
30. Tsukahara T, Haniu H, Matsuda Y. PTB-associated splicing factor (PSF) is a PPARγ-binding protein and growth regulator of colon cancer cells. PLoS One. 2013;8(3):e58749.
31. Tsukahara T, Matsuda Y, Haniu H. PSF knockdown enhances apoptosis via downregulation of LC3B in human colon cancer cells. Biomed Res Int. 2013;2013:204973.
32. Hefner Y, Borsch-Haubold AG, Murakami M, Wilde JI, Pasquet S, Schieltz D, et al. Serine 727 phosphorylation and activation of cytosolic phospholipase A2 by MNK1-related protein kinases. J Biol Chem. 2000;275(48):37542-51.
33. Linkous A, Yazlovitskaya E. Cytosolic phospholipase A2 as a mediator of disease pathogenesis. Cell Microbiol. 2010;12(10):1369-77.
34. Wendum D, Comperat E, Boëlle PY, Parc R, Masliah J, Trugnan G, et al. Cytoplasmic phospholipase A2 alpha overexpression in stromal cells is correlated with angiogenesis in human colorectal cancer. Mod Pathol. 2005;18(2):212-20.
35. Manne BK, Campbell RA, Bhatlekar S, Ajanel A, Denorme F, Portier I, et al. MAPK-interacting kinase 1 regulates platelet production, activation, and thrombosis. Blood. 2022;140(23):2477-89.
36. Merrick WC, Pavitt GD. Protein Synthesis Initiation in Eukaryotic Cells. Cold Spring Harb Perspect Biol. 2018;10(12).

37. Sonenberg N, Hinnebusch AG. Regulation of translation initiation in eukaryotes: mechanisms and biological targets. Cell. 2009;136(4):731-45.
38. Jackson RJ, Hellen CU, Pestova TV. The mechanism of eukaryotic translation initiation and principles of its regulation. Nat Rev Mol Cell Biol. 2010;11(2):113-27.
39. Martínez A, Sesé M, Losa JH, Robichaud N, Sonenberg N, Aasen T, et al. Phosphorylation of eIF4E Confers Resistance to Cellular Stress and DNA-Damaging Agents through an Interaction with 4E-T: A Rationale for Novel Therapeutic Approaches. PLoS One. 2015;10(4):e0123352.
40. Yi T, Papadopoulos E, Hagner PR, Wagner G. Hypoxia-inducible factor-1α (HIF-1α) promotes cap-dependent translation of selective mRNAs through up-regulating initiation factor eIF4E1 in breast cancer cells under hypoxia conditions. J Biol Chem. 2013;288(26):18732-42.
41. Shah OJ, Anthony JC, Kimball SR, Jefferson LS. 4E-BP1 and S6K1: translational integration sites for nutritional and hormonal information in muscle. Am J Physiol Endocrinol Metab. 2000;279(4):E715-29.
42. Lin CJ, Cencic R, Mills JR, Robert F, Pelletier J. c-Myc and eIF4F are components of a feedforward loop that links transcription and translation. Cancer Res. 2008;68(13):5326-34.
43. Siddiqui N, Sonenberg N. Signalling to eIF4E in cancer. Biochem Soc Trans. 2015;43(5):763-72.
44. Alain T, Morita M, Fonseca BD, Yanagiya A, Siddiqui N, Bhat M, et al. eIF4E/4E-BP ratio predicts the efficacy of mTOR targeted therapies. Cancer Res. 2012;72(24):6468-76.
45. Yang X, Zhong W, Cao R. Phosphorylation of the mRNA cap-binding protein eIF4E and cancer. Cell Signal. 2020;73:109689.
46. O'Loghlen A, González VM, Salinas M, Martín ME. Suppression of human Mnk1 by small interfering RNA increases the eukaryotic initiation factor 4F activity in HEK293T cells. FEBS Lett. 2004;578(1-2):31-5.
47. Scheper GC, van Kollenburg B, Hu J, Luo Y, Goss DJ, Proud CG. Phosphorylation of eukaryotic initiation factor 4E markedly reduces its affinity for capped mRNA. J Biol Chem. 2002;277(5):3303-9.
48. Slepenkov SV, Darzynkiewicz E, Rhoads RE. Stopped-flow kinetic analysis of eIF4E and phosphorylated eIF4E binding to cap analogs and capped oligoribonucleotides: evidence for a one-step binding mechanism. J Biol Chem. 2006;281(21):14927-38.
49. Wheater MJ, Johnson PW, Blaydes JP. The role of MNK proteins and eIF4E phosphorylation in breast cancer cell proliferation and survival. Cancer Biol Ther. 2010;10(7):728-35.
50. Konicek BW, Stephens JR, McNulty AM, Robichaud N, Peery RB, Dumstorf CA, et al. Therapeutic inhibition of MAP kinase interacting kinase blocks eukaryotic initiation factor 4E phosphorylation and suppresses outgrowth of experimental lung metastases. Cancer Res. 2011;71(5):1849-57.
51. Carter JH, Deddens JA, Spaulding NI, Lucas D, Colligan BM, Lewis TG, et al. Phosphorylation of eIF4E serine 209 is associated with tumour progression and reduced survival in malignant melanoma. Br J Cancer. 2016;114(4):444-53.
52. Fan S, Ramalingam SS, Kauh J, Xu Z, Khuri FR, Sun SY. Phosphorylated eukaryotic translation initiation factor 4 (eIF4E) is elevated in human cancer tissues. Cancer Biol Ther. 2009;8(15):1463-9.
53. Zhan Y, Guo J, Yang W, Goncalves C, Rzymski T, Dreas A, et al. MNK1/2 inhibition limits oncogenicity and metastasis of KIT-mutant melanoma. J Clin Invest. 2017;127(11):4179-92.
54. Huang F, Gonçalves C, Bartish M, Rémy-Sarrazin J, Issa ME, Cordeiro B, et al. Inhibiting the MNK1/2-eIF4E axis impairs melanoma phenotype switching and potentiates antitumor immune responses. J Clin Invest. 2021;131(8).
55. Furic L, Rong L, Larsson O, Koumakpayi IH, Yoshida K, Brueschke A, et al. eIF4E phosphorylation promotes tumorigenesis and is associated with prostate cancer progression. Proc Natl Acad Sci U S A. 2010;107(32):14134-9.

56. Topisirovic I, Ruiz-Gutierrez M, Borden KL. Phosphorylation of the eukaryotic translation initiation factor eIF4E contributes to its transformation and mRNA transport activities. Cancer Res. 2004;64(23):8639-42.
57. Holm N, Byrnes K, Johnson L, Abreo F, Sehon K, Alley J, et al. A prospective trial on initiation factor 4E (eIF4E) overexpression and cancer recurrence in node-negative breast cancer. Ann Surg Oncol. 2008;15(11):3207-15.
58. Chen YT, Tsai HP, Wu CC, Wang JY, Chai CY. Eukaryotic translation initiation factor 4E (eIF-4E) expressions are associated with poor prognosis in colorectal adenocarcinoma. Pathol Res Pract. 2017;213(5):490-5.
59. Jiang XM, Yu XN, Huang RZ, Zhu HR, Chen XP, Xiong J, et al. Prognostic significance of eukaryotic initiation factor 4E in hepatocellular carcinoma. J Cancer Res Clin Oncol. 2016;142(11):2309-17.
60. Fang D, Peng J, Wang G, Zhou D, Geng X. Upregulation of eukaryotic translation initiation factor 4E associates with a poor prognosis in gallbladder cancer and promotes cell proliferation in vitro and in vivo. Int J Mol Med. 2019;44(4):1325-32.
61. Salehi Z, Mashayekhi F, Shahosseini F. Significance of eIF4E expression in skin squamous cell carcinoma. Cell Biol Int. 2007;31(11):1400-4.
62. Salehi Z, Mashayekhi F. Expression of the eukaryotic translation initiation factor 4E (eIF4E) and 4E-BP1 in esophageal cancer. Clin Biochem. 2006;39(4):404-9.
63. Hou S, Du P, Wang P, Wang C, Liu P, Liu H. Significance of MNK1 in prognostic prediction and chemotherapy development of epithelial ovarian cancer. Clin Transl Oncol. 2017;19(9):1107-16.
64. Guo Q, Li VZ, Nichol JN, Huang F, Yang W, Preston SEJ, et al. MNK1/NODAL Signaling Promotes Invasive Progression of Breast Ductal Carcinoma In Situ. Cancer Res. 2019;79(7):1646-57.
65. Geter PA, Ernlund AW, Bakogianni S, Alard A, Arju R, Giashuddin S, et al. Hyperactive mTOR and MNK1 phosphorylation of eIF4E confer tamoxifen resistance and estrogen independence through selective mRNA translation reprogramming. Genes Dev. 2017;31(22):2235-49.
66. Wendel HG, Silva RL, Malina A, Mills JR, Zhu H, Ueda T, et al. Dissecting eIF4E action in tumorigenesis. Genes Dev. 2007;21(24):3232-7.
67. Mody PH, Dos Santos NL, Barron LR, Price TJ, Burton MD. eIF4E phosphorylation modulates pain and neuroinflammation in the aged. Geroscience. 2020;42(6):1663-74.
68. Robichaud N, del Rincon SV, Huor B, Alain T, Petruccelli LA, Hearnden J, et al. Phosphorylation of eIF4E promotes EMT and metastasis via translational control of SNAIL and MMP-3. Oncogene. 2015;34(16):2032-42.
69. Khosravi S, Tam KJ, Ardekani GS, Martinka M, McElwee KJ, Ong CJ. eIF4E is an adverse prognostic marker of melanoma patient survival by increasing melanoma cell invasion. J Invest Dermatol. 2015;135(5):1358-67.
70. Truitt ML, Conn CS, Shi Z, Pang X, Tokuyasu T, Coady AM, et al. Differential Requirements for eIF4E Dose in Normal Development and Cancer. Cell. 2015;162(1):59-71.
71. Prabhu SA, Moussa O, Miller WH, Jr., Del Rincón SV. The MNK1/2-eIF4E Axis as a Potential Therapeutic Target in Melanoma. Int J Mol Sci. 2020;21(11).
72. Hsu PP, Kang SA, Rameseder J, Zhang Y, Ottina KA, Lim D, et al. The mTOR-regulated phosphoproteome reveals a mechanism of mTORC1-mediated inhibition of growth factor signaling. Science. 2011;332(6035):1317-22.
73. Yu Y, Yoon SO, Poulogiannis G, Yang Q, Ma XM, Villén J, et al. Phosphoproteomic analysis identifies Grb10 as an mTORC1 substrate that negatively regulates insulin signaling. Science. 2011;332(6035):1322-6.

74. Choo AY, Blenis J. Not all substrates are treated equally: implications for mTOR, rapamycin-resistance and cancer therapy. Cell Cycle. 2009;8(4):567-72.
75. Harrington LS, Findlay GM, Lamb RF. Restraining PI3K: mTOR signalling goes back to the membrane. Trends Biochem Sci. 2005;30(1):35-42.
76. Soefje SA, Karnad A, Brenner AJ. Common toxicities of mammalian target of rapamycin inhibitors. Target Oncol. 2011;6(2):125-9.
77. Martins F, de Oliveira MA, Wang Q, Sonis S, Gallottini M, George S, et al. A review of oral toxicity associated with mTOR inhibitor therapy in cancer patients. Oral Oncol. 2013;49(4):293-8.
78. Yang W, Khoury E, Guo Q, Prabhu SA, Emond A, Huang F, et al. MNK1 signaling induces an ANGPTL4-mediated gene signature to drive melanoma progression. Oncogene. 2020;39(18):3650-65.
79. Kosciuczuk EM, Kar AK, Blyth GT, Fischietti M, Abedin S, Mina AA, et al. Inhibitory effects of SEL201 in acute myeloid leukemia. Oncotarget. 2019;10(67):7112-21.
80. Suarez M, Blyth GT, Mina AA, Kosciuczuk EM, Dolniak B, Dinner S, et al. Inhibitory effects of Tomivosertib in acute myeloid leukemia. Oncotarget. 2021;12(10):955-66.
81. Wang X, Yue P, Chan CB, Ye K, Ueda T, Watanabe-Fukunaga R, et al. Inhibition of mammalian target of rapamycin induces phosphatidylinositol 3-kinase-dependent and Mnk-mediated eukaryotic translation initiation factor 4E phosphorylation. Mol Cell Biol. 2007;27(21):7405-13.
82. Lineham E, Tizzard GJ, Coles SJ, Spencer J, Morley SJ. Synergistic effects of inhibiting the MNK-eIF4E and PI3K/AKT/ mTOR pathways on cell migration in MDA-MB-231 cells. Oncotarget. 2018;9(18):14148-59.
83. Eckerdt F, Beauchamp E, Bell J, Iqbal A, Su B, Fukunaga R, et al. Regulatory effects of a Mnk2-eIF4E feedback loop during mTORC1 targeting of human medulloblastoma cells. Oncotarget. 2014;5(18):8442-51.
84. Grzmil M, Huber RM, Hess D, Frank S, Hynx D, Moncayo G, et al. MNK1 pathway activity maintains protein synthesis in rapalog-treated gliomas. J Clin Invest. 2014;124(2):742-54.
85. Huang XB, Yang CM, Han QM, Ye XJ, Lei W, Qian WB. MNK1 inhibitor CGP57380 overcomes mTOR inhibitor-induced activation of eIF4E: the mechanism of synergic killing of human T-ALL cells. Acta Pharmacol Sin. 2018;39(12):1894-901.
86. Lock R, Ingraham R, Maertens O, Miller AL, Weledji N, Legius E, et al. Cotargeting MNK and MEK kinases induces the regression of NF1-mutant cancers. J Clin Invest. 2016;126(6):2181-90.
87. Cherian J, Nacro K, Poh ZY, Guo S, Jeyaraj DA, Wong YX, et al. Structure-Activity Relationship Studies of Mitogen Activated Protein Kinase Interacting Kinase (MNK) 1 and 2 and BCR-ABL1 Inhibitors Targeting Chronic Myeloid Leukemic Cells. J Med Chem. 2016;59(7):3063-78.
88. Zhang W, Su X, Li S, Wang Y, Wang Q, Zeng H. Inhibiting MNK Selectively Targets Cervical Cancer via Suppressing eIF4E-Mediated β-Catenin Activation. Am J Med Sci. 2019;358(3):227-34.
89. Yang ZY, Jiang CW, Zhang WL, Sun G. Treatment with eFT-508 increases chemosensitivity in breast cancer cells by modulating the tumor microenvironment. J Transl Med. 2022;20(1):276.
90. Pham TND, Kumar K, DeCant BT, Shang M, Munshi SZ, Matsangou M, et al. Induction of MNK Kinase-dependent eIF4E Phosphorylation by Inhibitors Targeting BET Proteins Limits Efficacy of BET Inhibitors. Mol Cancer Ther. 2019;18(2):235-44.
91. Prabhu SA, Moussa O, Gonçalves C, LaPierre JH, Chou H, Huang F, et al. Inhibition of the MNK1/2-eIF4E Axis Augments Palbociclib-Mediated Antitumor Activity in Melanoma and Breast Cancer. Mol Cancer Ther. 2023;22(2):192-204.
92. Pham TND, Spaulding C, Munshi HG. Controlling TIME: How MNK Kinases Function to Shape Tumor Immunity. Cancers (Basel). 2020;12(8).

93. Rowlett RM, Chrestensen CA, Nyce M, Harp MG, Pelo JW, Cominelli F, et al. MNK kinases regulate multiple TLR pathways and innate proinflammatory cytokines in macrophages. Am J Physiol Gastrointest Liver Physiol. 2008;294(2):G452-9.
94. Bartish M, Tong D, Pan Y, Wallerius M, Liu H, Ristau J, et al. MNK2 governs the macrophage antiinflammatory phenotype. Proc Natl Acad Sci U S A. 2020;117(44):27556-65.
95. Fortin CF, Mayer TZ, Cloutier A, McDonald PP. Translational control of human neutrophil responses by MNK1. J Leukoc Biol. 2013;94(4):693-703.
96. Robichaud N, Hsu BE, Istomine R, Alvarez F, Blagih J, Ma EH, et al. Translational control in the tumor microenvironment promotes lung metastasis: Phosphorylation of eIF4E in neutrophils. Proc Natl Acad Sci U S A. 2018;115(10):E2202-e9.
97. Cerezo M, Guemiri R, Druillennec S, Girault I, Malka-Mahieu H, Shen S, et al. Translational control of tumor immune escape via the eIF4F-STAT1-PD-L1 axis in melanoma. Nat Med. 2018;24(12):1877-86.
98. Xu Y, Poggio M, Jin HY, Shi Z, Forester CM, Wang Y, et al. Translation control of the immune checkpoint in cancer and its therapeutic targeting. Nat Med. 2019;25(2):301-11.
99. Guo Q, Bartish M, Gonçalves C, Huang F, Smith-Voudouris J, Krisna SS, et al. The MNK1/2-eIF4E Axis Supports Immune Suppression and Metastasis in Postpartum Breast Cancer. Cancer Res. 2021;81(14):3876-89.
100. Preston SEJ, Bartish M, Richard VR, Aghigh A, Gonçalves C, Smith-Voudouris J, et al. Phosphorylation of eIF4E in the stroma drives the production and spatial organisation of collagen type I in the mammary gland. Matrix Biol. 2022;111:264-88.
101. Berman AJ, Thoreen CC, Dedeic Z, Chettle J, Roux PP, Blagden SP. Controversies around the function of LARP1. RNA Biol. 2021;18(2):207-17.
102. Philippe L, van den Elzen AMG, Watson MJ, Thoreen CC. Global analysis of LARP1 translation targets reveals tunable and dynamic features of 5' TOP motifs. Proc Natl Acad Sci U S A. 2020;117(10):5319-28.
103. Lahr RM, Fonseca BD, Ciotti GE, Al-Ashtal HA, Jia JJ, Niklaus MR, et al. La-related protein 1 (LARP1) binds the mRNA cap, blocking eIF4F assembly on TOP mRNAs. Elife. 2017;6.
104. Philippe L, Vasseur JJ, Debart F, Thoreen CC. La-related protein 1 (LARP1) repression of TOP mRNA translation is mediated through its cap-binding domain and controlled by an adjacent regulatory region. Nucleic Acids Res. 2018;46(3):1457-69.
105. Lahr RM, Mack SM, Héroux A, Blagden SP, Bousquet-Antonelli C, Deragon JM, et al. The La-related protein 1-specific domain repurposes HEAT-like repeats to directly bind a 5'TOP sequence. Nucleic Acids Res. 2015;43(16):8077-88.
106. Fonseca BD, Zakaria C, Jia JJ, Graber TE, Svitkin Y, Tahmasebi S, et al. La-related Protein 1 (LARP1) Represses Terminal Oligopyrimidine (TOP) mRNA Translation Downstream of mTOR Complex 1 (mTORC1). J Biol Chem. 2015;290(26):15996-6020.
107. Al-Ashtal HA, Rubottom CM, Leeper TC, Berman AJ. The LARP1 La-Module recognizes both ends of TOP mRNAs. RNA Biol. 2021;18(2):248-58.
108. Hong S, Freeberg MA, Han T, Kamath A, Yao Y, Fukuda T, et al. LARP1 functions as a molecular switch for mTORC1-mediated translation of an essential class of mRNAs. Elife. 2017;6.
109. Haneke K, Schott J, Lindner D, Hollensen AK, Damgaard CK, Mongis C, et al. CDK1 couples proliferation with protein synthesis. J Cell Biol. 2020;219(3).
110. Ramani K, Robinson AE, Berlind J, Fan W, Abeynayake A, Binek A, et al. S-adenosylmethionine inhibits la ribonucleoprotein domain family member 1 in murine liver and human liver cancer cells. Hepatology. 2022;75(2):280-96.

111. Jia JJ, Lahr RM, Solgaard MT, Moraes BJ, Pointet R, Yang AD, et al. mTORC1 promotes TOP mRNA translation through site-specific phosphorylation of LARP1. Nucleic Acids Res. 2021;49(6):3461-89.
112. Ogami K, Oishi Y, Sakamoto K, Okumura M, Yamagishi R, Inoue T, et al. mTOR- and LARP1-dependent regulation of TOP mRNA poly(A) tail and ribosome loading. Cell Rep. 2022;41(4):111548.
113. Mura M, Hopkins TG, Michael T, Abd-Latip N, Weir J, Aboagye E, et al. LARP1 post-transcriptionally regulates mTOR and contributes to cancer progression. Oncogene. 2015;34(39):5025-36.
114. Hopkins TG, Mura M, Al-Ashtal HA, Lahr RM, Abd-Latip N, Sweeney K, et al. The RNA-binding protein LARP1 is a post-transcriptional regulator of survival and tumorigenesis in ovarian cancer. Nucleic Acids Res. 2016;44(3):1227-46.
115. Xie C, Huang L, Xie S, Xie D, Zhang G, Wang P, et al. LARP1 predict the prognosis for early-stage and AFP-normal hepatocellular carcinoma. J Transl Med. 2013;11:272.
116. Ye L, Lin ST, Mi YS, Liu Y, Ma Y, Sun HM, et al. Overexpression of LARP1 predicts poor prognosis of colorectal cancer and is expected to be a potential therapeutic target. Tumour Biol. 2016;37(11):14585-94.
117. Xu Z, Xu J, Lu H, Lin B, Cai S, Guo J, et al. LARP1 is regulated by the XIST/miR-374a axis and functions as an oncogene in non-small cell lung carcinoma. Oncol Rep. 2017;38(6):3659-67.
118. Schneider C, Erhard F, Binotti B, Buchberger A, Vogel J, Fischer U. An unusual mode of baseline translation adjusts cellular protein synthesis capacity to metabolic needs. Cell Rep. 2022;41(2):111467.
119. Polymenis M, Aramayo R. Translate to divide: control of the cell cycle by protein synthesis. Microb Cell. 2015;2(4):94-104.
120. Shahbazian D, Roux PP, Mieulet V, Cohen MS, Raught B, Taunton J, et al. The mTOR/PI3K and MAPK pathways converge on eIF4B to control its phosphorylation and activity. Embo j. 2006;25(12):2781-91.
121. Fingar DC, Richardson CJ, Tee AR, Cheatham L, Tsou C, Blenis J. mTOR controls cell cycle progression through its cell growth effectors S6K1 and 4E-BP1/eukaryotic translation initiation factor 4E. Mol Cell Biol. 2004;24(1):200-16.
122. Romero-Pozuelo J, Figlia G, Kaya O, Martin-Villalba A, Teleman AA. Cdk4 and Cdk6 Couple the Cell-Cycle Machinery to Cell Growth via mTORC1. Cell Rep. 2020;31(2):107504.
123. Mitchell DC, Menon A, Garner AL. Chemoproteomic Profiling Uncovers CDK4-Mediated Phosphorylation of the Translational Suppressor 4E-BP1. Cell Chem Biol. 2019;26(7):980-90.e8.
124. Liu J, Peng Y, Wei W. Cell cycle on the crossroad of tumorigenesis and cancer therapy. Trends Cell Biol. 2022;32(1):30-44.
125. Goel S, Bergholz JS, Zhao JJ. Targeting CDK4 and CDK6 in cancer. Nat Rev Cancer. 2022;22(6):356-72.
126. Sheppard KE, McArthur GA. The cell-cycle regulator CDK4: an emerging therapeutic target in melanoma. Clin Cancer Res. 2013;19(19):5320-8.
127. Peeper DS, Upton TM, Ladha MH, Neuman E, Zalvide J, Bernards R, et al. Ras signalling linked to the cell-cycle machinery by the retinoblastoma protein. Nature. 1997;386(6621):177-81.
128. Schmidt M, Fernandez de Mattos S, van der Horst A, Klompmaker R, Kops GJ, Lam EW, et al. Cell cycle inhibition by FoxO forkhead transcription factors involves downregulation of cyclin D. Mol Cell Biol. 2002;22(22):7842-52.
129. Muise-Helmericks RC, Grimes HL, Bellacosa A, Malstrom SE, Tsichlis PN, Rosen N. Cyclin D expression is controlled post-transcriptionally via a phosphatidylinositol 3-kinase/Akt-dependent pathway. J Biol Chem. 1998;273(45):29864-72.

130. Diehl JA, Cheng M, Roussel MF, Sherr CJ. Glycogen synthase kinase-3beta regulates cyclin D1 proteolysis and subcellular localization. Genes Dev. 1998;12(22):3499-511.
131. Averous J, Fonseca BD, Proud CG. Regulation of cyclin D1 expression by mTORC1 signaling requires eukaryotic initiation factor 4E-binding protein 1. Oncogene. 2008;27(8):1106-13.
132. Rosenwald IB, Lazaris-Karatzas A, Sonenberg N, Schmidt EV. Elevated levels of cyclin D1 protein in response to increased expression of eukaryotic initiation factor 4E. Mol Cell Biol. 1993;13(12):7358-63.
133. Serrano M, Hannon GJ, Beach D. A new regulatory motif in cell-cycle control causing specific inhibition of cyclin D/CDK4. Nature. 1993;366(6456):704-7.
134. Stepanova L, Leng X, Parker SB, Harper JW. Mammalian p50Cdc37 is a protein kinase-targeting subunit of Hsp90 that binds and stabilizes Cdk4. Genes Dev. 1996;10(12):1491-502.
135. Zhao Q, Boschelli F, Caplan AJ, Arndt KT. Identification of a conserved sequence motif that promotes Cdc37 and cyclin D1 binding to Cdk4. J Biol Chem. 2004;279(13):12560-4.
136. Lamphere L, Fiore F, Xu X, Brizuela L, Keezer S, Sardet C, et al. Interaction between Cdc37 and Cdk4 in human cells. Oncogene. 1997;14(16):1999-2004.
137. Cerqueira A, Martín A, Symonds CE, Odajima J, Dubus P, Barbacid M, et al. Genetic characterization of the role of the Cip/Kip family of proteins as cyclin-dependent kinase inhibitors and assembly factors. Mol Cell Biol. 2014;34(8):1452-9.
138. Guiley KZ, Stevenson JW, Lou K, Barkovich KJ, Kumarasamy V, Wijeratne TU, et al. p27 allosterically activates cyclin-dependent kinase 4 and antagonizes palbociclib inhibition. Science. 2019;366(6471).
139. Schachter MM, Merrick KA, Larochelle S, Hirschi A, Zhang C, Shokat KM, et al. A Cdk7-Cdk4 T-loop phosphorylation cascade promotes G1 progression. Mol Cell. 2013;50(2):250-60.
140. Ray A, James MK, Larochelle S, Fisher RP, Blain SW. p27Kip1 inhibits cyclin D-cyclin-dependent kinase 4 by two independent modes. Mol Cell Biol. 2009;29(4):986-99.
141. Santarius T, Shipley J, Brewer D, Stratton MR, Cooper CS. A census of amplified and overexpressed human cancer genes. Nat Rev Cancer. 2010;10(1):59-64.
142. Garcea G, Neal CP, Pattenden CJ, Steward WP, Berry DP. Molecular prognostic markers in pancreatic cancer: a systematic review. Eur J Cancer. 2005;41(15):2213-36.
143. Gautschi O, Ratschiller D, Gugger M, Betticher DC, Heighway J. Cyclin D1 in non-small cell lung cancer: a key driver of malignant transformation. Lung Cancer. 2007;55(1):1-14.
144. Li R, An SJ, Chen ZH, Zhang GC, Zhu JQ, Nie Q, et al. Expression of cyclin D1 splice variants is differentially associated with outcome in non-small cell lung cancer patients. Hum Pathol. 2008;39(12):1792-801.
145. Hardisson D. Molecular pathogenesis of head and neck squamous cell carcinoma. Eur Arch Otorhinolaryngol. 2003;260(9):502-8.
146. Qie S, Diehl JA. Cyclin D1, cancer progression, and opportunities in cancer treatment. J Mol Med (Berl). 2016;94(12):1313-26.
147. Thomas GR, Nadiminti H, Regalado J. Molecular predictors of clinical outcome in patients with head and neck squamous cell carcinoma. Int J Exp Pathol. 2005;86(6):347-63.
148. Li W, Sanki A, Karim RZ, Thompson JF, Soon Lee C, Zhuang L, et al. The role of cell cycle regulatory proteins in the pathogenesis of melanoma. Pathology. 2006;38(4):287-301.
149. Moreno-Bueno G, Rodríguez-Perales S, Sánchez-Estévez C, Marcos R, Hardisson D, Cigudosa JC, et al. Molecular alterations associated with cyclin D1 overexpression in endometrial cancer. Int J Cancer. 2004;110(2):194-200.

150. Wu W, Slomovitz BM, Soliman PT, Schmeler KM, Celestino J, Milam MR, et al. Correlation of cyclin D1 and cyclin D3 overexpression with the loss of PTEN expression in endometrial carcinoma. Int J Gynecol Cancer. 2006;16(4):1668-72.
151. Bertoni F, Rinaldi A, Zucca E, Cavalli F. Update on the molecular biology of mantle cell lymphoma. Hematol Oncol. 2006;24(1):22-7.
152. Italiano A, Bianchini L, Gjernes E, Keslair F, Ranchere-Vince D, Dumollard JM, et al. Clinical and biological significance of CDK4 amplification in well-differentiated and dedifferentiated liposarcomas. Clin Cancer Res. 2009;15(18):5696-703.
153. Korz C, Pscherer A, Benner A, Mertens D, Schaffner C, Leupolt E, et al. Evidence for distinct pathomechanisms in B-cell chronic lymphocytic leukemia and mantle cell lymphoma by quantitative expression analysis of cell cycle and apoptosis-associated genes. Blood. 2002;99(12):4554-61.
154. Ortega S, Malumbres M, Barbacid M. Cyclin D-dependent kinases, INK4 inhibitors and cancer. Biochim Biophys Acta. 2002;1602(1):73-87.
155. Tang B, Sheng X, Kong Y, Chi Z, Si L, Cui C, et al. Palbociclib for treatment of metastatic melanoma with copy number variations of CDK4 pathway: case report. Chin Clin Oncol. 2018;7(6):62.
156. Jr WHL, Sidransky D. Role of the p16 tumor suppressor gene in cancer. Journal of Clinical Oncology. 1998;16(3):1197-206.
157. Sherr CJ. The INK4a/ARF network in tumour suppression. Nat Rev Mol Cell Biol. 2001;2(10):731-7.
158. Straume O, Smeds J, Kumar R, Hemminki K, Akslen LA. Significant impact of promoter hypermethylation and the 540 C>T polymorphism of CDKN2A in cutaneous melanoma of the vertical growth phase. Am J Pathol. 2002;161(1):229-37.
159. Al-Kaabi A, van Bockel LW, Pothen AJ, Willems SM. p16INK4A and p14ARF gene promoter hypermethylation as prognostic biomarker in oral and oropharyngeal squamous cell carcinoma: a review. Dis Markers. 2014;2014:260549.
160. Ameri A, Alidoosti A, Hosseini SY, Parvin M, Emranpour MH, Taslimi F, et al. Prognostic Value of Promoter Hypermethylation of Retinoic Acid Receptor Beta (RARB) and CDKN2 (p16/MTS1) in Prostate Cancer. Chin J Cancer Res. 2011;23(4):306-11.
161. Asokan GS, Jeelani S, Gnanasundaram N. Promoter hypermethylation profile of tumour suppressor genes in oral leukoplakia and oral squamous cell carcinoma. J Clin Diagn Res. 2014;8(10):Zc09-12.
162. Igaki H, Sasaki H, Kishi T, Sakamoto H, Tachimori Y, Kato H, et al. Highly frequent homozygous deletion of the p16 gene in esophageal cancer cell lines. Biochem Biophys Res Commun. 1994;203(2):1090-5.
163. Zhao R, Choi BY, Lee MH, Bode AM, Dong Z. Implications of Genetic and Epigenetic Alterations of CDKN2A (p16(INK4a)) in Cancer. EBioMedicine. 2016;8:30-9.
164. Goldstein AM, Chan M, Harland M, Hayward NK, Demenais F, Bishop DT, et al. Features associated with germline CDKN2A mutations: a GenoMEL study of melanoma-prone families from three continents. J Med Genet. 2007;44(2):99-106.
165. Castellano M, Pollock PM, Walters MK, Sparrow LE, Down LM, Gabrielli BG, et al. CDKN2A/p16 is inactivated in most melanoma cell lines. Cancer Res. 1997;57(21):4868-75.
166. McConnell BB, Gregory FJ, Stott FJ, Hara E, Peters G. Induced expression of p16(INK4a) inhibits both CDK4- and CDK2-associated kinase activity by reassortment of cyclin-CDK-inhibitor complexes. Mol Cell Biol. 1999;19(3):1981-9.
167. Rossi M, Pellegrini C, Cardelli L, Ciciarelli V, Di Nardo L, Fargnoli MC. Familial Melanoma: Diagnostic and Management Implications. Dermatol Pract Concept. 2019;9(1):10-6.

168. VanderWel SN, Harvey PJ, McNamara DJ, Repine JT, Keller PR, Quin J, 3rd, et al. Pyrido[2,3-d]pyrimidin-7-ones as specific inhibitors of cyclin-dependent kinase 4. J Med Chem. 2005;48(7):2371-87.
169. DeSantis CE, Ma J, Gaudet MM, Newman LA, Miller KD, Goding Sauer A, et al. Breast cancer statistics, 2019. CA Cancer J Clin. 2019;69(6):438-51.
170. Hanker AB, Sudhan DR, Arteaga CL. Overcoming Endocrine Resistance in Breast Cancer. Cancer Cell. 2020;37(4):496-513.
171. García-Becerra R, Santos N, Díaz L, Camacho J. Mechanisms of resistance to endocrine therapy in breast cancer: focus on signaling pathways, miRNAs and genetically based resistance. Int J Mol Sci. 2012;14(1):108-45.
172. Jeong Y, Bae SY, You D, Jung SP, Choi HJ, Kim I, et al. EGFR is a Therapeutic Target in Hormone Receptor-Positive Breast Cancer. Cell Physiol Biochem. 2019;53(5):805-19.
173. Knowlden JM, Hutcheson IR, Jones HE, Madden T, Gee JM, Harper ME, et al. Elevated levels of epidermal growth factor receptor/c-erbB2 heterodimers mediate an autocrine growth regulatory pathway in tamoxifen-resistant MCF-7 cells. Endocrinology. 2003;144(3):1032-44.
174. Kurokawa H, Lenferink AE, Simpson JF, Pisacane PI, Sliwkowski MX, Forbes JT, et al. Inhibition of HER2/neu (erbB-2) and mitogen-activated protein kinases enhances tamoxifen action against HER2-overexpressing, tamoxifen-resistant breast cancer cells. Cancer Res. 2000;60(20):5887-94.
175. Sabbah M, Courilleau D, Mester J, Redeuilh G. Estrogen induction of the cyclin D1 promoter: involvement of a cAMP response-like element. Proc Natl Acad Sci U S A. 1999;96(20):11217-22.
176. Finn RS, Aleshin A, Slamon DJ. Targeting the cyclin-dependent kinases (CDK) 4/6 in estrogen receptor-positive breast cancers. Breast Cancer Res. 2016;18(1):17.
177. Hurvitz S, Martin M, Press M, Wijayawardana S, Brahmachary M, Ebert P, et al. Abstract PD2-10: Treatment with abemaciclib modulates the immune response in gene expression analysis of the neoMONARCH neoadjuvant study of abemaciclib in postmenopausal women with HR+, HER2 negative breast cancer. Cancer Research. 2019;79(4_Supplement):PD2-10-PD2-.
178. Malorni L, Curigliano G, Minisini AM, Cinieri S, Tondini CA, D'Hollander K, et al. Palbociclib as single agent or in combination with the endocrine therapy received before disease progression for estrogen receptor-positive, HER2-negative metastatic breast cancer: TREnd trial. Ann Oncol. 2018;29(8):1748-54.
179. Ma CX, Gao F, Luo J, Northfelt DW, Goetz M, Forero A, et al. NeoPalAna: Neoadjuvant Palbociclib, a Cyclin-Dependent Kinase 4/6 Inhibitor, and Anastrozole for Clinical Stage 2 or 3 Estrogen Receptor-Positive Breast Cancer. Clin Cancer Res. 2017;23(15):4055-65.
180. Johnston S, Puhalla S, Wheatley D, Ring A, Barry P, Holcombe C, et al. Randomized Phase II Study Evaluating Palbociclib in Addition to Letrozole as Neoadjuvant Therapy in Estrogen Receptor-Positive Early Breast Cancer: PALLET Trial. J Clin Oncol. 2019;37(3):178-89.
181. Finn RS, Martin M, Rugo HS, Jones S, Im SA, Gelmon K, et al. Palbociclib and Letrozole in Advanced Breast Cancer. N Engl J Med. 2016;375(20):1925-36.
182. Goetz MP, Toi M, Campone M, Sohn J, Paluch-Shimon S, Huober J, et al. MONARCH 3: Abemaciclib As Initial Therapy for Advanced Breast Cancer. J Clin Oncol. 2017;35(32):3638-46.
183. Garutti M, Targato G, Buriolla S, Palmero L, Minisini AM, Puglisi F. CDK4/6 Inhibitors in Melanoma: A Comprehensive Review. Cells. 2021;10(6).
184. Pacheco J, Schenk E. CDK4/6 inhibition alone and in combination for non-small cell lung cancer. Oncotarget. 2019;10(6):618-9.
185. Kosovec JE, Zaidi AH, Omstead AN, Matsui D, Biedka MJ, Cox EJ, et al. CDK4/6 dual inhibitor abemaciclib demonstrates compelling preclinical activity against esophageal adenocarcinoma: a novel therapeutic option for a deadly disease. Oncotarget. 2017;8(59):100421-32.

186. Jiggens E, Mortoglou M, Grant GH, Uysal-Onganer P. The Role of CDK4 in the Pathogenesis of Pancreatic Cancer. Healthcare (Basel). 2021;9(11).
187. Thoma OM, Neurath MF, Waldner MJ. Cyclin-Dependent Kinase Inhibitors and Their Therapeutic Potential in Colorectal Cancer Treatment. Front Pharmacol. 2021;12:757120.
188. Finn RS, Dering J, Conklin D, Kalous O, Cohen DJ, Desai AJ, et al. PD 0332991, a selective cyclin D kinase 4/6 inhibitor, preferentially inhibits proliferation of luminal estrogen receptor-positive human breast cancer cell lines in vitro. Breast Cancer Res. 2009;11(5):R77.
189. Konecny GE, Winterhoff B, Kolarova T, Qi J, Manivong K, Dering J, et al. Expression of p16 and retinoblastoma determines response to CDK4/6 inhibition in ovarian cancer. Clin Cancer Res. 2011;17(6):1591-602.
190. Dickson MA, Tap WD, Keohan ML, D'Angelo SP, Gounder MM, Antonescu CR, et al. Phase II trial of the CDK4 inhibitor PD0332991 in patients with advanced CDK4-amplified well-differentiated or dedifferentiated liposarcoma. J Clin Oncol. 2013;31(16):2024-8.
191. Geoerger B, Bourdeaut F, DuBois SG, Fischer M, Geller JI, Gottardo NG, et al. A Phase I Study of the CDK4/6 Inhibitor Ribociclib (LEE011) in Pediatric Patients with Malignant Rhabdoid Tumors, Neuroblastoma, and Other Solid Tumors. Clin Cancer Res. 2017;23(10):2433-41.
192. Raspé E, Coulonval K, Pita JM, Paternot S, Rothé F, Twyffels L, et al. CDK4 phosphorylation status and a linked gene expression profile predict sensitivity to palbociclib. EMBO Mol Med. 2017;9(8):1052-66.
193. Gong X, Litchfield LM, Webster Y, Chio LC, Wong SS, Stewart TR, et al. Genomic Aberrations that Activate D-type Cyclins Are Associated with Enhanced Sensitivity to the CDK4 and CDK6 Inhibitor Abemaciclib. Cancer Cell. 2017;32(6):761-76.e6.
194. Min A, Kim JE, Kim YJ, Lim JM, Kim S, Kim JW, et al. Cyclin E overexpression confers resistance to the CDK4/6 specific inhibitor palbociclib in gastric cancer cells. Cancer Lett. 2018;430:123-32.
195. Chandarlapaty S, Razavi P. Cyclin E mRNA: Assessing Cyclin-Dependent Kinase (CDK) Activation State to Elucidate Breast Cancer Resistance to CDK4/6 Inhibitors. J Clin Oncol. 2019;37(14):1148-50.
196. Asghar US, Barr AR, Cutts R, Beaney M, Babina I, Sampath D, et al. Single-Cell Dynamics Determines Response to CDK4/6 Inhibition in Triple-Negative Breast Cancer. Clin Cancer Res. 2017;23(18):5561-72.
197. Condorelli R, Spring L, O'Shaughnessy J, Lacroix L, Bailleux C, Scott V, et al. Polyclonal RB1 mutations and acquired resistance to CDK 4/6 inhibitors in patients with metastatic breast cancer. Ann Oncol. 2018;29(3):640-5.
198. O'Leary B, Cutts RJ, Liu Y, Hrebien S, Huang X, Fenwick K, et al. The Genetic Landscape and Clonal Evolution of Breast Cancer Resistance to Palbociclib plus Fulvestrant in the PALOMA-3 Trial. Cancer Discov. 2018;8(11):1390-403.
199. Formisano L, Lu Y, Servetto A, Hanker AB, Jansen VM, Bauer JA, et al. Aberrant FGFR signaling mediates resistance to CDK4/6 inhibitors in ER+ breast cancer. Nat Commun. 2019;10(1):1373.
200. Haines E, Chen T, Kommajosyula N, Chen Z, Herter-Sprie GS, Cornell L, et al. Palbociclib resistance confers dependence on an FGFR-MAP kinase-mTOR-driven pathway in KRAS-mutant non-small cell lung cancer. Oncotarget. 2018;9(60):31572-89.
201. de Leeuw R, McNair C, Schiewer MJ, Neupane NP, Brand LJ, Augello MA, et al. MAPK Reliance via Acquired CDK4/6 Inhibitor Resistance in Cancer. Clin Cancer Res. 2018;24(17):4201-14.
202. Romano G, Chen PL, Song P, McQuade JL, Liang RJ, Liu M, et al. A Preexisting Rare PIK3CA(E545K) Subpopulation Confers Clinical Resistance to MEK plus CDK4/6 Inhibition in NRAS Melanoma and Is Dependent on S6K1 Signaling. Cancer Discov. 2018;8(5):556-67.

203. Knudsen ES, Kumarasamy V, Ruiz A, Sivinski J, Chung S, Grant A, et al. Cell cycle plasticity driven by MTOR signaling: integral resistance to CDK4/6 inhibition in patient-derived models of pancreatic cancer. Oncogene. 2019;38(18):3355-70.
204. Michaloglou C, Crafter C, Siersbaek R, Delpuech O, Curwen JO, Carnevalli LS, et al. Combined Inhibition of mTOR and CDK4/6 Is Required for Optimal Blockade of E2F Function and Long-term Growth Inhibition in Estrogen Receptor-positive Breast Cancer. Mol Cancer Ther. 2018;17(5):908-20.
205. Zhang J, Xu K, Liu P, Geng Y, Wang B, Gan W, et al. Inhibition of Rb Phosphorylation Leads to mTORC2-Mediated Activation of Akt. Mol Cell. 2016;62(6):929-42.
206. AbuHammad S, Cullinane C, Martin C, Bacolas Z, Ward T, Chen H, et al. Regulation of PRMT5-MDM4 axis is critical in the response to CDK4/6 inhibitors in melanoma. Proc Natl Acad Sci U S A. 2019;116(36):17990-8000.
207. Maskey RS, Wang F, Lehman E, Wang Y, Emmanuel N, Zhong W, et al. Sustained mTORC1 activity during palbociclib-induced growth arrest triggers senescence in ER+ breast cancer cells. Cell Cycle. 2021;20(1):65-80.
208. O'Brien NA, McDermott MSJ, Conklin D, Luo T, Ayala R, Salgar S, et al. Targeting activated PI3K/mTOR signaling overcomes acquired resistance to CDK4/6-based therapies in preclinical models of hormone receptor-positive breast cancer. Breast Cancer Res. 2020;22(1):89.
209. Rodriguez MJ, Perrone MC, Riggio M, Palafox M, Salinas V, Elia A, et al. Targeting mTOR to overcome resistance to hormone and CDK4/6 inhibitors in ER-positive breast cancer models. Sci Rep. 2023;13(1):2710.
210. Yoshida A, Lee EK, Diehl JA. Induction of Therapeutic Senescence in Vemurafenib-Resistant Melanoma by Extended Inhibition of CDK4/6. Cancer Res. 2016;76(10):2990-3002.
211. Yoshida A, Bu Y, Qie S, Wrangle J, Camp ER, Hazard ES, et al. SLC36A1-mTORC1 signaling drives acquired resistance to CDK4/6 inhibitors. Sci Adv. 2019;5(9):eaax6352.
212. Kong T, Xue Y, Cencic R, Zhu X, Monast A, Fu Z, et al. eIF4A Inhibitors Suppress Cell-Cycle Feedback Response and Acquired Resistance to CDK4/6 Inhibition in Cancer. Mol Cancer Ther. 2019;18(11):2158-70.
213. Pancholi S, Ribas R, Simigdala N, Schuster E, Nikitorowicz-Buniak J, Ressa A, et al. Tumour kinome re-wiring governs resistance to palbociclib in oestrogen receptor positive breast cancers, highlighting new therapeutic modalities. Oncogene. 2020;39(25):4781-97.
214. Ziaei S, Shimada N, Kucharavy H, Hubbard K. MNK1 expression increases during cellular senescence and modulates the subcellular localization of hnRNP A1. Exp Cell Res. 2012;318(5):500-8.
215. Santag S, Siegel F, Wengner AM, Lange C, Bömer U, Eis K, et al. BAY 1143269, a novel MNK1 inhibitor, targets oncogenic protein expression and shows potent anti-tumor activity. Cancer Lett. 2017;390:21-9.
216. Zheng J, Li J, Xu L, Xie G, Wen Q, Luo J, et al. Phosphorylated Mnk1 and eIF4E are associated with lymph node metastasis and poor prognosis of nasopharyngeal carcinoma. PLoS One. 2014;9(2):e89220.
217. Pettersson F, Del Rincon SV, Emond A, Huor B, Ngan E, Ng J, et al. Genetic and pharmacologic inhibition of eIF4E reduces breast cancer cell migration, invasion, and metastasis. Cancer Res. 2015;75(6):1102-12.
218. Zhou S, Wang GP, Liu C, Zhou M. Eukaryotic initiation factor 4E (eIF4E) and angiogenesis: prognostic markers for breast cancer. BMC Cancer. 2006;6:231.
219. Pettersson F, Yau C, Dobocan MC, Culjkovic-Kraljacic B, Retrouvey H, Puckett R, et al. Ribavirin treatment effects on breast cancers overexpressing eIF4E, a biomarker with prognostic specificity for luminal B-type breast cancer. Clin Cancer Res. 2011;17(9):2874-84.

220. Guo Z, Peng G, Li E, Xi S, Zhang Y, Li Y, et al. MAP kinase-interacting serine/threonine kinase 2 promotes proliferation, metastasis, and predicts poor prognosis in non-small cell lung cancer. Scientific Reports. 2017;7(1):10612.
221. Liu T, Yu J, Deng M, Yin Y, Zhang H, Luo K, et al. CDK4/6-dependent activation of DUB3 regulates cancer metastasis through SNAIL1. Nature Communications. 2017;8(1):13923.
222. Zhang Z, Li J, Ou Y, Yang G, Deng K, Wang Q, et al. CDK4/6 inhibition blocks cancer metastasis through a USP51-ZEB1-dependent deubiquitination mechanism. Signal Transduction and Targeted Therapy. 2020;5(1):25.
223. Zhang QF, Li J, Jiang K, Wang R, Ge JL, Yang H, et al. CDK4/6 inhibition promotes immune infiltration in ovarian cancer and synergizes with PD-1 blockade in a B cell-dependent manner. Theranostics. 2020;10(23):10619-33.
224. Bai X, Guo Z-Q, Zhang Y-P, Fan Z-z, Liu L-J, Liu L, et al. CDK4/6 inhibition triggers ICAM1-driven immune response and sensitizes LKB1 mutant lung cancer to immunotherapy. Nature Communications. 2023;14(1):1247.
225. Deng J, Wang ES, Jenkins RW, Li S, Dries R, Yates K, et al. CDK4/6 Inhibition Augments Antitumor Immunity by Enhancing T-cell Activation. Cancer Discov. 2018;8(2):216-33.
226. Zhang J, Bu X, Wang H, Zhu Y, Geng Y, Nihira NT, et al. Cyclin D-CDK4 kinase destabilizes PD-L1 via cullin 3-SPOP to control cancer immune surveillance. Nature. 2018;553(7686):91-5.
227. Wang C-L, Chiang I-T, Hsu F-T, Chang Y. Abstract 1592: Palbociclib enhances anti-PD-L1 therapeutic efficacy in oral squamous cell carcinoma was associated with CXCR4 inactivation. Cancer Research. 2021;81(13_Supplement):1592-.
228. Scirocchi F, Scagnoli S, Botticelli A, Di Filippo A, Napoletano C, Zizzari IG, et al. Immune effects of CDK4/6 inhibitors in patients with HR(+)/HER2(-) metastatic breast cancer: Relief from immunosuppression is associated with clinical response. EBioMedicine. 2022;79:104010.
229. Yuan Y, Lee JS, Yost SE, Frankel PH, Ruel C, Egelston CA, et al. Phase I/II trial of palbociclib, pembrolizumab and letrozole in patients with hormone receptor-positive metastatic breast cancer. Eur J Cancer. 2021;154:11-20.
230. Burrows C, Abd Latip N, Lam SJ, Carpenter L, Sawicka K, Tzolovsky G, et al. The RNA binding protein Larp1 regulates cell division, apoptosis and cell migration. Nucleic Acids Res. 2010;38(16):5542-53.
231. Tcherkezian J, Cargnello M, Romeo Y, Huttlin EL, Lavoie G, Gygi SP, et al. Proteomic analysis of cap-dependent translation identifies LARP1 as a key regulator of 5'TOP mRNA translation. Genes Dev. 2014;28(4):357-71.
232. Schwenzer H, Abdel Mouti M, Neubert P, Morris J, Stockton J, Bonham S et al. LARP1 isoform expression in human cancer cell lines. RNA biology. 2021; 18(2): 237–247